MECHANISTIC MODELING OF MASS TRANSFER IN THE LAMINAR SUBLAYER IN DOWNHOLE SYSTEMS

By

SIVAKUMAR NATARAJAN

Bachelor of Engineering with Master of Science

Birla Institute of Technology and Science

Rajasthan, India

1997

Submitted to the Faculty of the
Graduate College of the
Oklahoma State University
in partial fulfillment of
the requirements for
the Degree of
MASTER OF SCIENCE
May, 2000

MECHANISTIC MODELING OF MASS TRANSFER

IN THE LAMINAR SUBLAYER IN DOWNHOLE

SYSTEMS

Thesis Approved:

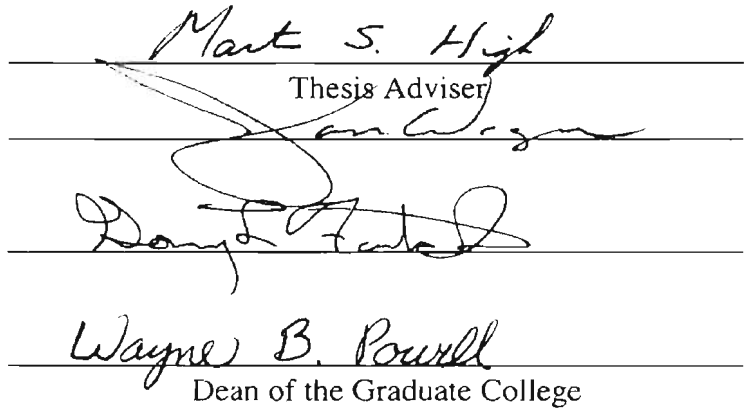

Thesis Adviser

Dean of the Graduate College

ACKNOWLEDGMENTS

First of all, I would like to thank my adviser, Dr. Martin S. High, for providing me this wonderful opportunity to work on this research. His active interest, valuable guidance, constant encouragement and an understanding attitude helped me stay focussed and motivated. I sincerely thank Dr. Jan Wagner for providing me academic guidance throughout my graduate studies. I would like to thank Dr. Gary L. Foutch for serving on my thesis committee.

I am very thankful to the Downhole Corrosion Consortium whose members, namely, Conoco, Chevron, and Phillips Petroleum, have been sponsors of this project. I also thank the entire faculty and staff of the School of Chemical Engineering for their generous assistance.

I would like to give special appreciation to my parents, my younger brother, and all my friends for their support and encouragement at times of difficulty, and for their love and understanding throughout this whole process.

TABLE OF CONTENTS

LIST OF TABLES

LIST OF FIGURES

NOMENCLATURE

$a_{i,k}$ coefficient of the second derivative of k^{th} variable in the i^{th} equation in the set of N coupled, linear differential equations represented by Equation (3.5)

A empirical constant in Equation (3.35), dimensionless

$A_{i,k}(j)$ coefficient of the k^{th} variable at grid point (j-1) in the i^{th} equation in the set of N coupled, linear difference equation represented by Equation (3.8)

$b_{i,k}$ coefficient of first derivative of k^{th} variable in the i^{th} equation in the set of N coupled, linear differential equation represented by Equation (3.5)

B empirical constant in Equation (3.35), dimensionless

$B_{i,k}(j)$ coefficient of the k^{th} variable at grid point (j) in the i^{th} equation in the set of N coupled, linear difference equation represented by Equation (3.8)

bbl barrels

BOPD barrels of oil produced per day, bbls/day

BWPD barrels of water produced per day, bbls/day

c_i concentration of species *i*, moles/dm^3

C_i concentration of species *i*, moles/dm^3

c_k k^{th} unknown variable in the set of N coupled, linear differential equation represented by Equation (3.5)

$C_k(j)$ k^{th} variable at grid point (j) in the set of N coupled, linear difference equation represented by Equation (3.8)

$c_{i,t}$ concentration of species *i* at turbulent laminar interface, moles/dm^3

CR corrosion rate, mils per inch

$d_{i,k}$ coefficient of k^{th} variable in the i^{th} equation in the set of N coupled, linear differential equation represented by Equation (3.5)

D_i diffusion coefficient of species *i*, dm^2/s

$D_{i,k}(j)$ coefficient of the k^{th} variable at grid point (j+1) in the i^{th} equation in the set of N coupled, linear difference equation represented by Equation (3.8)

D_t hydraulic diameter of pipe, dm

E_{corr} corrosion potential, V

EUE external Upset End - a tubing specification, dimensionless

F Faraday's constant, 96500 C/mole

F_0 Henstock-Hanratty dimensionless group defined by Equation (33), dimensionless

g_i constant in the i^{th} equation in the set of N coupled, linear differential equation represented by Equation (3.5)

$G_i(j)$ constant in the i^{th} equation in the set of N coupled, linear difference equation represented by Equation (3.8)

h spacing between two adjacent grid points, dm

i_a anodic current density, Amp/dm^2

i_{ao} anodic exchange current density, Amp/dm^2

i_c cathodic corrosion current, Amp/dm^2

i_{corr}	corrosion current, Amp/dm^2
I	ionic strength, Coulomb mol^2/kg^2
j	grid point, dimensionless
J_i	flux density of species *i*, mol/cm^2/s
J_r	reactive Flux, mol/dm^2/s
M_i	molecular weight of species *i*, g/mol
MPY	unit of corrosion rate measurement, mils per year
n	number of valence electrons, dimensionless
N_i	flux density of species *i*, mol/cm^2/s
N_{sp}	number of species in the system, dimensionless
N	number of dependent variables in the system = N_{sp}+ 1, dimensionless
NJ	number of grid points in the laminar sublayer, dimensionless
R	universal gas constant, J/mol/K
R_j	generation term in Equation (2.22), mol/dm^3/s
Re_{LF}	reynolds number of liquid flowing along the wall, dimensionless
Re_G	reynolds number of the core gas calculated as if the gas filled the whole tube, dimensionless
Sc	non-linear source term, dimensionless
Sc	Schmidt Number, dimensionless
t	time, s
t	temperature, K
T	temperature, K
u_i	mobility of species *i*, cm mol/J/s

v_{corr} corrosion rate, mm/yr

v_i fluid velocity, cm/s

V corrosion rate, mm/yr or mpy

X dimensionless length scale, dimensionless

$X_{i,k}(j)$ coefficient of the k^{th} variable at grid point (j+2) in the i^{th} equation in the set of N coupled, linear difference equation represented by Equation (3.11)

y axis along radial direction

$Y_{i,k}(j)$ coefficient of the k^{th} variable at grid point (j-2) in the i^{th} equation in the set of N coupled, linear difference equation represented by Equation (3.12)

z axis along well depth in the vertical upward direction

z_i charge number of species *i*, dimensionless

Greek Symbols

ε convergence criterion, dimensionless

Φ electrostatic potential, V

δ annular liquid film thickness, dm

δ_o laminar layer thickness, dm

ρ density, g/cc

ν kinematic viscosity, m^2/s

μ viscosity, g/cm/s

η_a anodic overpotential, V

α_a anodic transfer coefficient, dimensionless

γ function of liquid film Reynolds number used in Equation (2.33), dimensionless

λ_i ionic equivalent conductance, $S.cm^2/equiv$

Subscripts

abs absolute, dimensionless

g gas, dimensionless

i ith species, dimensionless

l liquid, dimensionless

new the last iteration, dimensionless

old the previous iteration, dimensionless

rel relative, dimensionless

δ wall property, dimensionless

t turbulent-laminar layer interface property, dimensionless

Superscript

$'$ first derivative with respect to y

$'$ second directive with respect to y

^{o} initial guess

CHAPTER I

INTRODUCTION

Corrosion is the destructive result of a chemical reaction between a metal or a metal alloy and its environment (Jones, 1992). Each year the economic losses attributable to corrosion amount to billions of dollars. Considerable research is performed to provide a better understanding of the mechanisms of corrosion. The findings from these studies can be used to reduce the impact of corrosion.

The first section illustrates the significance of corrosion in oil and natural gas production. The background and purpose of this research are discussed in the following sections.

1.1 Significance of Corrosion

Oil and natural gas producers are among those affected severely by corrosion. Pipes that bring the oil and/or gas to the surface of the earth are subject to CO_2 corrosion, and must either be replaced or abandoned when they are severely damaged. In most oil and gas wells, CO_2 occurs naturally, and in certain wells it is also added to enhance oil recovery. In addition, water vapor present in the formation condenses as rises because of the drop in pressure and temperature. The gaseous CO_2 dissolves in water to form carbonic acid which is corrosive (Newton, 1984). In this environment, destructive

chemical reactions occur at the pipe wall causing corrosion and potential destruction of the tubing.

Pipeline corrosion has a significant influence on petroleum production costs. Additional expenditures to combat pipeline corrosion include identification of the well sections where the tubes have to be replaced and the actual tube replacement costs. Further, lost revenues occurs due to shutdown for tube replacement and product losses due to leaks from corroded tubes.

Corrosion studies and research are aimed at reducing the financial losses. Maintenance averages 14% of the cost of products sold in many industries including the oil and gas industry. The ability to predict the corrosiveness of a well would be valuable to the corrosion engineer to schedule pipeline maintenance and repair work. The timely detection and replacement of tubes prevent product losses and also avoid unnecessary maintenance shutdowns.

1.2 Background

The economic impact of corrosion in downhole systems has resulted in the need for a better understanding of the corrosion process. There are many factors that influence the corrosion process, and to assimilate them in one study is a challenge. In modeling downhole corrosion, the factors to be studied include phase equilibrium, electrolyte equilibrium, hydrodynamics, mass transfer, and reaction kinetics. Studies have been undertaken to determine the effect of these factors on the corrosion process. However, very little work has been done to develop an overall model that integrates all the above factors.

A deterministic model to predict corrosion in downhole systems has been developed by the Downhole Corrosion Consortium at Oklahoma State University. The consortium work is one of the few studies that consider all of the above mentioned factors. The modeling approach began initially by simplifying the overall problem through assumptions involving the behavior of the well. Over the years, specific areas like flow regimes, pressure drop, and electrolyte equilibrium have been targeted to improve the models and to eliminate the more unreasonable assumptions. DREAM is the software tool developed at Oklahoma State University that implements the overall corrosion model. It has been developed using FORTRAN and Visual C++. This software is continually updated to reflect any modifications that occur in the model.

Understanding the mass transfer mechanism is very important in modeling the downhole system accurately. Chapter II discusses, in detail, the mass transfer model used and Chapter III discusses the modifications made in handling the mass transfer model.

1.3 Purpose of this work

The objective of this research is to obtain a better understanding of the fundamental physical phenomena influencing downhole corrosion to improve the accuracy of the corrosion model. Corrosion can be classified as uniform or localized. During the corrosion process there is also the possibility of a product film being formed on the pipe wall. This film may act as a protective coating reducing further corrosion. This study concentrates on modeling the mass transfer process at the wall to improve the accuracy of prediction of uniform corrosion rates without corrosion product film formation.

A finite difference numerical approach is used to solve the laminar layer mass transfer model equations. The numerical method used in the previous version of DREAM failed to correctly solve the mass transfer model. Parametric studies have been conducted to obtain a better understanding of corrosion process and the influence of various factors - temperature, pressure, CO_2 concentration, and diffusion layer thickness - on the corrosion rate.

CHAPTER II

REVIEW OF THE LITERATURE AND PREVIOUS WORK

This chapter gives an overview of previous work that has been undertaken in studying and modeling corrosion in downhole systems. Section 2.1 gives a brief summary of the corrosion prediction models that have been developed. Section 2.2 gives the details of previous models developed at Oklahoma State University. Aspects of the overall model, and the assumptions involved, are discussed briefly in the next section. Section 2.4 describes, in detail, the mass transfer model. In the last section the need for this work is illustrated by describing the shortcomings of the previous work.

2.1 Downhole Corrosion Models

The economic importance of CO_2 corrosion in downhole environments has led to a proliferation of corrosion prediction models. The ability to predict corrosion rates is particularly useful in scheduling maintenance of downhole tubulars. Some of these models are described briefly.

2.1.1 de Waard and Coworkers (1975-1995)

In the work of de Waard and Milliams (1975), the influence of partial pressure of CO_2 on the corrosion rate of steel in carbonic acid was studied. Weight loss and

polarization resistance measurements were made, and a relation between corrosion rate and CO_2 partial pressure was determined. For grit-blasted steel the relation between the corrosion rate and CO_2 partial pressure is

$$\log v = 7.96 - \left(\frac{2.32 * 10^3}{t + 273} \right) - 5.55 * 10^{-3} t + 0.67 \log p_{CO_2} \qquad (2.1)$$

where v is the corrosion rate in mm/yr, t is the temperature in Celsius, and p_{CO2} is the CO_2 partial pressure in bars. A mechanism was proposed for the cathodic reaction, which quantitatively explains the relation obtained. The influences of temperature and surface preparation on the corrosion rate at constant pH were also studied.

In 1991, de Waard, Lotz and Milliams proposed a model, which systematically modified the de Waard and Milliams work to obtain a more conservative estimate of CO_2 corrosion rates. The de Waard-Milliams relation (Equation (2.1)), was able to predict the "worst case" corrosion rates. Further, it was valid only for a certain temperature range and was based on the assumption that the water is saturated with corrosion product. In the de Waard Lotz and Milliams model, correction factors were estimated which quantified the effect of different physical and chemical effects that were not accounted for in the de Waard-Milliams (1975) model. The effect of dissolved Fe^{2+}, film formation, increasing temperature, presence of a liquid hydrocarbon phase, and glycol injection were some of the effects that have been included in the de Waard, Lotz and Milliams model.

In 1993, de Waard and Lotz reviewed previous models and suggested modifications to make the models more comprehensive and accurate. The effects of protective corrosion product layers, high flow rates, pH changes due to dissolved corrosion products, glycol additions and localized corrosion were studied. Correction factors were proposed for the de Waard and Milliams equation, to include these effects

and to improve the accuracy of corrosion rate predictions. Computer-based spreadsheets were used to calculate the influence of these parameters on corrosion prediction.

2.1.2 University of Southwestern Louisiana (1996)

A model has been developed which is comprised of correlations for predicting life of tubing strings in gas condensate wells containing CO_2. The data for developing the correlations were obtained from 12 sweet gas condensate wells in the Gulf of Mexico. The correlations predict that the minimum tubing life for a mass-transfer controlled annular-flow well containing CO_2 is 14 months. Based on the correlations, a computer implementation of the model was developed, which presents results in both graphical and tabulated formats (Perkins and Garber, 1996).

2.1.3 Ohio University (1994-1999)

The effects of wall shear stress, CO_2 partial pressure, flow velocity, and oil/water composition on corrosion rates in multiphase slug systems in horizontal pipelines were modeled. The modeling was based on experiments conducted on carbon steel for a range of temperatures, pressures, and water cut. The model showed that temperature, CO_2 partial pressure, pressure gradient across slug, and water cut have a significant effect on the corrosion rate (Jepson and Kanwar, 1994).

A mechanistic model of CO_2 corrosion in multiphase flow conditions has also been developed. The electrochemistry, reaction kinetics, and mass transfer effects were taken into account, and the model predictions were found to be in good agreement with experimental results (Zhang et al., 1997).

2.1.4 Kvarekval (1997)

Kvarekval developed a mathematical model that treats the conditions in the diffusion layer close to the corroding steel surface. The simultaneous diffusion and homogeneous chemical reactions involving the dissolved species in the CO_2-H_2O system were considered. The model uses kinetic data for the CO_2-H_2O reactions and attempts to simulate the corrosion mechanism in the diffusion layer close to the pipe wall.

The diffusion and chemical reaction models, make up the overall model of Kvarekval. The temperature, total pressure, mole fraction of CO_2 in the gas phase, pH, mean flow velocity and pipe diameter are used to calculate the partial pressures, diffusion coefficients, rate constants, bulk concentrations and other fluid properties. These parameters are then passed to the diffusion model which estimates the concentration profiles of different species in the diffusion layer due to one-dimensional diffusion. The model assumes that the ionic migration contribution is negligible. The results from the diffusion model are then passed to the chemical reaction model. The chemical reaction model assumes complete reduction of the protons and carbonic acid transported to the metal surface. The concentration profiles obtained from the chemical reaction model are then passed back as inputs to the diffusion model. This procedure is carried out until the desired convergence is achieved. The iterative model has been solved using Excel 5.0.

The corrosion current, i_{corr}, is defined as the flux of H^+ ions and H_2CO_3 in the Nernst layer and is given by the following expression

$$i_{corr} = F\left(D_{H^+} \frac{\left\{\left(c_{H^+}\right)_1 - \left(c_{H^+}\right)_0\right\}}{\delta_N} + D_{H_2CO_3} \frac{\left\{\left(c_{H_2CO_3}\right)_1 - \left(c_{H_2CO_3}\right)_0\right\}}{\delta_N} \right) \qquad (2.2)$$

where subscripts $_0$ and $_1$ represent the metal surface and inner boundary of the Nernst layer respectively, and δ_N (cm) is the thickness of the Nernst layer. The corrosion rate, v_{corr} (mm/yr), is obtained from the corrosion current, i_{corr} (Amp/cm^2), using the following expression

$$v_{corr} = 11550\left(\frac{\text{mm cm}^2}{\text{yr Amp}}\right) * i_{corr}\left(\frac{\text{Amp}}{\text{cm}^2}\right) \tag{2.3}$$

The model demonstrates that incorporating the reaction kinetics in the mathematical modeling of corrosion gives meaningful results. The model, when tested against published cases, yielded plausible worst case corrosion rates in 80% of the test cases (Treseder, 1998).

2.2 Corrosion Prediction Models at OSU

Research on downhole corrosion started at Oklahoma State University in 1986. A number of models have been developed, each with their own advantages and limitations. These models are constantly updated and modified in an effort to improve their accuracy in predicting corrosion rates; well pressures and temperatures; and phase and electrolyte equilibrium calculations. This section details some of these models developed prior to this work.

2.2.1 Robertson (1988)

This work resulted in a computer program that identified the location in the well where corrosion would be expected. For corrosion to occur, liquid water must be present

and the computer program, DOWN*HOLE Production String Simulation Package, was designed to identify the water condensation zone in the string.

To determine the water condensation zone the fluid phase behavior and flow characteristics must be estimated. For this purpose the entire well has been divided into 500-foot sections, which are then treated as a series of flash drums. Phase equilibrium calculations are then performed for each flash drum using GPA*SIM, an industrially tested thermodynamic simulator developed by John Erbar at Oklahoma State University (Robertson, 1988). To calculate the pressure drop and fluid properties, models from related research work have been incorporated as subroutines into this package. In certain wells the hydrocarbons condense along with the water. In this package additional subroutines that predict the water/oil ratios in wells are included (Robertson, 1988).

2.2.2 Liu and Erbar (1990)

The Liu and Erbar model predicted uniform corrosion rates in downhole systems by incorporating the fundamental concepts of thermodynamic phase equilibrium, mass transfer, and surface reaction kinetics. The model considers the hydrogen ion in the downhole system to be the key corrosive species. The DOWN*HOLE program, designed by Robertson (1988), was used to identify the water condensation zone. The model calculates the equilibrium concentration of the hydrogen ion at the interface of the gas core and the liquid condensate. These were then used along with mass transfer coefficients and reaction rate constants from literature data to evaluate the corrosion rates in a section. These steps are then repeated for other sections to generate the corrosion rate profile along the well depth. In certain wells the corrosion product, iron carbonate,

precipitates and forms a layer on the pipe wall. This layer may act as a protective barrier by decreasing the rate at which the hydrogen ions diffuse to the wall iron. However, the Liu and Erbar model did not account for the possibility of corrosion product film formation (Sundaram, 1996).

2.2.3 Liu (1991)

The Liu model, which includes the corrosion product film formation, is a further extension of the Liu and Erbar (1990) model. Here the downhole system is modeled as an annular two-phase system. The liquid layer is divided into a turbulent layer, a laminar layer and a corrosion product layer (if formed). The mass transfer calculations are performed individually for these layers. The electrolyte equilibrium calculations are modified based on the reactions proposed in this work. Slug flow regions, if any, are handled based on the assumption that the film formed can be modeled as annular flow (Sundaram, 1996; Liu, 1991).

2.2.4 Achour (1993)

An attempt was made in this work to understand the concepts underlying pitting corrosion in downhole systems. Pitting corrosion analysis is very useful for failure analysis of downhole tubing. A theoretical model for flow induced CO_2 pitting corrosion was developed. The model predicts the extent of propagation of an existing pit under turbulent conditions since pitting corrosion is most likely within this layer. However, the pit initiation is not included due to its highly random behavior. The model is not

currently implemented in the DREAM software developed as a part of the Downhole Corrosion Consortium Project at OSU (Archour et al., 1993).

2.2.5 Liu and High (1993)

A simulation model, named DREAM, was developed by incorporating the modifications of Liu (1991) into DOWN*HOLE. The modifications included restructuring the GPA*SIM code used in thermodynamic calculations and updating the pressure drop models using better correlations for slug and bubble flow modeling. Further, the numerical method used to solve for the mass transfer equations in the diffusion layer was altered. Localized corrosion rate calculations have also been added which give an approximate estimate of the time required for corrosion product film failure, the pit propagation rate, and the corrosion rate (Liu, 1993).

2.2.6 Raman (1996)

Several pressure drop models were studied for annular and slug flow regimes in upward, vertical, two-phase flow. Pressure drop is a function of the liquid holdup, the flow velocity, the direction of flow, and the flow regime. To identify the flow regime the Barnea (1987) flow map was used. Comparing the flow map predictions with experimental data of Golan (1970) validated the use of the Barnea (1987) flow map. The map was then used to identify the flow regimes in 140 well cases that were obtained from the work of Camacho (1970) and Reinicke et al. (1987). The pressure drop predictions from the Ansari et al. (1994) and Sylvester (1987) slug flow models were compared against the wells with slug flow. In the wells with annular flow regime, the Ansari et al.

(1994) model was compared against the Yao and Sylvester (1987) model predictions. Based on the comparisons, the Sylvester (1987) model that had been used in DREAM was replaced by the Ansari et al. (1994) model for the slug-flow regime. In the annular flow regime the Yao and Sylvester (1987) model was retained as it performed better than the Ansari et al. (1994) model.

The impact of the modifications made to the pressure drop correlations on the corrosion rate was also investigated. Three sample cases were employed, and it was observed that the pressure drop models did not have a significant impact on the corrosion rate predictions. Coding errors were also identified in the previous version of DREAM. These were corrected to make the software package more robust and accurate.

2.2.7 Sundaram (1996)

This work focussed on improving the phase and electrolyte equilibrium models used in DREAM. Phase and electrolyte equilibrium calculations are performed to estimate the quantities of the liquid and vapor phases and the compositions of species present at the gas-liquid interface. The electrolytes that are of significance for the corrosion process are CO_2 and H_2S and their dissociation products. In the earlier Liu and High (1993) model, the phase equilibrium calculations were performed to estimate the species concentrations on the liquid side. These were then used for the electrolyte equilibrium calculations to determine the ionic species concentration. However, the species disassociation reactions have an influence on the phase equilibrium. In Sundaram's work the effect of liquid phase dissociation of electrolytes on the phase equilibrium has been studied and modeled. In this model the phase and electrolyte

equilibrium calculations are coupled. This has been done by integrating the extent of dissociation of the electrolytes with the equilibrium K values (Sundaram, 1996).

The generalized framework for phase and electrolyte equilibrium model has been developed using a combination of molecular and empirical models. The dissociation constants for species, K_i, were evaluated using the following correlation

$$\ln K_i = \frac{B_{i,1}}{T} + B_{i,2} \ln T + B_{i,3} T + B_{i,4} \tag{2.4}$$

where $B_{i,j}$ are constants which were obtained from the work of Edwards (1978) and Kawazuishi and Prausnitz (1987). The framework uses the Chen et al. (1994) model to estimate the single molecular interaction parameters, which are then used in the Soave-Redlich-Kwong equation of state to model the phase equilibrium. The Chen et al. (1994) correlations for the single molecular interaction parameters, C_{ij}, of CO_2-H_2O and H_2S-H_2O binary systems are given below

$$C_{ij,CO_2} = 0.457 - \frac{131}{T} \tag{2.5}$$

$$C_{ij,H_2S} = 0.432 - \frac{104}{T} \tag{2.6}$$

The accuracy of the bubble point pressure predictions using Chen et al. (1994) model was compared against the performance of the Liu and High (1994) model. The data for the CO_2-H_2O system were obtained from the work of Stewart and Munjal (1970), Takenouchi and Kennedy (1964), Wiebe and Gaddy (1939), Zawisza and Malesinka (1981), Gillespie et al. (1986), and Muller et al. (1988). Data points from Selleck et al. (1952), Gillespie and Wilson (1980), Clarke and Glew (1971), Wright and Maass (1932) and Lee and Mather (1977) were used for the H_2S-H_2O system. A statistical analysis was

performed and it was found that the average absolute percentage difference in the predictions were significantly lower for both the binary systems when the Chen et al. (1994) model was used. The Chen et al. (1994) model was then incorporated in the next version of DREAM, Version 3.3. The impact of modifying the phase and electrolyte models on the corrosion rate predictions was investigated. The modifications did not significantly affect the corrosion rate predictions.

2.2.8 Dugan (1998)

The work of Dugan focused on the mass transfer model in the laminar layer. The modeling of the mass transfer in the laminar layer is critical to the accurate prediction of corrosion rate. Two methods have been employed to account for the reactions at the pipe wall. The de Waard and Milliams (1975) empirical flux expressions for CO_2 and H_2S, illustrated later in Section 2.5 (Equations (2.46) - (2.50)), were used in the first method to calculate the Fe^{2+} reactive flux at the wall. The second method used the Bockris and Reddy (1970) current density expression to account for the reactions at the wall.

$$i_a = i_{ao} \exp\left(\alpha_a F \eta_a / RT\right) \tag{2.7}$$

where i_a is the anodic current density, i_{ao} is the anodic exchange current density, η_a is the anodic overpotential and α_a is the anodic transfer coefficient (Dugan, 1998). The current density was then used to evaluate the reactive flux at the wall. It was also observed that the numerical method previously used (Liu, 1991) to solve the laminar layer model did not provide an accurate solution. Therefore, another numerical method based on fifth-order Runge-Kutta shooting method and Newton Raphson convergence method (Press et

al., 1997) was used to solve the proposed laminar layer model. The current density model was found to be more accurate than the de Waard and Milliams (1975) model in predicting corrosion rates for the downhole systems. The current density model was capable of predicting not only when a high corrosion rate is probable, but also when a low corrosion rate would occur. The proposed model was found to predict the maximum corrosion rates within 10% of those obtained from field data (Dugan, 1997). However, this work has not been incorporated into DREAM.

2.3 Overall Corrosion Prediction Model

The different aspects of the mechanistic models that form the basis for downhole corrosion modeling at OSU are illustrated in this section. In downhole wells, natural gas, with or without formation water, flows up the pipe to the wellhead. The temperature and pressure at the bottom of the well are usually very high and depend on the depth of the well. As the gas flows up the tubing string, there is a pressure drop accompanied with a reduction in the temperature. This reduction in temperature may cause water to condense from the vapor phase. In some wells, hydrocarbons may also condense. In this model, the presence of liquid water in contact with the wall is considered essential for corrosion to occur. This is because the condensed or formation water is the electrolytic medium in the electrochemical corrosion process.

Understanding the hydrodynamic flow patterns in upward, multiphase flow is critical for pressure drop calculations. From the above discussion it is clear that there is more than one phase in the downhole system. These are the uncondensed gas phase and the condensed liquid phase or phases. The multi-phase mixture can flow through the pipe

in a variety of patterns and further complicate the modeling process. Some of the most commonly encountered flow regimes in upward vertical multiphase flow in downhole systems include slug flow, churn flow and annular flow. In slug flow, there exists bullet shaped gas bubbles that are termed 'Taylor bubbles'. The condensed liquid is the continuous phase, and the Taylor bubbles are large with diameters approximately equal to that of the pipe and separated from each other by liquid slugs. The transition from slug to annular flow is classified as the churn flow regime (Chisholm, 1983). Due to its complexity, churn flow has been modeled as being part of the slug flow regime in Section 2.2. In annular flow, the liquid phase exists as a thin layer around the central gas core. Flow is characterized by very high gas flow rates when compared to the liquid flow rates. The gas phase exerts a shear stress on the liquid film that results in large amplitude waves at the gas liquid interface. This, in turn, results in some of the liquid being entrained as droplets in the gas core (Robertson, 1988).

Apart from the relative flow rates of the two phases the flow pattern also depends on the pipe size and fluid properties (Raman, 1996). Flow pattern maps developed by Taitel et al. (1980) and later modified by Barnea (1987) are used to identify the flow regimes in the different sections of the tubing string.

2.3.1 Phase and Electrolyte Equilibrium

The presence of two phases and the electrochemical nature of the system necessitate phase and electrolyte equilibrium predictions. The corrosive gases, CO_2 and H_2S, dissolve in the condensed water, and phase equilibrium dictates the amount of

species in the two phases. The equilibrium relations that are to be considered in this respect are given below

$$H_2O_{(g)} \leftrightarrow H_2O_{(l)} \tag{2.8}$$

$$CO_{2(g)} \leftrightarrow CO_{2(l)} \tag{2.9}$$

$$H_2S_{(g)} \leftrightarrow H_2S_{(l)} \tag{2.10}$$

In the liquid phase, the following reactions take place

$$H_2O + CO_2 \leftrightarrow H_2CO_3 \tag{2.11}$$

$$H_2CO_3 \leftrightarrow HCO_3^- + H^+ \tag{2.12}$$

$$HCO_3^- \leftrightarrow CO_3^{2-} + H^+ \tag{2.13}$$

$$H_2O \leftrightarrow OH^- + H^+ \tag{2.14}$$

$$H_2S \leftrightarrow HS^- + H^+ \tag{2.15}$$

$$HS^- \leftrightarrow S^{2-} + H^+ \tag{2.16}$$

Other reactions that have to be considered in cases where species saturation, which may result in film formation, becomes significant are listed below.

$$(FeCO_3)_s \leftrightarrow Fe^{2+} + CO_3^{2-} \tag{2.17}$$

$$(CaCO_3)_s \leftrightarrow Ca^{2+} + CO_3^{2-} \tag{2.18}$$

$$(FeS)_s \leftrightarrow Fe^{2+} + S^{2-} \tag{2.19}$$

The reactions given by Equations (2.8) - (2.19) have an influence on the thermodynamic phase equilibrium. The Chen et al. (1994) model outlines an approach that couples the phase and electrolyte equilibrium calculations. The model updates the vapor-liquid equilibrium constants based on the liquid phase dissociation of the

molecular species. The Soave-Redlich-Kwong equation of state is used for modeling the phase equilibrium (Sundaram, 1996). The details of the equations involved and the numerical approach used to solve these equations are provided in the thesis work of Sundaram (1996).

2.3.2 Pressure Drop

A number of correlations are available in literature to evaluate pressure drop in different flow regimes in upward, vertical, two-phase flow. Some of these models have been studied and their predictions have been compared against data sets from Camacho (1970) and Reinicke et al. (1987). Based on the evaluations made, the most accurate correlations have been incorporated into the DREAM software.

The Yao and Sylvester (1987) model and Ansari et al. (1994) model are used in DREAM to predict pressure drop in downhole systems. The Yao and Sylvester (1987) model was found to accurately predict the pressure drop in annular flow regimes. It takes into consideration the effect of the liquid droplets entrained in the gas core. In the slug flow regime, the Ansari et al. (1994) model was evaluated to be superior to the Sylvester (1987) model. The evaluation and description of these pressure drop models are provided by Raman (1996).

2.4 Mass Transfer Model

The mass transfer model and the fundamental equations are discussed in this section. Modeling the mass transfer of the different species present in the downhole system is critical in determining the corrosion rate profiles. This involves determining

the amount of reactive species present at the wall. A four-layer model has been developed for the mass transfer process. The primary focus is on the laminar section of this four-layer model. However a thorough understanding of the entire mass transfer model is important.

The annular flow regime forms the basis for the model. The two-phase flow regimes most commonly encountered in gas wells are annular and slug flow. In the DREAM model the thickness of the liquid layer between the Taylor bubble and the pipe wall is assumed to be the annular film thickness (Liu, 1991). This assumption is made due to the complexity in handling mass transfer in slug flow regimes.

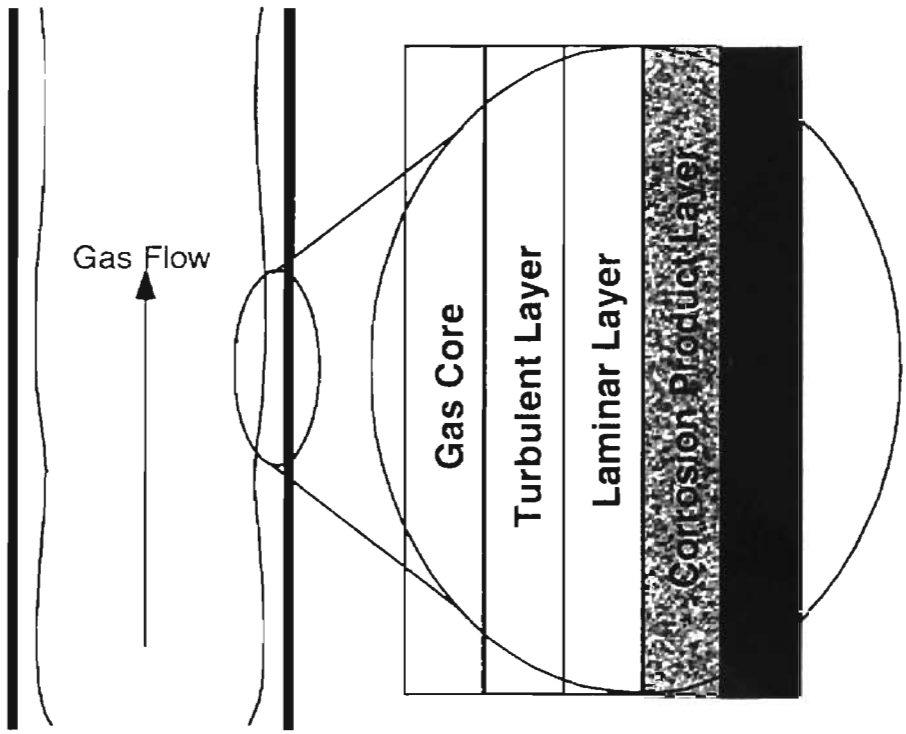

Figure 1. Schematic representation of the Mass Transfer Model

As discussed in Section 2.3, a thin liquid layer wetting the surface of the pipe characterizes annular flow. The gas flows along the center section of the pipe. This

forms the first layer in the four-layer model, which is schematically described in Figure 1. The annular liquid region is further divided into a turbulent and a laminar sublayer. If a corrosion product film is formed on the wall surface then it is modeled as the fourth layer. The modeling of these layers is discussed below.

2.4.1 Gas-Liquid Interface

In Section 2.3.1, the reactions that occur at the interface of the gas core and the annular liquid are identified. The phase and electrolyte equilibria calculations are used to estimate the concentration of different ionic species on the liquid side of the interface.

To model the mass transfer across the gas-liquid interface, certain assumptions have been made. Thermodynamic equilibrium is assumed across the gas-liquid interface. Further, the liquid phase ionic dissociation reactions are assumed to occur so rapidly that they reach equilibrium immediately in the liquid side of the interface.

2.4.2 Turbulent Layer

Liu (1991) modeled the turbulent layer mass transfer in the two-phase annular downhole system. The model considers the effect of interfacial shear stress and wall roughness. Sand type correlations are assumed due to the unavailability of a more accurate corrosion wall roughness correlation. The model estimates the turbulent mass transfer coefficients based on these assumptions. The species concentrations at the gas-liquid interface are already available from the phase and electrolyte equilibria calculations mentioned above. These, along with other species properties, such as

diffusivities, are then used to determine the concentrations at the other boundary of the turbulent layer, namely the turbulent-laminar interface (Figure 1).

2.4.3 Laminar Layer

In this section, the fundamental equations involved in modeling the laminar layer are explained in detail. "The number of moles passing per unit time through a unit area oriented perpendicular to the velocity is referred to as flux density" (Newman, 1991). There are three different factors - migration, diffusion and convection - which can contribute to the movement of an ionic species. The contributions of these is

$$N_i = -z_i u_i F c_i \nabla\Phi - D_i \nabla c_i + c_i v \qquad (2.20)$$

where c_i is the concentration of i^{th} ionic species in moles/dm^3, u_i is the ionic mobility, z_i is the species ionic charge (dimensionless), D_i is the ionic diffusion coefficient in dm^2/s, Φ is the electric potential in Volts, v is the bulk fluid velocity in dm/s, and F is the Faraday's constant in C/mole.

The entire pipe is divided into 500-foot sections. The annular liquid layer is very thin when compared to the pipe diameter. Hence the system can be modeled as a two dimensional problem using a rectangular coordinate system instead of the cylindrical coordinate system. The variations along the z-axis, which is in the upward direction of flow, in any particular section are neglected.

The focus of the modeling effort is on the concentration variations in the radial direction, which is now represented by the y-axis, in the annular layer. In this system the third term in the right hand side of Equation (2.20), which is the contribution due to

convection, is neglected because we assume that the bulk velocity in the radial direction is negligible. This reduces the above equation to the following form

$$N_i = -z_i u_i F c_i \frac{\partial \Phi}{\partial y} - D_i \frac{\partial c_i}{\partial y} \tag{2.21}$$

The equation of continuity is given by the following relation

$$\frac{\partial c_i}{\partial t} = -\nabla \cdot N_i + R_i \tag{2.22}$$

The corrosion rate in any particular 500-foot section of the downhole system is assumed to be constant with respect to time. Assuming steady state, the term on the left-hand side of Equation (2.22) can be eliminated.

The term R_i is the generation term that accounts for the production or consumption of any species within the system, namely the laminar layer. This term is also neglected, because the reactions are assumed to occur either at the core gas-turbulent liquid interface or at the pipe wall. Since no reaction occurs within the diffusion layer this term becomes zero. These assumptions reduce Equation (2.22) to

$$\nabla \cdot N_i = 0 \tag{2.23}$$

Further, the previous assumption that only the y-axis variations are significant results in

$$\frac{\partial N_i}{\partial y} = 0 \tag{2.24}$$

Substituting the expression for N_i from Equation (2.21) into (2.24) results in the following governing differential equation

$$D_i \frac{\partial^2 (c_i)}{\partial y^2} + z_i u_i F \frac{\partial (c_i \Phi')}{\partial y} = 0 \tag{2.25}$$

The above expression, when written for each species, forms the set of governing equations for the downhole system. The product, $c_i\Phi'$, makes these equations non-linear. The equations are also coupled through the electric potential. These would hence form a set of coupled, nonlinear, ordinary differential equations.

It is also assumed that the inorganic ions present in the formation water do not take part in the corrosion reactions. However their contribution to the electroneutrality of the solution is taken into account by using the following equation

$$\sum z_i c_i = 0 \tag{2.26}$$

Boundary conditions are needed to solve this set of equations. The turbulent layer-laminar layer interface forms one of the boundaries of the laminar layer. This is henceforth be referred to as the left boundary. The pipe wall where the corrosion reactions take place forms the right boundary of the laminar layer.

The species concentrations at the left boundary of the laminar layer are known from the solution of the turbulent layer mass transfer calculations. Hence the left boundary conditions are given by :

$$c_i = c_{i,t} \tag{2.27}$$

Additionally the electric potential, Φ, is set to zero at this boundary as shown below

$$\Phi = 0 \tag{2.28}$$

The pipe wall, which forms the right boundary, is where the corrosion reactions take place. The dissolution reaction of iron is given by

$$Fe + 2H^+ \leftrightarrow Fe^{2+} + H_{2(g)} \tag{2.29}$$

The species Fe^{2+} and H^{+} are considered to be the only species that react at the wall. The flux of these reactive species at the wall would be equal to the reactive flux based on the above reaction. For other species the flux would be zero since they are non-reactive species and also cannot diffuse through the wall. This forms the basis for the formulation of boundary conditions at right boundary of the laminar layer. The relation is

$$D_{mol}\frac{dC_i}{dy}+z_i u_i F C_i \frac{d\Phi}{dy} \quad = \quad J_r \,, \tag{2.30}$$

where J_r represents the reactive flux, which would be zero for non-reactive species. The evaluation of J_r for reactive species is discussed in Section 2.5 and again in Chapter III. Apart from the above boundary conditions the assumption of electroneutrality, given by Equation (2.26), is also applied to the right boundary. Recall that the electroneutrality assumption is also applied at the interior grid points, but the zero electric potential, given by Equation (2.28), replaces the electroneutrality condition at the leftmost grid point.

The total annular film thickness, δ, is obtained from the Henstock and Hanratty (1976) correlation shown below.

$$\frac{\delta}{D_i}=\frac{6.59F_o}{(1+1400F)^{1/2}} \tag{2.31}$$

$$F_o=\frac{\gamma(\mathrm{Re}_{LF})}{\mathrm{Re}_G^{0.90}}\frac{\nu_L}{\nu_G}\sqrt{\frac{\rho_L}{\rho_G}} \tag{2.32}$$

$$\gamma=\left[\left(0.707\,\mathrm{Re}_{LF}^{0.5}\right)^{2.5} \quad + \quad \left(0.0379\,\mathrm{Re}_{LF}^{0.9}\right)^{2.5}\right]^{0.40} \quad , \tag{2.33}$$

where F_o is a dimensionless group containing flow rates and fluid properties, Re_{LF} is the Reynolds number of the liquid flowing in the wall layer, Re_G is the gas Reynolds number

calculated as if the gas filled the whole tube, D_t is the hydraulic diameter of the pipe, and ρ and ν represent the density and kinematic viscosity of the respective fluids.

The following empirical relation relates the diffusion layer thickness, δ_0, to the thickness of the annular film, δ (Levich, 1962).

$$\delta_o \approx \frac{\delta}{Sc^{1/3}} \tag{2.34}$$

$$Sc = \frac{\nu}{D} = \frac{\mu}{D\rho} \quad . \tag{2.35}$$

where D is the diffusivity, μ is the viscosity, ρ the density and Sc represents the Schmidt number.

The numerical method previously used to solve this system of equations is explained in Section 2.5. Chapter III discusses the new approach used for modeling the laminar layer along with the details of the numerical scheme employed.

2.4.4 Corrosion Product Layer

The corrosion product, iron carbonate, sometimes precipitates and forms a protective layer on the pipe wall. The Liu (1991) model handled this layer simply as another diffusion layer. However the Liu and High (1993) model has a different approach. The diffusion coefficients of the different species in the iron carbonate layer would be different from those in the laminar layer. These coefficients are estimated from the following expressions (Liu and High, 1993) which are correlated from the temperature dependence studies of Choi et al. (1989), Ikeda et al. (1984), and Hausler (1984).

$$D_{eff} = D_i/2.0 \qquad t < 60^\circ C \tag{2.36}$$

$$D_{eff} = D_i/2.5 \qquad 60^\circ C \le t < 75^\circ C \tag{2.37}$$

$$D_{eff} = 159.9\exp(0.017815t)D_i/2.5 \qquad 75^\circ C \le t < 150^\circ C \tag{2.38}$$

$$D_{eff} = D_i/1000 \qquad 150^\circ C \le t \tag{2.39}$$

Using effective diffusivities the corrosion rate at the wall is calculated based on the assumption that the corrosion process is diffusion limited in the corrosion product layer. The expression used to calculate the corrosion flux J_D, is given by

$$J_D = D_{eff}\, C_{if}/\delta_f \tag{2.40}$$

where C_{if} is the species concentration at the interface of the laminar liquid layer and the corrosion product film, and δ_f is the thickness of the corrosion product layer and is assumed to be 30 μm (Palacios and Shadley, 1991).

2.5 Previous Numerical Solution Technique

The numerical method that had been used in the previous version of DREAM, version 3.0, for solving for the laminar layer is explained in this section. This method was found to contain certain shortcomings and these are identified here.

The model eliminated the potential term from the set of equations by using the zero net current condition given below

$$\sum z_i N_i = 0 = -\sum D_i z_i \frac{\partial c_i}{\partial y} - \sum z_i^2 u_i F c_i \frac{\partial \Phi}{\partial y} \tag{2.41}$$

This on rearrangement gives

$$\frac{\partial \Phi}{\partial y} = -\frac{RT}{F}\frac{\sum D_i z_i \frac{\partial c_i}{\partial y}}{\sum z_i^2 D_i c_i} \tag{2.42}$$

This expression for Φ' is then substituted in Equation (2.25) to eliminate Φ (Sundaram et al., 1996) resulting in

$$D_i \frac{\partial^2 (c_i)}{\partial y^2} - z_i \frac{d}{\partial y}\left(c_i \frac{\sum D_i z_i \frac{\partial c_i}{\partial y}}{\sum z_i^2 D_i c_i} \right) = 0 \tag{2.43}$$

The summations were expanded and dimensionless length variable X was introduced to rewrite the above governing equation as follows

$$\frac{d^2 c_i}{dX^2} + S_c = 0 \tag{2.44}$$

where $X = \frac{y}{\delta_D}$, δ_D is the laminar layer thickness and S_c is the non linear source term given by

$$S_c = -z_i \left(\frac{dc_i}{dX} \frac{\sum_j z_j D_j \frac{dc_j}{dX}}{\sum_j z_j^2 D_j c_j} + c_i \left(\frac{(\sum_j z_j D_j \frac{d^2 c_j}{dX^2})(\sum_j z_j^2 D_j c_j) - (\sum_j z_j D_j \frac{dc_j}{dX})(\sum_j z_j^2 D_j \frac{dc_j}{dX})}{(\sum_j z_j^2 D_j c_j)^2} \right) \right) \tag{2.45}$$

To solve this set of governing equations defined by Equations (2.44) and (2.45), along with the boundary conditions given by Equation (2.27) and (2.30), a discretization method was used. The nonlinearity of the equations necessitated the use of an iterative

procedure. The nature of the equation was found to be similar to a one dimensional heat conduction problem. Patankar (1980) had solved the heat transfer problems and Liu (1993) adopted this approach to solve these mass transfer equations.

In the previous method the species CO_2, H_2S, Fe^{2+}, HS^- and HCO_3^- were all considered having a reactive flux at the wall. For the reactive fluxes, J_r, which appear in the right boundary condition shown in Equation (2.30), the following expressions based on the experimental data of de Waard and Milliams (1975) were used for species CO_2 and H_2S.

$$J_{r,CO_2} = -52.5 \exp\left(\frac{-5385}{T}\right) a_{CO_2} \tag{2.46}$$

$$J_{r,H_2S} = -9.8 10^6 \exp\left(\frac{-9261}{T}\right) a_{H_2S} \tag{2.47}$$

The expressions for other reactive species were related to the above fluxes in the following manner

$$J_{r,Fe^{2+}} = 2 * (J_{r,CO_2} + J_{r,H_2S}) \tag{2.48}$$

$$J_{r,HCO_3^-} = J_{r,CO_2} \tag{2.49}$$

$$J_{r,HS^-} = J_{r,H_2S} \tag{2.50}$$

However the numerical method used by Liu (1993) was found to be incorrect as it always predicted corrosion rates of zero MPY. It became evident that the subroutines, which handled the differential equation solver, contained an error. The solver assigned the known concentrations of species at the left boundary to all the grid points in the discretization procedure. However it failed to solve the governing equation and update these values thereafter. This resulted in the concentration gradient of all the species

including that of the ferrous ion, Fe^{2+}, to be zero. This incorrect solution when used to calculate the corrosion rate at the wall resulted in corrosion rates of zero MPY.

The code was carefully studied with an aim to correct it. However lack of proper code documentation made it impossible to achieve this. It was then decided to use a different approach to solve these differential equations. The new approach is explained in the next chapter.

CHAPTER III

MODEL DEVELOPMENT

The mass transfer model for the laminar sublayer and the numerical scheme used to solve the model equations are illustrated in this chapter. The new approach used to model the corrosion kinetics at the pipe wall is also explained. A numerical scheme different from the previous method has been used. The first section describes the system of equations that constitute the laminar layer mass transfer model. Some of the different numerical methods that have been used in an attempt to solve the system of differential equations are discussed in the next section. One of these methods, namely the BAND(J) method, was found to be a suitable and efficient way to solve the mass transfer model. The numerical scheme used to solve the mass transfer model by making use of the BAND(J) method is explained in detail in the last section.

3.1 System of Equations

A system of differential equations has been developed that models the mass transfer process in the laminar sublayer as a boundary value problem. The basic equations that constitute the laminar layer mass transfer model are summarized in this section.

The expression for the flux density of an ionic species

$$N_i = -z_i u_i F c_i \nabla\Phi - D_i \nabla c_i + c_i v \tag{3.1}$$

is used along with the mass balance equation

$$\frac{\partial c_i}{\partial t} = -\nabla \cdot N_i + R_i \tag{3.2}$$

to obtain the mass transfer model equations in the laminar layer. The derivation of the governing equation and the assumptions made are discussed in Chapter II. The governing equation for the mass transfer of species *i* in the laminar sublayer is given by the following equation

$$D_i \frac{\partial^2 (c_i)}{\partial y^2} + z_i u_i F \frac{\partial (c_i \Phi')}{\partial y} = 0 \tag{3.3}$$

Equation (3.3) is a second order non-linear ordinary differential equation. In the downhole system there are many ionic and molecular species that are significant in the overall modeling. A list of the different species taken into account is in Appendix A. Equation (3.3) has to be applied to all of the N_{sp} species (i.e. i=1,2,...,N_{sp}). This results in a set of N_{sp} equations with (N_{sp}+1) unknowns. The concentrations of the N_{sp} species (c_1, c_2... c_{Nsp}) along with the electric potential, Φ, are the unknown variables in the system of equations. An additional equation is needed to complete the set of governing equations. The charged species interact with each other through the electric potential thereby coupling the equations. Thus the electroneutrality equation forms the required $(N_{sp}+1)^{th}$ equation.

Boundary conditions are needed to solve the set of governing equations. As illustrated in Chapter II, the known species concentrations and zero electric potential form the left hand boundary conditions which is at the turbulent-laminar interface. At the right boundary, namely the pipe wall, the flux boundary condition is applied to all the N_{sp}

species along with the electroneutrality condition. The equations along with the details of the numerical scheme used to solve the entire system are explained later in Section 3.3.

3.2 Numerical Methods

One of the most challenging tasks of this research work has been to find a suitable numerical technique that can be used to solve the above mentioned boundary value problem. This section gives a brief overview of the different methods that have been tried at different stages of this work. All these numerical methods make use of the finite difference approach where derivatives are approximated by Taylor expansions. Some of the finite differences used in this work are the central and backward differences of first and second order derivatives.

To use the finite difference approach the laminar sub-layer has been divided into equally spaced nodes. These nodes are also referred to as grid points. The turbulent-laminar interface, which forms the left boundary of the laminar layer, represents the first grid point. The last grid point lies on the right boundary, which physically represents the pipe wall where the corrosion reactions take place. Figure 2 is a visual representation of the grid points in the laminar sublayer. The figure does not include the corrosion product layer since this study focuses on uniform corrosion rates without corrosion product film formation.

The left-hand boundary conditions are applied at the first grid point. The right hand boundary conditions are applied at the last grid point and the governing equations are applied at all the interior grid points. A numerical method is then used to solve the

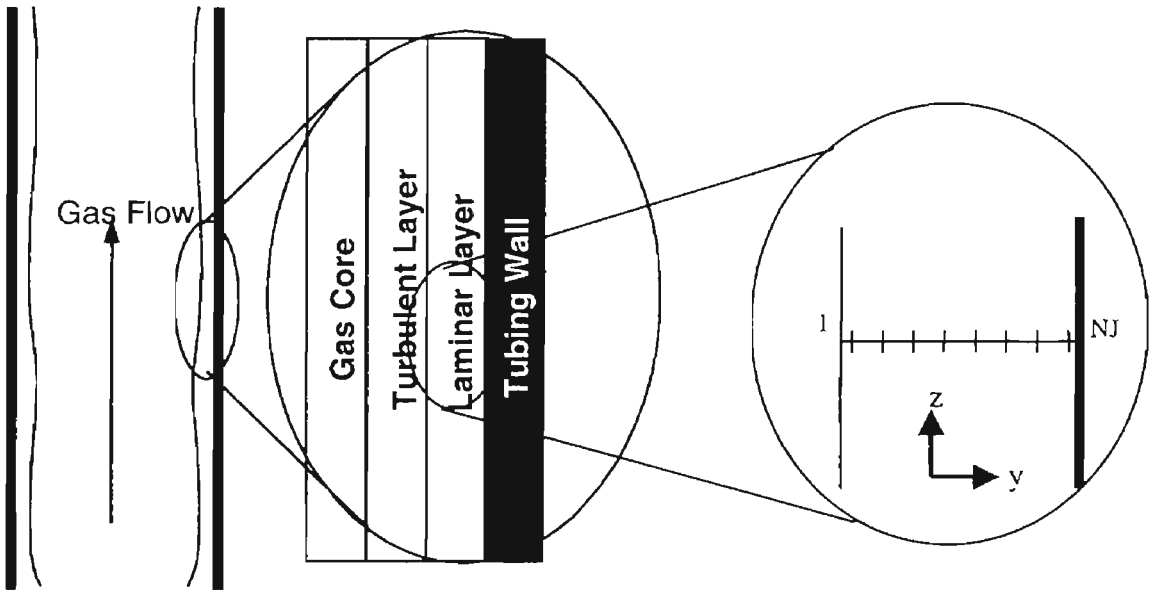

Figure 2: Grid Point Representation of the Laminar Sublayer

model equations for the unknown variables at these grid points thereby resulting in the concentration profiles of different species across the laminar sublayer.

3.2.1 Source term Method

Liu(1993) used the condition of no net current to eliminate the electric potential term from the system of governing equations. This resulted in the following system

$$\frac{\partial^2 (c_i)}{\partial X^2} + Sc = 0 \tag{3.4}$$

where Sc is the non-linear source term as derived in the Chapter II. Since this is similar to a heat conduction problem with a nonlinear source term, Liu used a numerical method which involved iterating on the nonlinear source term (Patankar, 1991). In the present work, it was found that the numerical method did not generate the correct results. The method did not correctly solve for the concentration profiles and always resulted in a

corrosion rate of zero mpy. Initially the computer code was studied with an aim to find out the exact reason for the failure of the numerical method. However due to the inadequate documentation and commenting of the code, this could not be achieved. It was then decided to start afresh with a new numerical approach.

3.2.2 Shooting Method

A shooting method approach was studied and found to be not efficient to solve the system of equations encountered in this work. The second order differential equations represented by Equation (3.4) were rewritten as a set of first order differential equations. These were then solved by using a shooting method approach (Press et al., 1992). The method was initially used for an imaginary case where only two species are considered and was later extended to systems with more species. Convergence was found to be dependent on the choice of the initial guesses made. The method was found to be suitable for systems with few unknowns (<5). However, as the number of species was increased the method failed to converge. The method was, hence, found to be less efficient for nonlinear systems with more variables

3.2.3 BAND(J)

BAND(J) is a FORTRAN subroutine which incorporates a numerical scheme to solve coupled linear difference equations (Newman, 1991). A system of N coupled linear ordinary differential equations is shown below:

$$\sum_{k=1}^{N} a_{i,k}(x)\frac{\partial^2(c_k)}{\partial x^2} + b_{i,k}(x)\frac{\partial(c_k)}{\partial x} + d_{i,k}(x)c_k = g_i(x) \qquad (3.5)$$

This system can be approximated using the following central difference approximations

$$\frac{\partial^2(c_k)}{\partial x^2} = \frac{c_k(x_j + h) + c_k(x_j - h) - 2c_k(x_j)}{h^2} \tag{3.6}$$

$$\frac{\partial\ (c_k)}{\partial x} = \frac{c_k(x_j + h) - c_k(x_j - h)}{2h} \tag{3.7}$$

where j represents a grid point and h is the distance between two adjacent grid points. This reduces the set of differential equations represented by Equation (3.5) to the following difference equations

$$\sum_{k=1}^{N} A_{i,k}(j)C_k(j-1) + B_{i,k}(j)C_k(j) + D_{i,k}(j)C_k(j+1) = G_i(j) \tag{3.8}$$

where

$$\begin{aligned} A_{i,k}(j) &= a_{i,k}(x_j) - \frac{h}{2}b_{i,k}(x_j) \\ B_{i,k}(j) &= -2a_{i,k}(x_j) + h^2 d_{i,k}(x_j) \\ D_{i,k}(j) &= a_{i,k}(x_j) + \frac{h}{2}b_{i,k}(x_j) \\ C_k(j) &= c_k(x_j) \\ G_i(j) &= h^2 g_i(x_j) \end{aligned} \tag{3.9}$$

For the left boundary, the boundary conditions are rewritten using the following forward difference approximation for the first order derivatives,

$$\frac{\partial\ (c_k)}{\partial x} = \frac{-3c_k(x_j) + 4c_k(x_j + h) - c_k(x_j + 2h)}{2h} \tag{3.10}$$

to result in equations of the form

$$\sum_{k=1}^{N} B_{i,k}(1)C_k(1) + D_{i,k}(1)C_k(2) + X_{i,k}C_k(3) = G_i(1) \tag{3.11}$$

Similar treatment at the right boundary (j = *NJ*) using appropriate backward difference approximations gives difference equations of the form

$$\sum_{k=1}^{N} Y_{i,k} C_k(NJ-2) + A_{i,k}(NJ) C_k(NJ-1) + B_{i,k}(NJ) C_k(NJ) = G_i(NJ) \qquad (3.12)$$

The steps to solve such a system of coupled linear difference equations are explained in detail in Newman (1991). BAND(J) is the FORTRAN subroutine which implements the solution method. The subroutine requires as inputs, the coefficient matrices A, B, D, and G at each grid point and the values of coefficient matrix X for the left boundary and of matrix Y at the right boundary. Using these inputs the subroutine solves for the unknowns, namely matrix C. This is the numerical method that has been used in this work to solve for the concentration profiles of different species in the laminar layer in each well section.

3.3 Configuring the System for BAND(J)

The BAND(J) subroutine has been used to solve the set of coupled, non-linear, ordinary differential equations representing the mass transfer model. Since BAND(J) handles only coupled, linear, ordinary differential equations, all the equations representing this system have been linearized. Further, BAND(J) also requires some inputs which are the coefficient matrices. The linearization of all applicable equations and the derivations of expressions for the coefficient matrices are discussed in this section.

3.3.1 Interior Governing Equation.

The governing differential equation, given by Equation (2.25), is applied at all the interior grid points (j = 2, 3.. (*NJ*-1)). The equation for species *i* is shown below:

$$D_i \frac{\partial^2 (c_i)}{\partial y^2} + z_i u_i F \frac{\partial (c_i \Phi')}{\partial y} = 0 \tag{3.13}$$

$$D_i \frac{\partial^2 (c_i)}{\partial y^2} + z_i u_i F \left(c_i \Phi'' + c_i' \Phi' \right) = 0 \tag{3.14}$$

The equation has to be applied at every internal grid point (j = 2, 3.. *NJ*-1) and for all the different species present in the downhole system. However, if a species is not present in a particular well, then its concentration is set equal to zero at all the grid points. Together these give us N_{sp} equations and the condition of electroneutrality forms the requisite $(N_{sp}+1)^{th}$ equation.

The coefficient matrices are evaluated from the above governing equations. First, these equations, represented by Equation (3.14), have to be linearized in order to use BAND(J). Newman (1991) outlines the linearization method, which uses the following approximations for linearizing the nonlinear terms in the system of equations

$$c_i \Phi'' \approx \left(c_i \Phi^{0''} + c_i^0 \Phi'' - c_i^0 \Phi^{0''} \right) \tag{3.15}$$

and

$$c_i \Phi' \approx \left(c_i \Phi^{0'} + c_i^0 \Phi' - c_i^0 \Phi^{0'} \right) \tag{3.16}$$

where c_i^0, $\Phi^{0'}$, and $\Phi^{0''}$ are initial guesses of the respective variables. Using the above approximation the governing equations at an internal grid point is reduced to the difference form as shown below

$$
\begin{aligned}
&c_i(j-1)\left(D_i-\frac{1}{2}z_iu_iFh\Phi^{0'}\right)+c_i(j)\left(-2D_i+z_iu_iFh^2\Phi^{0''}\right)\\
&+c_i(j+1)\left(D_i+\frac{1}{2}z_iu_iFh\Phi^{0'}\right)+\Phi(j-1)z_iu_iF\left(c_i^0-\frac{1}{2}hc_i^{0'}\right)\\
&+\Phi(j)\left(-2z_iu_iFc_i^0\right)+\Phi(j+1)z_iu_iF\left(c_i^0+\frac{1}{2}hc_i^{0'}\right)\\
&=z_iu_iF\left(c_i^0\Phi^{0''}+c_i^{0'}\Phi^{0'}\right)
\end{aligned}
\tag{3.17}
$$

Now configuring this in BAND(J) terminology results in

$$
\begin{aligned}
&C(i,j-1)\left(D_i-\frac{1}{2}z_iu_iFh\Phi^{0'}\right)+C(i,j)\left(-2D_i+z_iu_iFh^2\Phi^{0''}\right)\\
&+C(i,j+1)\left(D_i+\frac{1}{2}z_iu_iFh\Phi^{0'}\right)+C(N,j-1)z_iu_iF\left(c_i^0-\frac{1}{2}hc_i^{0'}\right)\\
&+C(N,j)\left(-2z_iu_iFc_i^0\right)+C(N,j+1)z_iu_iF\left(c_i^0+\frac{1}{2}hc_i^{0'}\right)\\
&=z_iu_iFh^2\left(c_i^0\Phi^{0''}+c_i^{0'}\Phi^{0'}\right)
\end{aligned}
\tag{3.18}
$$

From the above equation the coefficient matrices for BAND(J) can be identified as

$$
\begin{aligned}
A(i,i)&=D_i-\frac{1}{2}z_iu_iFh\Phi^{0'}\\
B(i,i)&=-2D_i+z_iu_iFh^2\Phi^{0''}\\
D(i,i)&=D_i+\frac{1}{2}z_iu_iFh\Phi^{0'}\\
A(i,N)&=c_i^0-\frac{1}{2}hc_i^{0'}\\
B(i,N)&=-2z_iu_iFc_i^0\\
D(i,N)&=c_i^0+\frac{1}{2}hc_i^{0'}\\
G(i)&=z_iu_iFh^2\left(c_i^0\Phi^{0''}+c_i^{0'}\Phi^{0'}\right)
\end{aligned}
\tag{3.19}
$$

The above equations are valid for all species that are present in the system. For those species, k, that are not present in a particular well case then

$$c_k = 0 \tag{3.20}$$

gives the coefficients

$$B(k,k) = 1.0 \tag{3.21}$$

$$\text{and} \qquad G(k) = 0. \tag{3.22}$$

However, the number of variables is one more than the number of species because of the electric potential involved. This demands the need for one more equation. The $N(N_{sp}+1)^{th}$ equation is obtained from the assumption of electroneutrality. The determination of coefficients from the electroneutrality equation is discussed separately, as it is applicable not only at the interior grid points but also at the right boundary of the laminar sublayer. It should be noted that the potential is set to zero at the left boundary making it a reference point.

3.3.2 Left Boundary Condition

The interface between the turbulent and diffusion layers in the annular film forms the left-hand boundary of the system. The turbulent layer mass transfer calculations provide the concentrations of different species at this interface. These known concentrations form the left-hand boundary conditions and are as shown below

$$c_i = c_{i,t} \qquad\qquad i = 1, 2.. N_{sp} \tag{3.23}$$

This is a linear equation and the coefficient matrices for BAND(J) can be easily identified as

$$B(i,i) = 1.0 \tag{3.24}$$

$$\text{and} \qquad G(i) = c_{i,t} \qquad\qquad i = 1, 2.. N_{sp} \tag{3.25}$$

The zero electric potential at the left boundary,

$$\Phi = 0 \tag{3.26}$$

forms the N^{th} boundary condition and results in the following coefficients

$$B(N,N) = 0 \quad \text{and} \quad G(N) = 0. \tag{3.27}$$

3.3.3 Right Boundary Condition

For solving the set of differential equations the boundary conditions at the right boundary have to be formulated. Since the corrosion rates without corrosion product film is the quantity that is of interest, the pipe wall becomes the right boundary. The concentration of different species at the wall is not known at this stage and so the simple concentration boundary conditions that are applicable at the left boundary are not applicable here. Instead the flux of species is used to obtain the necessary boundary conditions at the wall. The flux of any species is given by

$$J_i = -\left(D_i \frac{dc_i}{dy} + z_i u_i F c_i \frac{d\Phi}{dy} \right) \tag{3.28}$$

Depending on whether the species is reactive or not, the flux at the wall will either be equal to a reactive flux or will equal zero (Sundaram et al., 1996). The procedure for calculating the coefficient matrices for BAND(J) in the case of nonreactive and reactive species are illustrated next.

For nonreactive species i.e. i =1...N-1(i≠ 7(Fe^{2+}),12(H^+),N(Φ)):

Equating the flux of nonreactive species at the wall to zero gives

$$-\left[D_i \frac{dc_i}{dy} + z_i u_i F c_i \frac{d\Phi}{dy} \right] = 0. \tag{3.29}$$

The nonlinear term in the above equation, namely $c_i(d\Phi/dy)$, is linearized as shown below by using Equation (3.16).

$$-\left[D_i \frac{dc_i}{dy} + z_i u_i F\left(c_i \Phi^{0'} + c_i^0 \Phi' - c_i^0 \Phi^{0'}\right)\right] = 0. \tag{3.30}$$

Backward differences are then used (since it the right most grid point) to obtain the expressions for the coefficient matrices.

$$\left[\begin{array}{l} D_i\left(\dfrac{3C(i,NJ) - 4C(i,NJ-1) + 1C(i,NJ-2)}{2h}\right) + \\ z_i u_i F\left(\begin{array}{l} C(i,NJ)\Phi^{0'} + \\ c_i^0\left(\dfrac{3C(N,NJ) - 4C(N,NJ-1) + 1C(N,NJ-2)}{2h}\right) \end{array}\right) \end{array}\right] = z_i u_i F c_i^0 \Phi^{0'} \tag{3.31}$$

From Equation (3.31) the terms of the coefficient matrices for nonreactive species can be identified as

$$\begin{aligned} B(i,i) &= +3D_i/(2h) + z_i u_i F \Phi^{0'} \\ A(i,i) &= -4D_i/(2h) \\ Y(i,i) &= +1D_i/(2h) \\ B(i,N) &= +3 z_i u_i F c_i^0/(2h) \\ A(i,N) &= -4 z_i u_i F c_i^0/(2h) \\ Y(i,N) &= +1 z_i u_i F c_i^0/(2h) \\ G(i) &= z_i u_i F c_i^0 \Phi^{0'} \end{aligned} \tag{3.32}$$

where c_i^0 is the concentration of species i at the wall obtained from either the initial guess or from the previous iteration.

For reactive species i.e. i =7(Fe^{2+}),12(H^+):

The treatment of boundary conditions for the reactive species, namely Fe^{2+} and H^+, is illustrated here. The reaction that occurs at the pipe wall, which leads to corrosion, is shown below

$$Fe + 2H^+ \leftrightarrow Fe^{2+} + H_{2(g)} \tag{3.33}$$

The following relation (Sundaram et al., 1996) relates the flux of the reactive species to the corrosion current density

$$-\left[D_i \frac{dc_i}{dy} + z_i u_i F c_i \frac{d\Phi}{dy}\right] = \frac{i_c}{nF}. \tag{3.34}$$

where i_c is the corrosion current density, F is Faraday's constant, and n is the number of valence electrons. The corrosion current density is related to the pH by the following expression (de Waard and Milliams, 1975)

$$\log i_c = -A.pH + B \tag{3.35}$$

The experimental value of A is 1.3 while the calculated value, based on a mechanism proposed in the above reference, is 1.25 and the value of B is 0.001 (Dugan, 1997). Using these values along with the general expression for pH gives

$$\log i_c = -A.\left(-\log\left[H^+\right]\right) + B \tag{3.36}$$

$$i_c = \exp(B)\left[H^+\right]^A \tag{3.37}$$

Further, since BAND(J) can handle only linear equations, the nonlinear term $[H^+]^A$ is linearized by approximating the value of A to 1. Initially a Taylor series expansion was used to linearize this term, resulting in

$$i_c = \exp(B)\left\{\left(c^o_{H^+}\right)^A + A\left(c^o_{H^+}\right)^{A-1}\left(c_{H^+} - c^o_{H^+}\right)\right\} \tag{3.38}$$

However mathematical computational difficulties were encountered in the iterative procedure scheme and the numerical method crashed frequently. The value of c^0_{H+}, which starts off with an initial guess at the beginning of the iterative scheme, is updated at the end of each iteration until the convergence criteria is satisfied. Sometimes during this process a negative value is temporarily assigned to the variable. This in turn resulted in a mathematical error in the calculations because a negative number was being raised to

the power of 1.3. The approximation of A to 1 solves this problem. This is a reasonable approximation because this will overpredict the corrosion current, and hence result in a more conservative estimate of the corrosion rate. This approximation reduces Equation (3.37) to

$$i_c \approx \exp(B)\left[H^+\right] \tag{3.39}$$

Plugging in the above expression into the right hand boundary condition Equation (3.34) gives

$$-\left[D_i \frac{dc_i}{dy} + z_i u_i F c_i \frac{d\Phi}{dy}\right] = \frac{\exp(B)}{nF} c_H. \tag{3.40}$$

The derivation of the coefficient matrices for H^+ (i = 12) is given below.

$$-\left[D_i \frac{dc_i}{dy} + z_i u_i F\left(c_i \Phi^{0'} + c_i^0 \Phi' - c_i^0 \Phi^{0'}\right)\right] = \left(\frac{i_c}{nF}\right)_H. \tag{3.41}$$

$$-\left[D_i \frac{dc_i}{dy} + z_i u_i F\left(c_i \Phi^{0'} + c_i^0 \Phi' - c_i^0 \Phi^{0'}\right)\right] = \frac{\exp(B)}{nF} c_H. \tag{3.42}$$

Using the appropriate backward finite differences for the derivatives and rearranging Equation (3.42) gives

$$\left[\begin{array}{l} D_i\left(\dfrac{3C(i,NJ) - 4C(i,NJ-1) + 1C(i,NJ-2)}{2h}\right) + \\ z_i u_i F\left(\begin{array}{l} C(i,NJ)\Phi^{0'} + \\ c_i^0\left(\dfrac{3C(N,NJ) - 4C(N,NJ-1) + 1C(N,NJ-2)}{2h}\right) \end{array}\right) + \\ \dfrac{\exp(B)}{nF} c_H. \end{array}\right] = \left(z_i u_i F c_i^0 \Phi^{0'}\right) \tag{3.43}$$

The coefficient matrices terms for i=12 can now be identified, and are given below:

$$
\begin{aligned}
B(i,i) &= +3D_i/(2h) + z_i u_i F\Phi^{0'} + (\exp(B)/nF) \\
A(i,i) &= -4D_i/(2h) \\
Y(i,i) &= +1D_i/(2h) \\
B(i,N) &= +3z_i u_i F c_i^0/(2h) \\
A(i,N) &= -4z_i u_i F c_i^0/(2h) \\
Y(i,N) &= +1z_i u_i F c_i^0/(2h) \\
G(i) &= z_i u_i F c_i^0 \Phi^{0'}
\end{aligned}
\tag{3.44}
$$

It should be noted that $c^0{}_{H+}$ and $c^0{}_i$ are the same in the above equations.

The derivation of the coefficient matrices for Fe^{2+} (i = 7) is illustrated. The flux of ferrous ions from the wall is related to the flux of the protons to the pipe wall. This relation between the reactive fluxes is used in the boundary condition of the ferrous species.

$$
-\left[D_i\frac{dc_i}{dy}+z_i u_i F\left(c_i\Phi^{0'}+c_i^0\Phi'-c_i^0\Phi^{0'}\right)\right]=\left(\frac{i_c}{nF}\right)_{Fe^{2+}}=-\frac{1}{2}\left(\frac{i_c}{nF}\right)_{H^+} \tag{3.45}
$$

$$
-\left[D_i\frac{dc_i}{dy}+z_i u_i F\left(c_i\Phi^{0'}+c_i^0\Phi'-c_i^0\Phi^{0'}\right)\right]=\left(-\frac{1}{2}\right)\frac{\exp(B)}{nF}c_{H^+} \tag{3.46}
$$

Rewriting Equation (3.46) using finite differences gives

$$
\left[\begin{array}{l}
D_i\left(\dfrac{3C(i,NJ)-4C(i,NJ-1)+1C(i,NJ-2)}{2h}\right)+ \\
z_i u_i F\left(\begin{array}{l} C(i,NJ)\Phi^{0'}+ \\ c_i^0\left(\dfrac{3C(N,NJ)-4C(N,NJ-1)+1C(N,NJ-2)}{2h}\right)\end{array}\right) \\
+\left(-\dfrac{1}{2}\right)\dfrac{\exp(B)}{nF}C(12,NJ)
\end{array}\right]=\left(z_i u_i F c_i^0\Phi^{0'}\right) \tag{3.47}
$$

The coefficient matrices terms for i=7 can now be identified, and are given below:

$$
\begin{aligned}
B(i.i) &= +3D_i/(2h) + z_i u_i F\Phi^0 \\
B(i,12) &= (-1/2)(\exp(B)/nF) \\
A(i,i) &= -4D_i/(2h) \\
Y(i,i) &= +1D_i/(2h) \\
B(i,N) &= +3z_i u_i F c_i^0/(2h) \\
A(i,N) &= -4z_i u_i F c_i^0/(2h) \\
Y(i,N) &= +1z_i u_i F c_i^0/(2h) \\
G(i) &= z_i u_i F c_i^0 \Phi^0
\end{aligned}
\tag{3.48}
$$

3.3.4 Electroneutrality Equation

The assumption of electroneutrality results in the following expression

$$\sum z_i c_i = 0 \tag{3.49}$$

This becomes the N^{th} equation for all the interior grid points and the right boundary grid point, thus completing the set of equations required to represent the system. The terms for the coefficient matrices of BAND(J) can be identified from this condition and are

$$\text{B(N,i)} = z_i \quad \text{and} \quad \text{G(N)} = 0 \ \text{ where i} = 1, 2, \ldots N_{sp}. \tag{3.50}$$

3.4 Ionic Diffusivity Calculation

The ionic mobility and diffusion coefficient of ionic species are related by the Nernst-Einstein equation (Newman, 1991)

$$D_i = RTu_i \tag{3.51}$$

However, literature data are usually available for ionic equivalent conductances and not for ionic mobilities. The ionic equivalent conductance is related to the ionic mobility by the following expression

$$\lambda_i = |z_i| F^2 u_i \tag{3.52}$$

Substituting the expression for ionic mobility from Equation (3.52) into the Nernst-Einstein relation gives

$$D_i = \frac{RT\lambda_i}{|z_i| F^2} \tag{3.53}$$

The temperature dependence of the ionic diffusion coefficient is also taken into account by using the following relation

$$\frac{D_i \mu}{T} = \text{constant}. \tag{3.54}$$

where μ is the viscosity of the solution.

3.5 Corrosion Rate Calculation

The flux of the ferrous ions is used to calculate the corrosion rate. For each section of a well, a number of iterations are to be performed until convergence is attained. The convergence criteria used are discussed in the next section. At the end of an iteration for a section in the well, BAND(J) provides the profiles for the concentration of all species as well as the potential across the laminar layer. The flux of Fe^{2+} is given by

$$J_i = -\left(D_i \frac{dc_i}{dy} + z_i u_i F c_i \frac{d\Phi}{dy} \right) \tag{3.55}$$

where $i = 7$ represent Fe^{2+}. The above expression is used to calculate the flux of Fe^{2+} from the wall. This flux is in units of mol/dm^2/s. The conversion of the above flux to a corrosion rate is shown below

$$Rate\left(\frac{dm}{s}\right) = J\left(\frac{mol}{dm^2.s}\right) * M_i\left(\frac{g}{mol}\right) * \frac{1}{\rho}\left(\frac{cc}{g}\right) * \frac{1dm^3}{1000cc} \tag{3.56}$$

Further the corrosion rate in dm/s can be converted to units of mpy using the following relations

$$1 \text{ dm} = 10^{11} \text{ pm} \tag{3.57}$$

$$1 \text{ mpy} = .805 \text{ pm/s} \tag{3.58}$$

$$1 \text{dm/s} = 10^{11} \text{ pm/s} = (10^{11}/0.805) \text{ mpy} \tag{3.59}$$

3.6 Convergence Criteria

Absolute and relative convergence criteria are used to determine when to terminate the iterative numerical calculations. For solving the mass transfer model, which consists of nonlinear differential equations, an iterative procedure has been employed. Initial guesses are made for the first and second derivatives of the electric potential, $\Phi^{0'}$ and $\Phi^{0''}$, and these are used to linearize the system of equations. The BAND(J) subroutine then solves the linearized system. The values of corrosion rate, $\Phi^{0'}$ and $\Phi^{0''}$ are calculated using the solution obtained. The procedure is repeated with the calculated values of $\Phi^{0'}$ and $\Phi^{0''}$, and a new corrosion rate is obtained. Such iterations are performed until the corrosion rates obtained from two successive iterations converge. The absolute and relative convergence criteria used are given below

$$\left|CR_{new} - CR_{old}\right| \leq \varepsilon_{abs} \tag{3.60}$$

$$\left|\frac{CR_{new} - CR_{old}}{CR_{old}}\right| \leq \varepsilon_{rel} \tag{3.61}$$

where ε_{abs} and ε_{rel} define the absolute and relative convergence criteria.

CHAPTER IV

RESULTS AND DISCUSSION

The mass transfer model illustrated in Chapter III has been incorporated into DREAM, which has been used to model corrosion in 18 different cases. The corrosion rate predictions of DREAM using the new model have been compared with field data. In addition, studies have been conducted with the new model, which illustrate the usefulness of this mechanistic model.

4.1 Data Source

The input data for the 18 cases have been compiled from case histories of actual wells that have been in production in several fields. The case histories were obtained from different industrial collaborators. Sundaram (1996) had previously tested his model for 16 out of the 18 wells discussed here. However, some of the data used by Sundaram (1996) could not be traced back to the case histories. It was concluded that some assumptions had been made and since these were not clearly stated in Sundaram's (1997) work it was decided to document the source of input data for future references. The input data for the 18 cases used in the present work is given in Tables I – XVIII. The well names identify the well number and the field in which the well is located. In these tables the sources of the input data have been documented and also include any assumptions

made in their compilation. This will serve as a reference for future downhole corrosion research work.

The input data needed to execute DREAM include well specifications, operating conditions, water and gas analysis data. A list of the inputs required is summarized in the data sheet in Table XIX. In practice, the well conditions change over a period of time sometimes even as often as daily. The results from our calculations reflect the instantaneous corrosion rate given the conditions represented by the most recent well and product analysis. Further the well head conditions have been assumed to be the same as the separator conditions.

The bottomhole temperature data are not explicitly available in all cases. The bottomhole temperature are available for Cases IV, X, XI, XII, XIII, XIV, XVII and XVIII. Among these, Cases XIII and XIV are wells in the Flores field. The average of the bottomhole temperatures of these two wells has been used as the bottomhole temperature for the other Flores field wells, namely Cases I, II, III, V, VI, VII, VIII, IX, XV and XVI.

The well depth for all cases except case IX has been taken from the Kinley Survey report. It was observed that the well length measured (WLM) obtained from the Kinley Survey was usually a few hundred feet less than the depth of the section last perforated. Therefore, in Case IX the well depth has been assumed to be 10300 ft. since the last section to be perforated was at 10476 – 10650 ft.

In Case IV, the water analysis data were in units of mg/l and this was converted to units of parts per million (ppm) using the assumption that the density of the solution

TABLE I

INPUT DATA FOR CASE I : YTURRIA L&L -C- #2, Flores

Well Geometry and Production Data		Water Analysis		Gas Analysis	
Completion	8/15/1985 *WDS	Sampled	9/26/1985	Sampled	11/20/1990
Kinley Survey	3/14/1991	Constituent	ppm	Component	mole %
Tubing type	2 7/8" 6.5#EUE *K	Na^+	6490	CH_4	90.94
ID (in.)	2.441 *K	Ca^{2+}	298	C_2H_6	4.37
Depth (ft.)	9700 *K	Mg^{2+}	38	C_3H_8	1.14
Water Production (bbl/day)	42 *WDS $	Ba^{2+}	4	$I\text{-}C_4H_{10}$	0.27
Gas Production (MSCFD)	5532 *WDS $	Sr^{2+}	0	$N\text{-}C_4H_{10}$	0.23
Oil Production (bbl/day)	63 *WDS $	K^+	0	$I\text{-}C_5H_{12}$	0.13
Wellhead Temp. (°F)	110 *G	Fe^{2+}	36	$N\text{-}C_5H_{12}$	0.08
Wellhead Pressure (psia)	1170 *G	Cl^-	10100	C_6H_{14}	0.11
Bottomhole Temp. (°F)	272 *AA	SO_4^{2-}	111	C_{7+}	0.27
Bottomhole Pressure (psia)	6765 *WDS $	CO_3^{2-}	0	N_2	0.25
		HCO_3^-	879	CO_2	2.21
				H_2S	0.00

Comments :

*G from Gas Analysis; *K from Kinley Survey; *WDS from Workover Data Sheet; *W from Water Analysis;

*AA assumed average of Bottomhole Temp. of Flores Fields JAGARCIA 2 (284°F) & JAGARCIA 3 (261°F)

$ measured in 1987

TABLE II

INPUT DATA FOR CASE II : IY GARCIA #8, Flores

Well Geometry and Production Data		Water Analysis		Gas Analysis	
Completion	3/1/1985 *WDS	Sampled	06/17/1988	Sampled	11/19/1990
Kinley Survey	2/22/1991	Constituent	ppm	Component	mole %
Tubing type	2 7/8" 6.5#AB MOD EUE *K	Na^+	6280	CH_4	91.60
ID (in.)	2.441 *K	Ca^{2+}	454	C_2H_6	4.39
Depth (ft.)	9420 *K	Mg^{2+}	50	C_3H_8	1.18
Water Production (bbl/day)	112 *WDS $	Ba^{2+}	2	$I\text{-}C_4H_{10}$	0.33
Gas Production (MSCFD)	6734 *WDS $	Sr^{2+}	0	$N\text{-}C_4H_{10}$	0.25
Oil Production (bbl/day)	11.8 *WDS $	K^+	0	$I\text{-}C_5H_{12}$	0.14
Wellhead Temp. (°F)	127 *G	Fe^{2+}	0	$N\text{-}C_5H_{12}$	0.09
Wellhead Pressure (psia)	1170 *G	Cl^-	10300	C_6H_{14}	0.13
Bottomhole Temp. (°F)	272 *AA	SO_4^{2-}	196	C_{7+}	0.33
Bottomhole Pressure (psia)	5623 *WDS $	CO_3^{2-}	0	N_2	0.30
		HCO_3^-	313	CO_2	1.26
				H_2S	0.00

Comments :

*G from Gas Analysis; *K from Kinley Survey; *WDS from Workover Data Sheet; *W from Water Analysis;

*AA assumed average of Bottomhole Temp. of Flores Fields JAGARCIA 2 (284°F) & JAGARCIA 3 (261°F)

$ measured in 03/1987

TABLE III

INPUT DATA FOR CASE III : YTURRIA L&L -C- #5, Flores

Well Geometry and Production Data		Water Analysis		Gas Analysis	
Completion	11/21/1987 *WDS	Sampled	06/07/1988	Sampled	11/21/1990
Kinley Survey	02/20/1991	Constituent	ppm	Component	mole %
Tubing type	2 7/8" 6.5#EUE *K	Na^+	127	CH_4	90.10
ID (in.)	2.441 *K	Ca^{2+}	21	C_2H_6	6.00
Depth (ft.)	9600 *K	Mg^{2+}	0	C_3H_8	1.68
Water Production (bbl/day)	72 *WDS $	Ba^{2+}	3	$I\text{-}C_4H_{10}$	0.45
Gas Production (MSCFD)	6134 *WDS $	Sr^{2+}	0	$N\text{-}C_4H_{10}$	0.34
Oil Production (bbl/day)	124.6 *WDS $	K^+	0	$I\text{-}C_5H_{12}$	0.20
Wellhead Temp. (°F)	149 *G	Fe^{2+}	0	$N\text{-}C_5H_{12}$	0.12
Wellhead Pressure (psia)	1200 *G	Cl^-	195	C_6H_{14}	0.18
Bottomhole Temp. (°F)	272 *AA	SO_4^{2-}	0	C_{7+}	0.40
Bottomhole Pressure (psia)	6250 *WDS $	CO_3^{2-}	0	N_2	0.22
		HCO_3^-	60	CO_2	0.31
				H_2S	0.00

Comments .

*G from Gas Analysis; *K from Kinley Survey; *WDS from Workover Data Sheet; *W from Water Analysis;

*AA assumed average of Bottomhole Temp. of Flores Fields JAGARCIA 2 (284°F) & JAGARCIA 3 (261°F)

$ measured in 1/18/1988

TABLE IV

INPUT DATA FOR CASE IV : EC 33 A#3, East Cameron 33

Well Geometry and Production Data		Water Analysis		Gas Analysis	
Completion	07/14/1988 *FCS	Sampled	12/14/1973	Sampled	02/19/1989
Kinley Survey	03/24/1990	Constituent	ppm	Component	mole %
Tubing type	2 7/8" 6.5#Lockit *K	Na^+	20104	CH_4	95.10
ID (in.)	2.441 *K	Ca^{2+}	326	C_2H_6	1.92
Depth (ft.)	10735 *K	Mg^{2+}	166	C_3H_8	0.49
Water Production (bbl/day)	20 *CMP	Ba^{2+}	6	$I\text{-}C_4H_{10}$	0.12
Gas Production (MSCFD)	4000 *CMP	Sr^{2+}	0	$N\text{-}C_4H_{10}$	0.11
Oil Production (bbl/day)	20 *CMP	K^+	0	$I\text{-}C_5H_{12}$	0.05
Wellhead Temp. (°F)	100 *CMP	Fe^{2+}	3	$N\text{-}C_5H_{12}$	0.03
Wellhead Pressure (psia)	415 *CMP	Cl^-	30540	C_6H_{14}	0.11
Bottomhole Temp. (°F)	230 *CMP	SO_4^{2-}	800	C_{7+}	0.15
Bottomhole Pressure (psia)	1015 *CMP	CO_3^{2-}	0	N_2	0.08
		HCO_3^-	1648	CO_2	1.84
				H_2S	0.00

Comments :

*G from Gas Analysis; *K from Kinley Survey; *FCS from Final Completion Sketch; *W from Water Analysis; *CMP from CMP Input Data Sheet

*AA assumed average of Bottomhole Temp. of Flores Fields JAGARCIA 2 (284°F) & JAGARCIA 3 (261°F)

water analysis mg/l to ppm

TABLE V

INPUT DATA FOR CASE V : IY GARCIA #7, Flores

Well Geometry and Production Data		Water Analysis		Gas Analysis	
Completion	04/01/1984 *WDS	Sampled	06/13/1988	Sampled	11/19/1990
Kinley Survey	02/21/1991	Constituent	ppm	Component	mole %
Tubing type	2 7/8" 6.5#Lockit *K	Na^+	35	CH_4	90.17
ID (in.)	2.441 *K	Ca^{2+}	7	C_2H_6	5.49
Depth (ft.)	9100 *K	Mg^{2+}	1	C_3H_8	1.70
Water Production (bbl/day)	1.5 *WDS $	Ba^{2+}	1	$I\text{-}C_4H_{10}$	0.54
Gas Production (MSCFD)	2385 *WDS $	Sr^{2+}	0	$N\text{-}C_4H_{10}$	0.41
Oil Production (bbl/day)	62.5 *WDS $	K^+	0	$I\text{-}C_5H_{12}$	0.22
Wellhead Temp. (°F)	166 *G	Fe^{2+}	0	$N\text{-}C_5H_{12}$	0.15
Wellhead Pressure (psia)	1345 *G	Cl^-	15	C_6H_{14}	0.24
Bottomhole Temp. (°F)	272 *AA	SO_4^{2-}	0	C_{7+}	0.59
Bottomhole Pressure (psia)	7800 *WDS $	CO_3^{2-}	0	N_2	0.23
		HCO_3^-	90	CO_2	0.26
				H_2S	0.00

Comments :

*G from Gas Analysis; *K from Kinley Survey; *WDS from Workover Data Sheet; *W from Water Analysis;

*AA assumed average of Bottomhole Temp. of Flores Fields JAGARCIA 2 (284°F) & JAGARCIA 3 (261°F)

$ measured in 1984

TABLE VI

INPUT DATA FOR CASE VI : JA GARCIA #1, Flores

Well Geometry and Production Data		Water Analysis		Gas Analysis	
Completion	01/01/1988 *WDS	Sampled	09/26/1985	Sampled	06/18/1990
Kinley Survey	02/23/1991	Constituent	ppm	Component	mole %
Tubing type	2 3/8" 4.7#EUE *K	Na^+	4580	CH_4	88.31
ID (in.)	1.995 *K	Ca^{2+}	197	C_2H_6	6.9
Depth (ft.)	9172 *K	Mg^{2+}	1140	C_3H_8	2.21
Water Production (bbl/day)	6 *WDS $	Ba^{2+}	4	$I\text{-}C_4H_{10}$	0.66
Gas Production (MSCFD)	4974 *WDS $	Sr^{2+}	0	$N\text{-}C_4H_{10}$	0.5
Oil Production (bbl/day)	147 *WDS $	K^+	0	$I\text{-}C_5H_{12}$	0.26
Wellhead Temp. (°F)	141 *G	Fe^{2+}	0	$N\text{-}C_5H_{12}$	0.17
Wellhead Pressure (psia)	1245 *G	Cl^-	10300	C_6H_{14}	0.23
Bottomhole Temp. (°F)	272 *AA	SO_4^{2-}	32	C_{7+}	0.52
Bottomhole Pressure (psia)	5780 *WDS $	CO_3^{2-}	0	N_2	0.12
		HCO_3^-	696	CO_2	0.12
				H_2S	0.00

Comments :

*G from Gas Analysis; *K from Kinley Survey; *WDS from Workover Data Sheet; *W from Water Analysis;

*AA assumed average of Bottomhole Temp. of Flores Fields JAGARCIA 2 (284°F) & JAGARCIA 3 (261°F)

$ measured in 1988

TABLE VII

INPUT DATA FOR CASE VII : YTURRIA L&C -B- #1, Flores

Well Geometry and Production Data		Water Analysis		Gas Analysis	
Completion	05/09/1986 *WDS	Sampled	11/09/1988	Sampled	03/21/1991
Kinley Survey	02/20/1991	Constituent	ppm	Component	mole %
Tubing type	3 1/2" 9.3#Hydril *K	Na^+	4740	CH_4	88.52
ID (in.)	2.92 *K	Ca^{2+}	200	C_2H_6	5.70
Depth (ft.)	10521 *K	Mg^{2+}	17	C_3H_8	1.77
Water Production (bbl/day)	114 *WDS $	Ba^{2+}	1	$I\text{-}C_4H_{10}$	0.47
Gas Production (MSCFD)	2567 *WDS $	Sr^{2+}	0	$N\text{-}C_4H_{10}$	0.40
Oil Production (bbl/day)	151 *WDS $	K^+	0	$I\text{-}C_5H_{12}$	0.22
Wellhead Temp. (°F)	110 *G	Fe^{2+}	0	$N\text{-}C_5H_{12}$	0.13
Wellhead Pressure (psia)	1020 *G	Cl^-	7490	C_6H_{14}	0.17
Bottomhole Temp. (°F)	272 *AA	SO_4^{2-}	94	C_{7+}	0.35
Bottomhole Pressure (psia)	6725 *WDS $	CO_3^{2-}	0	N_2	0.09
		HCO_3^-	257	CO_2	2.18
				H_2S	0.00

Comments :

*G from Gas Analysis; *K from Kinley Survey; *WDS from Workover Data Sheet; *W from Water Analysis;

*AA assumed average of Bottomhole Temp. of Flores Fields JAGARCIA 2 (284°F) & JAGARCIA 3 (261°F)

$ measured in 7/11/1986

TABLE VIII

INPUT DATA FOR CASE VIII : YTURRIA L&C -B- #3, Flores

Well Geometry and Production Data	
Completion	03/10/1987 *WDS
Kinley Survey	02/18/1991
Tubing type	2 3/8" 4.7#EUE *K
ID (in.)	1.995 *K
Depth (ft.)	9530 *K
Water Production (bbl/day)	95 *WDS $
Gas Production (MSCFD)	4036 *WDS $
Oil Production (bbl/day)	60.6 *WDS $
Wellhead Temp. (°F)	130 *G
Wellhead Pressure (psia)	1035 *G
Bottomhole Temp. (°F)	272 *AA
Bottomhole Pressure (psia)	7110 *WDS $

Water Analysis		
Sampled	11/09/1988	
Constituent	ppm	
Na^+	7110	
Ca^{2+}	371	
Mg^{2+}	21	
Ba^{2+}	20	
Sr^{2+}	0	
K^+	0	
Fe^{2+}	0	
Cl^-	11500	
SO_4^{2-}	0	
CO_3^{2-}	0	
HCO_3^-	335	

Gas Analysis	
Sampled	03/21/1991
Component	mole %
CH_4	90.44
C_2H_6	5.07
C_3H_8	1.36
$I\text{-}C_4H_{10}$	0.32
$N\text{-}C_4H_{10}$	0.27
$I\text{-}C_5H_{12}$	0.15
$N\text{-}C_5H_{12}$	0.09
C_6H_{14}	0.14
C_{7+}	0.32
N_2	0.12
CO_2	1.72
H_2S	0.00

Comments .

*G from Gas Analysis; *K from Kinley Survey; *WDS from Workover Data Sheet; *W from Water Analysis;

*AA assumed average of Bottomhole Temp. of Flores Fields JAGARCIA 2 (284°F) & JAGARCIA 3 (261°F)

$ measured in 5/29/1987

TABLE IX

INPUT DATA FOR CASE IX : IY GARCIA #14, Flores

Well Geometry and Production Data		Water Analysis		Gas Analysis	
Completion	08/01/1987 *WDS	Sampled	09/26/1985	Sampled	11/18/1990
Kinley Survey	02/21/1991	Constituent	ppm	Component	mole %
Tubing type	2 3/8" 4.7#EUE *K	Na^+	4580	CH_4	93.55
ID (in.)	1.995 *K	Ca^{2+}	197	C_2H_6	2.50
Depth (ft.)	10300 *AWDS	Mg^{2+}	1140	C_3H_8	0.47
Water Production (bbl/day)	144 *WDS $	Ba^{2+}	4	$I\text{-}C_4H_{10}$	0.10
Gas Production (MSCFD)	6517 *WDS $	Sr^{2+}	0	$N\text{-}C_4H_{10}$	0.08
Oil Production (bbl/day)	18 *WDS $	K^+	0	$I\text{-}C_5H_{12}$	0.06
Wellhead Temp. (°F)	148 *G	Fe^{2+}	0	$N\text{-}C_5H_{12}$	0.04
Wellhead Pressure (psia)	1270 *G	Cl^-	10300	C_6H_{14}	0.07
Bottomhole Temp. (°F)	272 *AA	SO_4^{2-}	32	C_{7+}	0.58
Bottomhole Pressure (psia)	6590 *WDS $	CO_3^{2-}	0	N_2	0.10
		HCO_3^-	696	CO_2	2.45
				H_2S	0.00

Comments :

*G from Gas Analysis; *K from Kinley Survey; *WDS from Workover Data Sheet; *W from Water Analysis;

*AA assumed average of Bottomhole Temp. of Flores Fields JAGARCIA 2 (284°F) & JAGARCIA 3 (261°F)

*AWDS assumed from Workover Data Sheet as being above the last perforated section (10476' - 10650'); $ measured in 11/1987

TABLE X

INPUT DATA FOR CASE X : VAQ A-91, Lobo

Well Geometry and Production Data		Water Analysis		Gas Analysis	
Completion	02/24/1992 *WDS	Sampled		Sampled	12/12/1993
Kinley Survey	12/08/1994	Constituent	ppm	Component	mole %
Tubing type	2 7/8" 6.5#EUE *K	Na^+	31000	CH_4	84.60
ID (in.)	2.441 *K	Ca^{2+}	7000	C_2H_6	7.88
Depth (ft.)	9995 *K	Mg^{2+}	900	C_3H_8	2.64
Water Production (bbl/day)	7.54 *IDS	Ba^{2+}	40	$I\text{-}C_4H_{10}$	0.65
Gas Production (MSCFD)	440 *IDS	Sr^{2+}	200	$N\text{-}C_4H_{10}$	0.57
Oil Production (bbl/day)	0.77 *IDS	K^+	130	$I\text{-}C_5H_{12}$	0.32
Wellhead Temp. (°F)	78 *G	Fe^{2+}	100	$N\text{-}C_5H_{12}$	0.18
Wellhead Pressure (psia)	275 *G	Cl^-	62000	C_6H_{14}	0.00
Bottomhole Temp. (°F)	190 *IDS	SO_4^{2-}	280	C_{7+}	0.17
Bottomhole Pressure (psia)	450 *IDS	CO_3^{2-}	0	N_2	0.60
		HCO_3^-	260	CO_2	2.40
				H_2S	0.00

Comments :

*G from Gas Analysis; *K from Kinley Survey; *IDS from Input Data Sheet; *W from Water Analysis; water analysis from Mahesh (orig source missing)

TABLE XI

INPUT DATA FOR CASE XI : LUNDELL A-9, Lobo

Well Geometry and Production Data		Water Analysis		Gas Analysis	
Completion	11/19/1992 *WDS	Sampled		Sampled	09/09/1994
Kinley Survey	11/23/1994	Constituent	ppm	Component	mole %
Tubing type	2 7/8" 6.5#EUE *K	Na^+	31000	CH_4	92.04
ID (in.)	2.441 *K	Ca^{2+}	7000	C_2H_6	3.72
Depth (ft.)	11246 *K	Mg^{2+}	900	C_3H_8	0.60
Water Production (bbl/day)	2.86 *IDS	Ba^{2+}	40	$I\text{-}C_4H_{10}$	0.14
Gas Production (MSCFD)	413 *IDS	Sr^{2+}	200	$N\text{-}C_4H_{10}$	0.00
Oil Production (bbl/day)	0.2 *IDS	K^+	130	$I\text{-}C_5H_{12}$	0.00
Wellhead Temp. (°F)	81 *IDS	Fe^{2+}	100	$N\text{-}C_5H_{12}$	0.00
Wellhead Pressure (psia)	470 *IDS	Cl^-	62000	C_6H_{14}	0.00
Bottomhole Temp. (°F)	191 *IDS	SO_4^{2-}	280	C_{7+}	0.06
Bottomhole Pressure (psia)	2050 *IDS	CO_3^{2-}	0	N_2	0.09
		HCO_3^-	260	CO_2	3.34
				H_2S	0.00

Comments :

*G from Gas Analysis; *K from Kinley Survey; *IDS from Input Data Sheet; *W from Water Analysis;

water analysis from Mahesh (orig source missing)

TABLE XII

INPUT DATA FOR CASE XII : VAQ A-99, Lobo

Well Geometry and Production Data		Water Analysis		Gas Analysis	
Completion	09/30/92 *WDS	Sampled		Sampled	06/10/1994
Kinley Survey	12/08/1994	Constituent	ppm	Component	mole %
Tubing type	2 7/8" 6.5#EUE *K	Na^+	31000	CH_4	92.75
ID (in.)	2.441 *K	Ca^{2+}	7000	C_2H_6	3.24
Depth (ft.)	10883 *K	Mg^{2+}	900	C_3H_8	0.42
Water Production (bbl/day)	10.68 *IDS	Ba^{2+}	40	$I\text{-}C_4H_{10}$	0.08
Gas Production (MSCFD)	905 *IDS	Sr^{2+}	200	$N\text{-}C_4H_{10}$	0.00
Oil Production (bbl/day)	0.1 *IDS	K^+	130	$I\text{-}C_5H_{12}$	0.00
Wellhead Temp. (°F)	95 *IDS	Fe^{2+}	100	$N\text{-}C_5H_{12}$	0.00
Wellhead Pressure (psia)	350 *IDS	Cl^-	62000	C_6H_{14}	0.00
Bottomhole Temp. (°F)	204 *IDS	SO_4^{2-}	280	C_{7+}	0.05
Bottomhole Pressure (psia)	2850 *IDS	CO_3^{2-}	0	N_2	0.07
		HCO_3^-	260	CO_2	3.40
				H_2S	0.00

Comments :

*G from Gas Analysis; *K from Kinley Survey; *IDS from Input Data Sheet; *W from Water Analysis; water analysis from Mahesh (orig source missing)

TABLE XIII

INPUT DATA FOR CASE XIII : JA GARCIA #2, Flores

Well Geometry and Production Data		Water Analysis		Gas Analysis	
Completion	08/01/1988 *WDS	Sampled	09/26/1985	Sampled	11/17/1990
Kinley Survey	03/19/1991	Constituent	ppm	Component	mole %
Tubing type	2 3/8" 4.7#EUE *K	Na^+	4580	CH_4	89.03
ID (in.)	1.995 *K	Ca^{2+}	197	C_2H_6	6.74
Depth (ft.)	9320 *K	Mg^{2+}	1140	C_3H_8	1.98
Water Production (bbl/day)	181 *WDS $	Ba^{2+}	4	$I\text{-}C_4H_{10}$	0.54
Gas Production (MSCFD)	829 *WDS $	Sr^{2+}	0	$N\text{-}C_4H_{10}$	0.40
Oil Production (bbl/day)	17 *WDS $	K^+	0	$I\text{-}C_5H_{12}$	0.17
Wellhead Temp. (°F)	93 *G	Fe^{2+}	0	$N\text{-}C_5H_{12}$	0.12
Wellhead Pressure (psia)	1190 *G	Cl^-	10300	C_6H_{14}	0.12
Bottomhole Temp. (°F)	284 *WDS	SO_4^{2-}	32	C_{7+}	0.22
Bottomhole Pressure (psia)	3500 *WDS $	CO_3^{2-}	0	N_2	0.28
		HCO_3^-	696	CO_2	0.40
				H_2S	0.00

Comments :

*G from Gas Analysis; *K from Kinley Survey; *WDS from Workover Data Sheet; *W from Water Analysis;

*AA assumed average of Bottomhole Temp. of Flores Fields JAGARCIA 2 (284°F) & JAGARCIA 3 (261°F)

$ measured in 2/1989

TABLE XIV

INPUT DATA FOR CASE XIV : JA GARCIA #3, Flores

Well Geometry and Production Data		Water Analysis		Gas Analysis	
Completion	01/01/1989 *WDS	Sampled	09/26/1985	Sampled	11/15/1990
Kinley Survey	03/18/1991	Constituent	ppm	Component	mole %
Tubing type	2 3/8" 4.7#EUE *K	Na^+	4580	CH_4	88.79
ID (in.)	1.995 *K	Ca^{2+}	197	C_2H_6	6.73
Depth (ft.)	9300 *K	Mg^{2+}	1140	C_3H_8	2.14
Water Production (bbl/day)	182 *WDS $	Ba^{2+}	4	$I\text{-}C_4H_{10}$	0.64
Gas Production (MSCFD)	838 *WDS $	Sr^{2+}	0	$N\text{-}C_4H_{10}$	0.48
Oil Production (bbl/day)	14 *WDS $	K^+	0	$I\text{-}C_5H_{12}$	0.24
Wellhead Temp. (°F)	106 *G	Fe^{2+}	0	$N\text{-}C_5H_{12}$	0.16
Wellhead Pressure (psia)	1200 *G	Cl^-	10300	C_6H_{14}	0.20
Bottomhole Temp. (°F)	261 *WDS	SO_4^{2-}	32	C_{7+}	0.34
Bottomhole Pressure (psia)	3260 *WDS $	CO_3^{2-}	0	N_2	0.24
		HCO_3^-	696	CO_2	0.04
				H_2S	0.00

Comments :

*G from Gas Analysis; *K from Kinley Survey; *WDS from Workover Data Sheet; *W from Water Analysis;

*AA assumed average of Bottomhole Temp. of Flores Fields JAGARCIA 2 (284°F) & JAGARCIA 3 (261°F)

$ measured in 4/1989

TABLE XV

INPUT DATA FOR CASE XV : YTURRIA L&C -B- #4, Flores

Well Geometry and Production Data		Water Analysis		Gas Analysis	
Completion	04/08/1988 *WDS	Sampled	11/09/1988	Sampled	03/21/1991
Kinley Survey	02/19/1991	Constituent	ppm	Component	mole %
Tubing type	2 3/8" 4.7#AB MOD EUE *K	Na^+	7830	CH_4	88.87
ID (in.)	1.995 *K	Ca^{2+}	319	C_2H_6	5.58
Depth (ft.)	9930 *K	Mg^{2+}	14	C_3H_8	1.65
Water Production (bbl/day)	73 *WDS $	Ba^{2+}	13	$I\text{-}C_4H_{10}$	0.42
Gas Production (MSCFD)	1534 *WDS $	Sr^{2+}	0	$N\text{-}C_4H_{10}$	0.36
Oil Production (bbl/day)	102 *WDS $	K^+	0	$I\text{-}C_5H_{12}$	0.20
Wellhead Temp. (°F)	117 *G	Fe^{2+}	0	$N\text{-}C_5H_{12}$	0.12
Wellhead Pressure (psia)	1177 *G	Cl^-	12600	C_6H_{14}	0.16
Bottomhole Temp. (°F)	272 *AA	SO_4^{2-}	0	C_{7+}	0.37
Bottomhole Pressure (psia)	6400 *WDS $	CO_3^{2-}	0	N_2	0.13
		HCO_3^-	146	CO_2	2.14
				H_2S	0.00

Comments :

*G from Gas Analysis; *K from Kinley Survey; *WDS from Workover Data Sheet; *W from Water Analysis;

*AA assumed average of Bottomhole Temp. of Flores Fields JAGARCIA 2 (284°F) & JAGARCIA 3 (261°F)

$ measured in 5/5//1988

TABLE XVI

INPUT DATA FOR CASE XVI : YTURRIA L&L -C- #4, Flores

Well Geometry and Production Data		Water Analysis		Gas Analysis	
Completion	04/15/1987 *WDS	Sampled	06/03/1988	Sampled	11/20/1990
Kinley Survey	03/15/1991	Constituent	ppm	Component	mole %
Tubing type	2 3/8" 4.7#EUE *K	Na^+	5850	CH_4	89.42
ID (in.)	1.995 *K	Ca^{2+}	564	C_2H_6	6.00
Depth (ft.)	9500 *K	Mg^{2+}	33	C_3H_8	1.84
Water Production (bbl/day)	33 *WDS $	Ba^{2+}	1	$I\text{-}C_4H_{10}$	0.50
Gas Production (MSCFD)	7096 *WDS $	Sr^{2+}	0	$N\text{-}C_4H_{10}$	0.40
Oil Production (bbl/day)	258 *WDS $	K^+	0	$I\text{-}C_5H_{12}$	0.22
Wellhead Temp. (°F)	130 *G	Fe^{2+}	0	$N\text{-}C_5H_{12}$	0.14
Wellhead Pressure (psia)	1230 *G	Cl^-	9800	C_6H_{14}	0.20
Bottomhole Temp. (°F)	272 *AA	SO_4^{2-}	218	C_{7+}	0.40
Bottomhole Pressure (psia)	5940 *WDS $	CO_3^{2-}	0	N_2	0.23
		HCO_3^-	263	CO_2	0.65
				H_2S	0.00

Comments :

*G from Gas Analysis; *K from Kinley Survey; *WDS from Workover Data Sheet; *W from Water Analysis;

*AA assumed average of Bottomhole Temp. of Flores Fields JAGARCIA 2 (284°F) & JAGARCIA 3 (261°F)

$ measured in 11/1987

TABLE XVII

INPUT DATA FOR CASE XVII : Phillips Case 1 A#1, Orchard

Well Geometry and Production Data		Water Analysis		Gas Analysis	
Completion	10/27/1985 *BD	Sampled	05/21/1990	Sampled	10/31/1989
Kinley Survey	12/13/1989	Constituent	ppm	Component	mole %
Tubing type	2 7/8" 6.4#VAM *K	Na^+	8734.25	CH_4	89.17
ID (in.)	2.441 *K	Ca^{2+}	441.06	C_2H_6	4.77
Depth (ft.)	9596 *K	Mg^{2+}	243.03	C_3H_8	1.62
Water Production (bbl/day)	31 *usl	Ba^{2+}	8.24	$I\text{-}C_4H_{10}$	0.29
Gas Production (MSCFD)	11500 *usl	Sr^{2+}	0	$N\text{-}C_4H_{10}$	0.37
Oil Production (bbl/day)	110 *usl	K^+	0	$I\text{-}C_5H_{12}$	0.14
Wellhead Temp. (°F)	185 *usl	Fe^{2+}	0	$N\text{-}C_5H_{12}$	0.10
Wellhead Pressure (psia)	2515 *usl	Cl^-	14998.2	C_6H_{14}	0.00
Bottomhole Temp. (°F)	297 *usl	SO_4^{2-}	19	C_{7+}	0.28
Bottomhole Pressure (psia)	4230 *usl	CO_3^{2-}	0	N_2	0.24
		HCO_3^-	134.23	CO_2	3.03
				H_2S	0.001

Comments :

*G from Gas Analysis; *K from Kinley Survey; *USL from USL Data Sheet; *W from Water Analysis;

TABLE XVIII

INPUT DATA FOR CASE XVIII : Phillips Case 2 S#1, Orchard

Well Geometry and Production Data		Water Analysis		Gas Analysis	
Completion	12/01/1986 *BD	Sampled	05/21/1990	Sampled	10/31/1989
Kinley Survey	11/28/1989	Constituent	ppm	Component	mole %
Tubing type	2 7/8" 8.7#NEW VAM *K	Na^+	14542.4	CH_4	88.25
ID (in.)	2.375 *usl	Ca^{2+}	6776.26	C_2H_6	5.15
Depth (ft.)	12072 *K	Mg^{2+}	534.66	C_3H_8	1.68
Water Production (bbl/day)	15.6 *usl	Ba^{2+}	68.63	$I\text{-}C_4H_{10}$	0.32
Gas Production (MSCFD)	7550	Sr^{2+}	0	$N\text{-}C_4H_{10}$	0.39
Oil Production (bbl/day)	53 *usl	K^+	0	$I\text{-}C_5H_{12}$	0.16
Wellhead Temp. (°F)	95 *usl	Fe^{2+}	0	$N\text{-}C_5H_{12}$	0.10
Wellhead Pressure (psia)	1790 *usl	Cl^-	35995.7	C_6H_{14}	0.00
Bottomhole Temp. (°F)	320 *usl	SO_4^{2-}	0.12	C_{7+}	0.38
Bottomhole Pressure (psia)	3645 *usl	CO_3^{2-}	0	N_2	0.31
		HCO_3^-	359.98	CO_2	3.27
				H_2S	0.001

Comments :

*G from Gas Analysis; *K from Kinley Survey; *USL from USL Data Sheet; *W from Water Analysis;

TABLE XIX

DREAM INPUT DATA SHEET

Well Geometry and Production Data		Water Analysis		Gas Analysis	
		Constituent	ppm	Component	mole %
ID (in.)		Na^+		CH_4	
Depth (ft.)		Ca^{2+}		C_2H_6	
Water Production (bbl/day)		Mg^{2+}		C_3H_8	
Gas Production (MSCFD)		Ba^{2+}		$I\text{-}C_4H_{10}$	
Oil Production (bbl/day)		Sr^{2+}		$N\text{-}C_4H_{10}$	
Separator Temp. (°F)		K^+		$I\text{-}C_5H_{12}$	
Separator Pressure (psia)		Fe^{2+}		$N\text{-}C_5H_{12}$	
Wellhead Temp. (°F)		Cl^-		C_6H_{14}	
Wellhead Pressure (psia)		SO_4^{2-}		C_{7+}	
Bottomhole Temp. (°F)		CO_3^{2-}		N_2	
Bottomhole Pressure (psia)		HCO_3^-		CO_2	
				H_2S	

analyzed is 1 g/cc. From the above assumption it follows that 1 mg/l = 1 ppm.

The corrosion rate profiles are obtained from the Kinley Caliper Survey and are then used for comparison with the DREAM predictions. The Kinley Survey reports the actual conditions of the tubing as surveyed by running caliper feelers along the length of the well. The model results, however, are predictions of uniform corrosion rates with the assumption that no protective corrosion product layer is formed. The Kinley Caliper Survey is available in all the 18 cases. In all cases, the first Kinley Survey report was used to calculate the corrosion rate. The Kinley Survey provides a tabulation of the joint number and the maximum well body penetration (inches). The well depth is equally divided depending on the number of joints available. This is based on the assumption that all joints are of equal length. The maximum body penetration is converted to corrosion rate (MPY) using the following expression

$$CR = \left(\frac{\text{maximum well body penetration (inch)}}{\text{years between well completion and first survey}} * \frac{1000 \text{ mil}}{1 \text{ inch}} \right) \qquad (4.1)$$

In Cases VII, XV, and XVI Sundaram (1996) had used the total iron concentration from the water analysis instead of the dissolved iron content as the input data for the Fe^{2+} ion concentration from the water analysis. The amount of dissolved iron should be used, as this would represent the amount of iron present as ions (Fe^{2+}). This has been accounted for in the inputs used in the present work. However, in future work, provision should be made for also using the total iron concentration, as this will provide a way to account for the precipitation of iron as iron carbonates and sulfides.

4.2 DREAM Predictions

The developed model has been used to predict corrosion rates in the 18 cases mentioned in the previous section. Studies have also been conducted which gives us a better understanding of the effect of different parameters on the corrosion process. The corrosion rates predicted by DREAM are for uniform corrosion without film formation. In reality, it is very rare to find such a situation. The constantly changing well conditions along with the low accuracy of the collected field data lead to limitations in the accuracy with which corrosion rates can be predicted. These limitations have to be kept in mind when such corrosion predictions tools are evaluated. However, the purpose of this work has been to develop a model based on fundamental principles that would help us gain a better understanding of the corrosion mechanism. The observations made from these studies are described next.

4.2.1 Case Studies

The model gives reasonable estimates of the corrosion rates however the model does significantly underpredicts corrosion rates. The DREAM corrosion rate predictions using the proposed model are compared against the Kinley Survey reports for the 18 cases in Figures 3-20. The order of magnitude of predicted corrosion rates is consistently much smaller when compared to that obtained from the caliper data. However, the trends predicted parallel reasonably well with those observed in the caliper data.

The predicted corrosion profiles in Cases IV, V, VI, X, and XI indicates that the corrosion rate gradually increases as we approach the top of the well. In Cases I, XVII, and XVIII, the overall trend is very similar to that mentioned above, however, there are

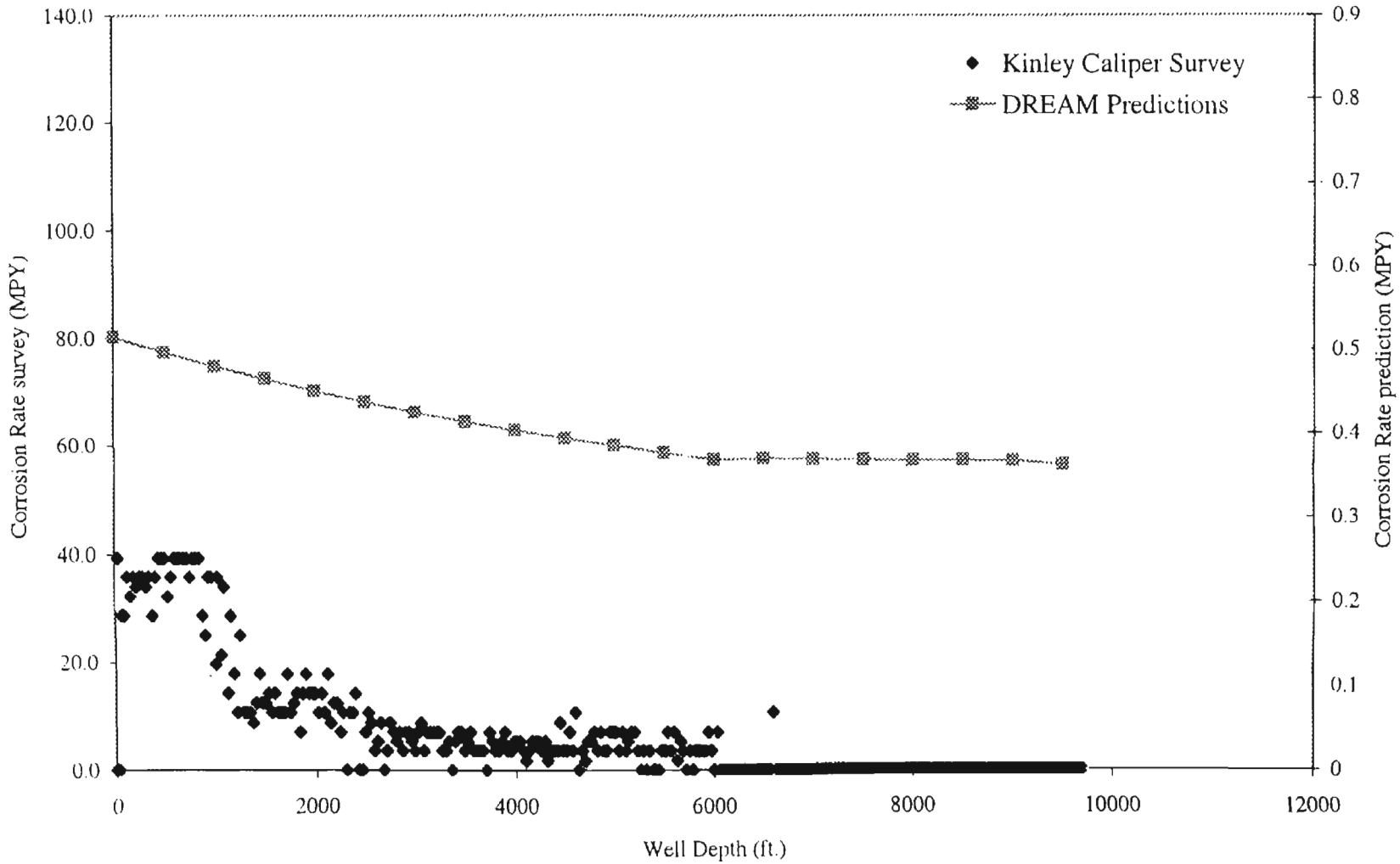

Figure 3. Corrosion Rate Profile along Well Depth: CASE I

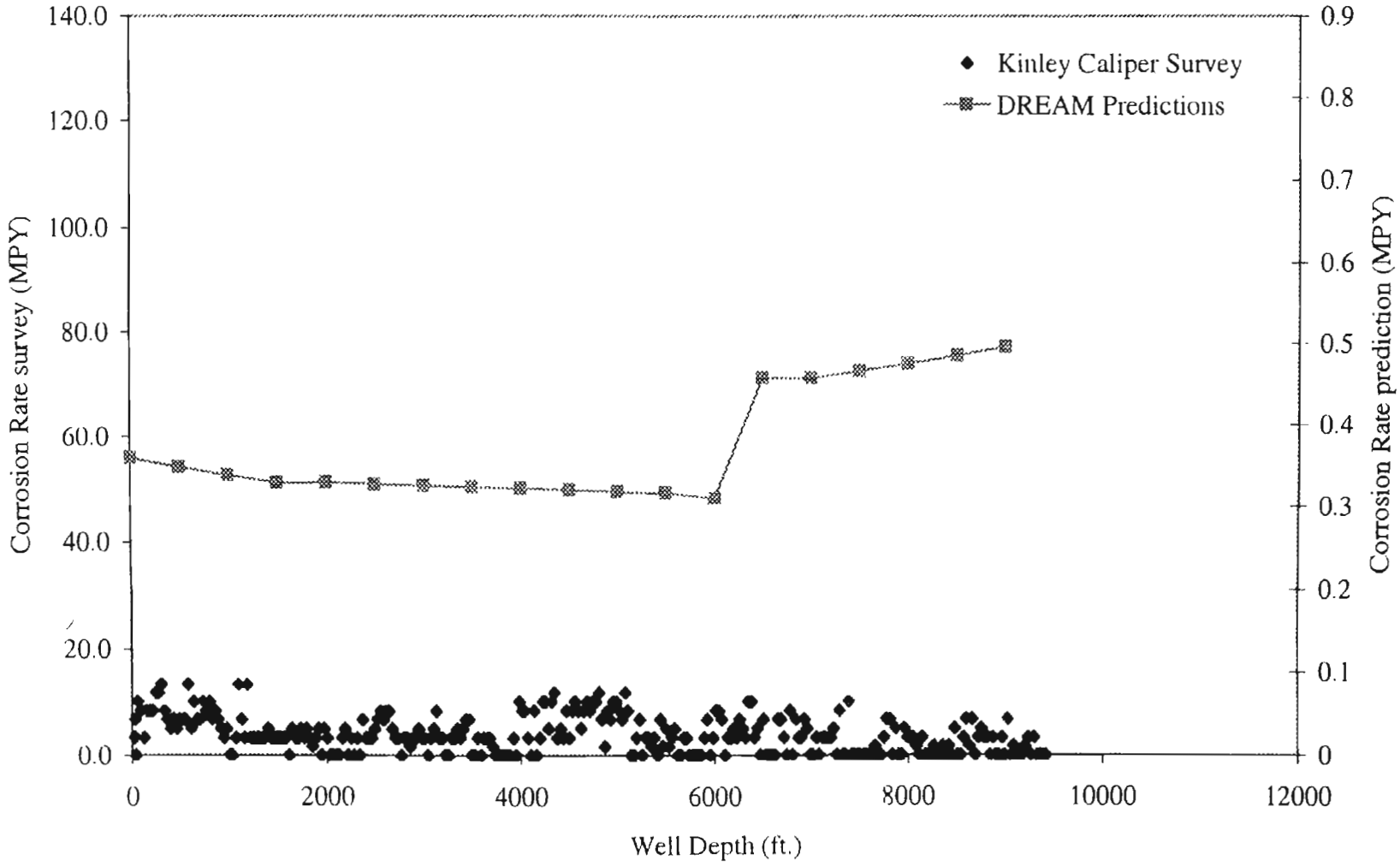

Figure 4. Corrosion Rate Profile along Well Depth: CASE II

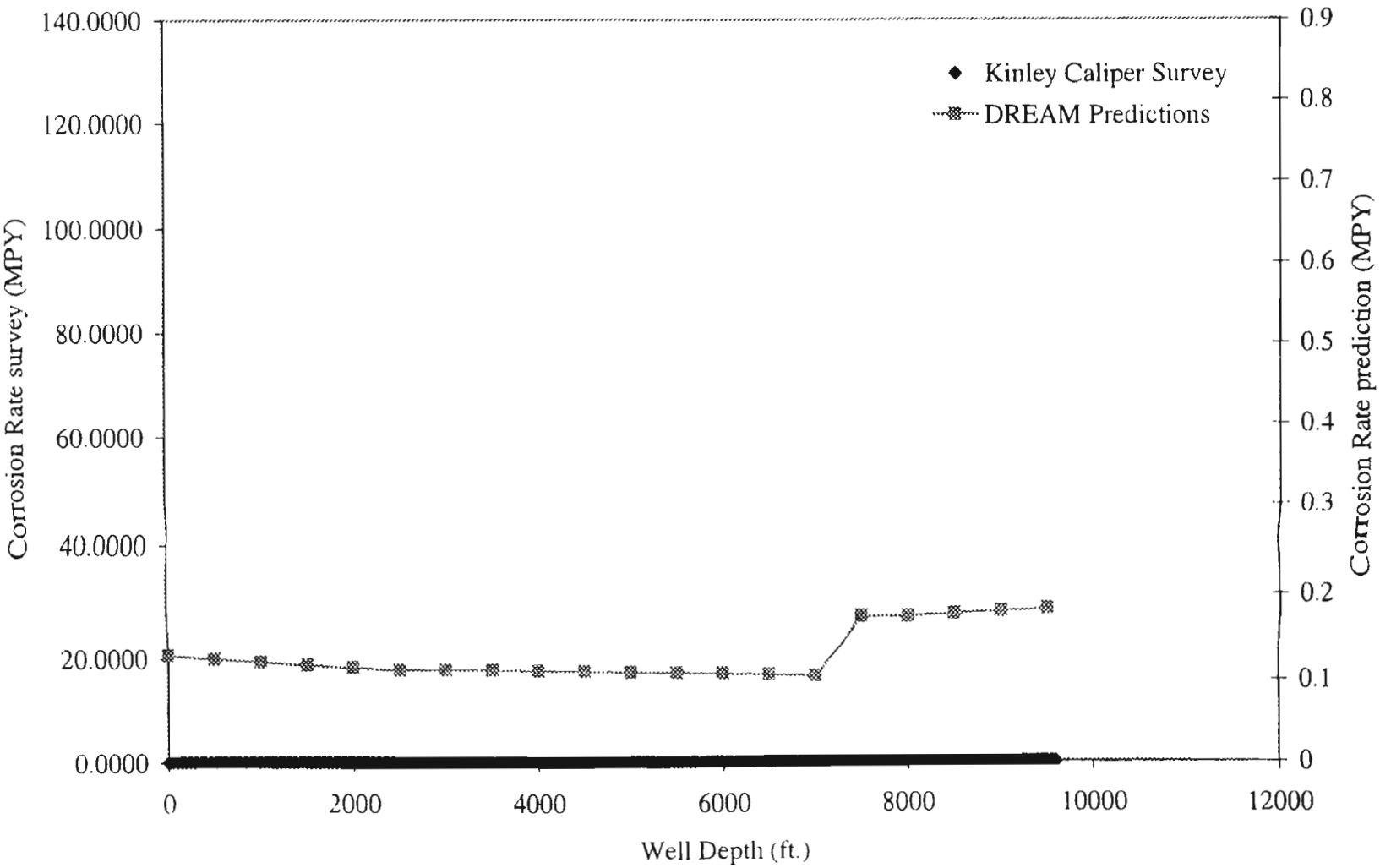

Figure 5. Corrosion Rate Profile along Well Depth: CASE III

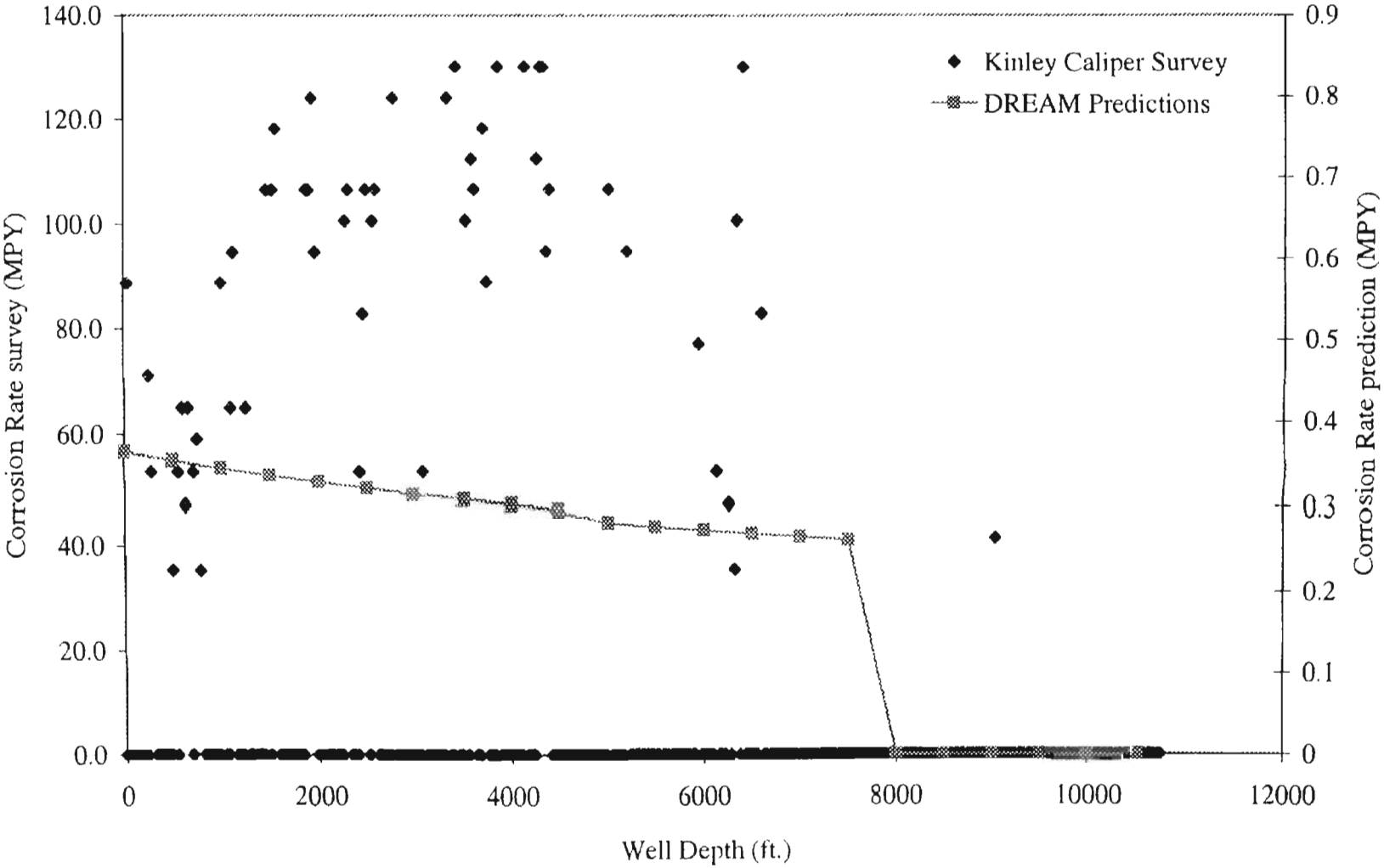

Figure 6. Corrosion Rate Profile along Well Depth: CASE IV

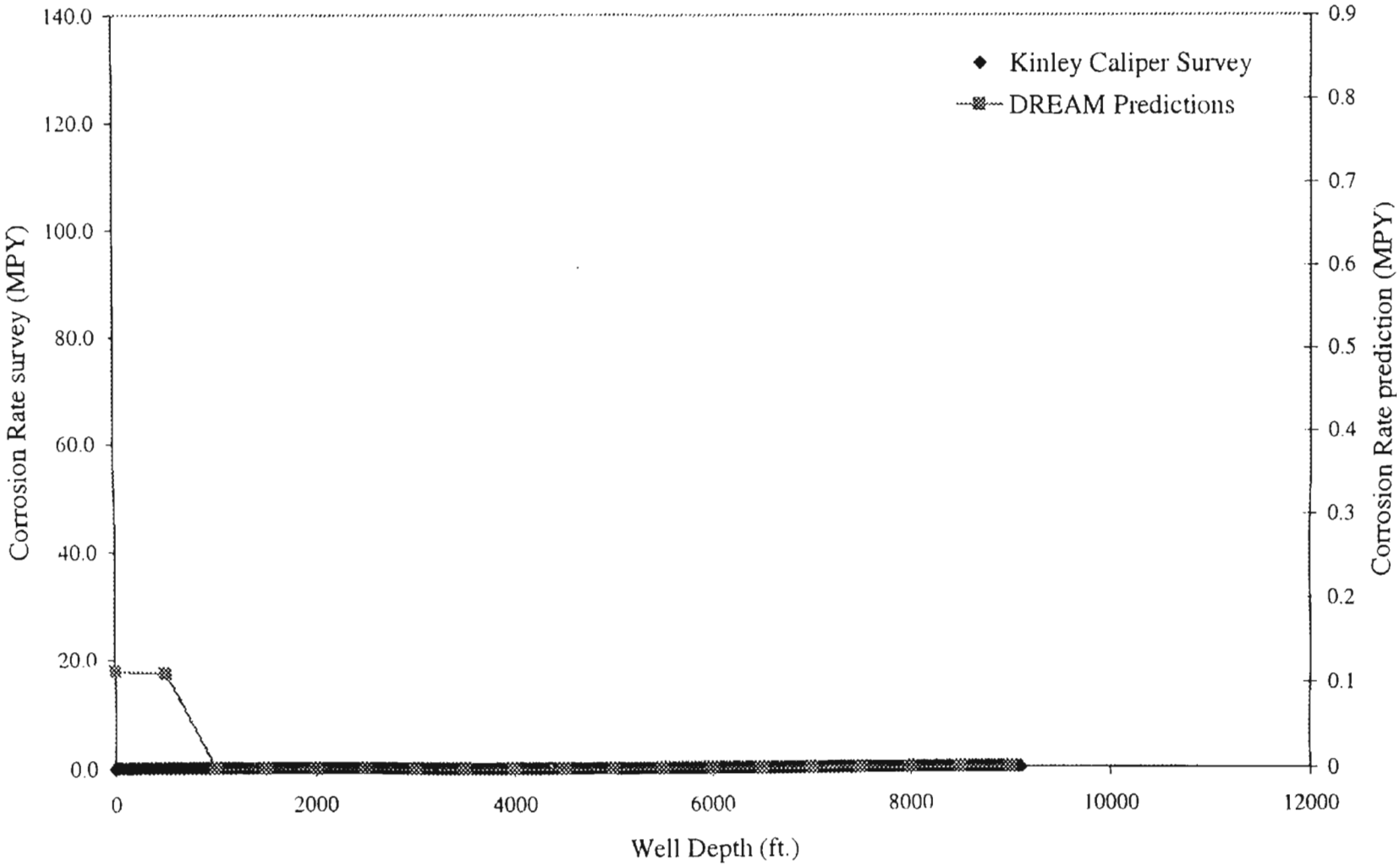

Figure 7. Corrosion Rate Profile along Well Depth: CASE V

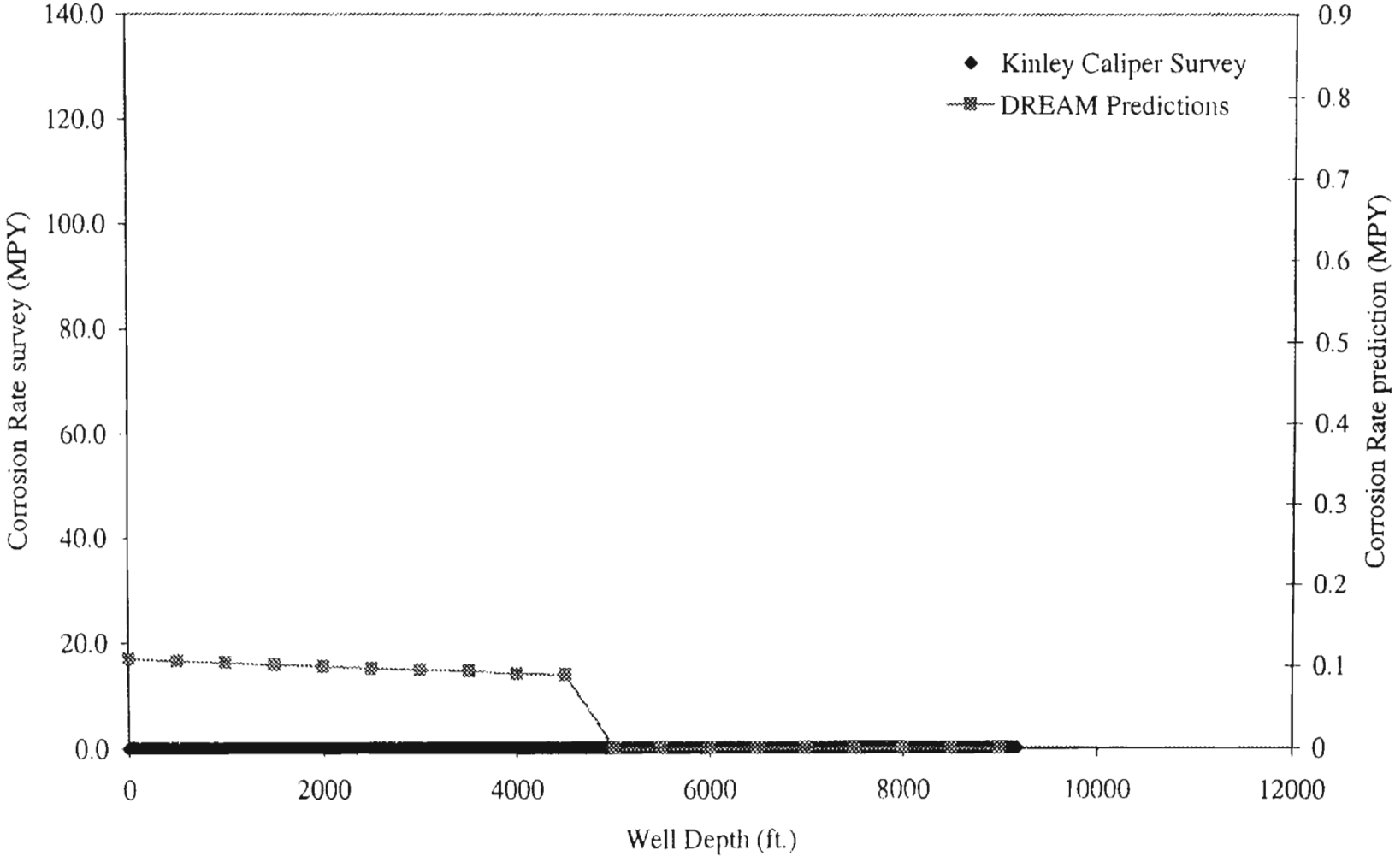

Figure 8. Corrosion Rate Profile along Well Depth: CASE VI

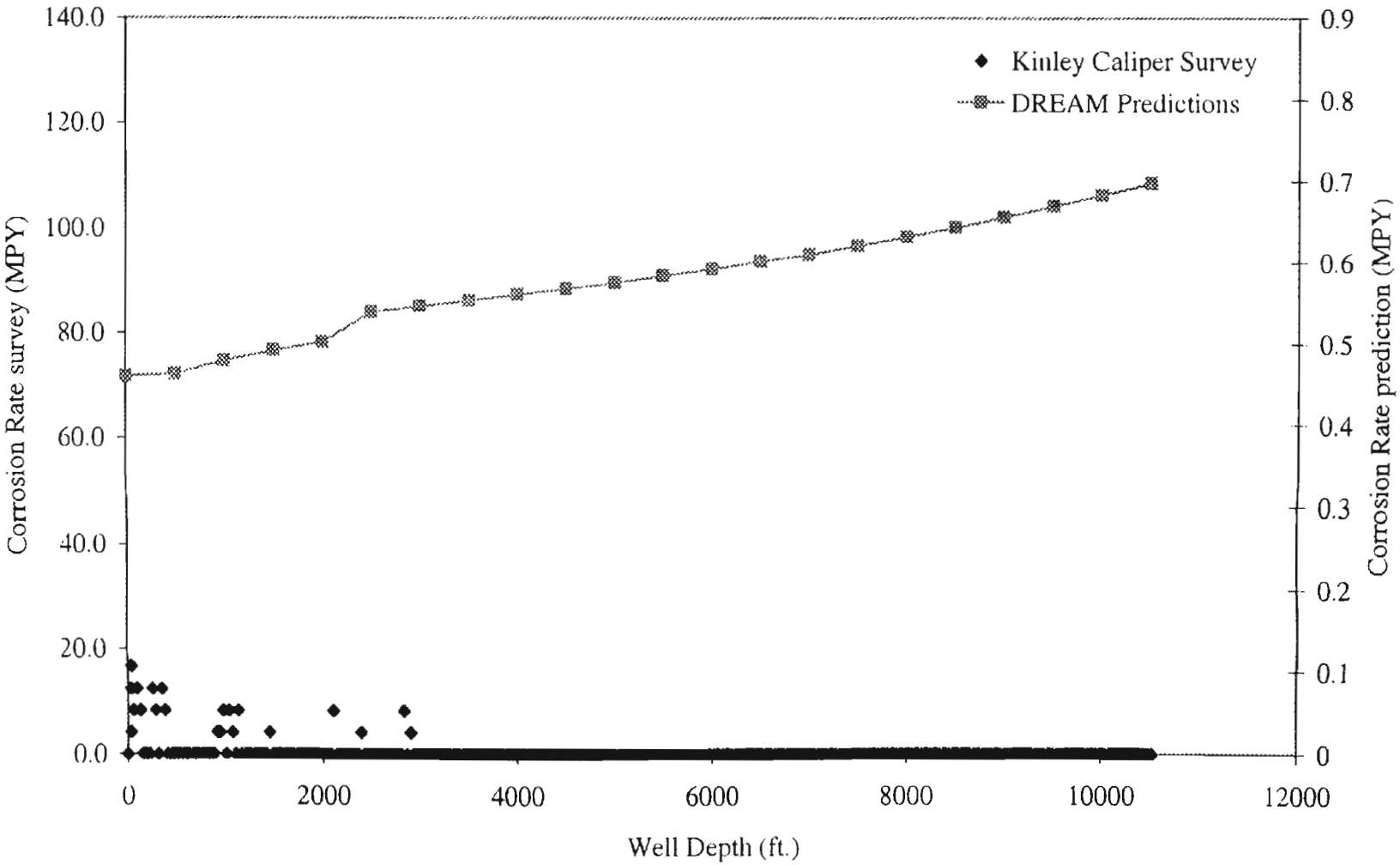

Figure 9. Corrosion Rate Profile along Well Depth: CASE VII

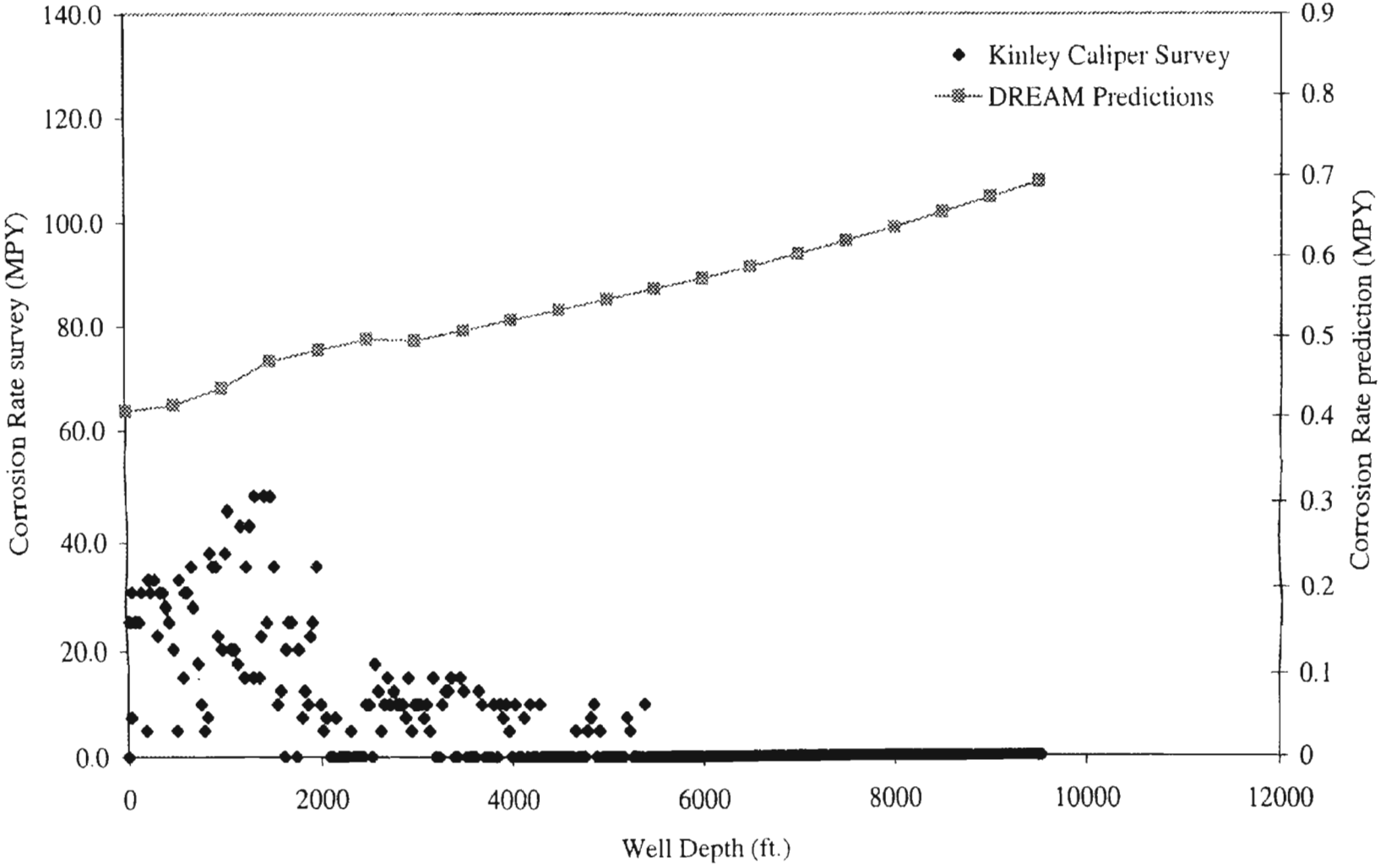

Figure 10. Corrosion Rate Profile along Well Depth: CASE VIII

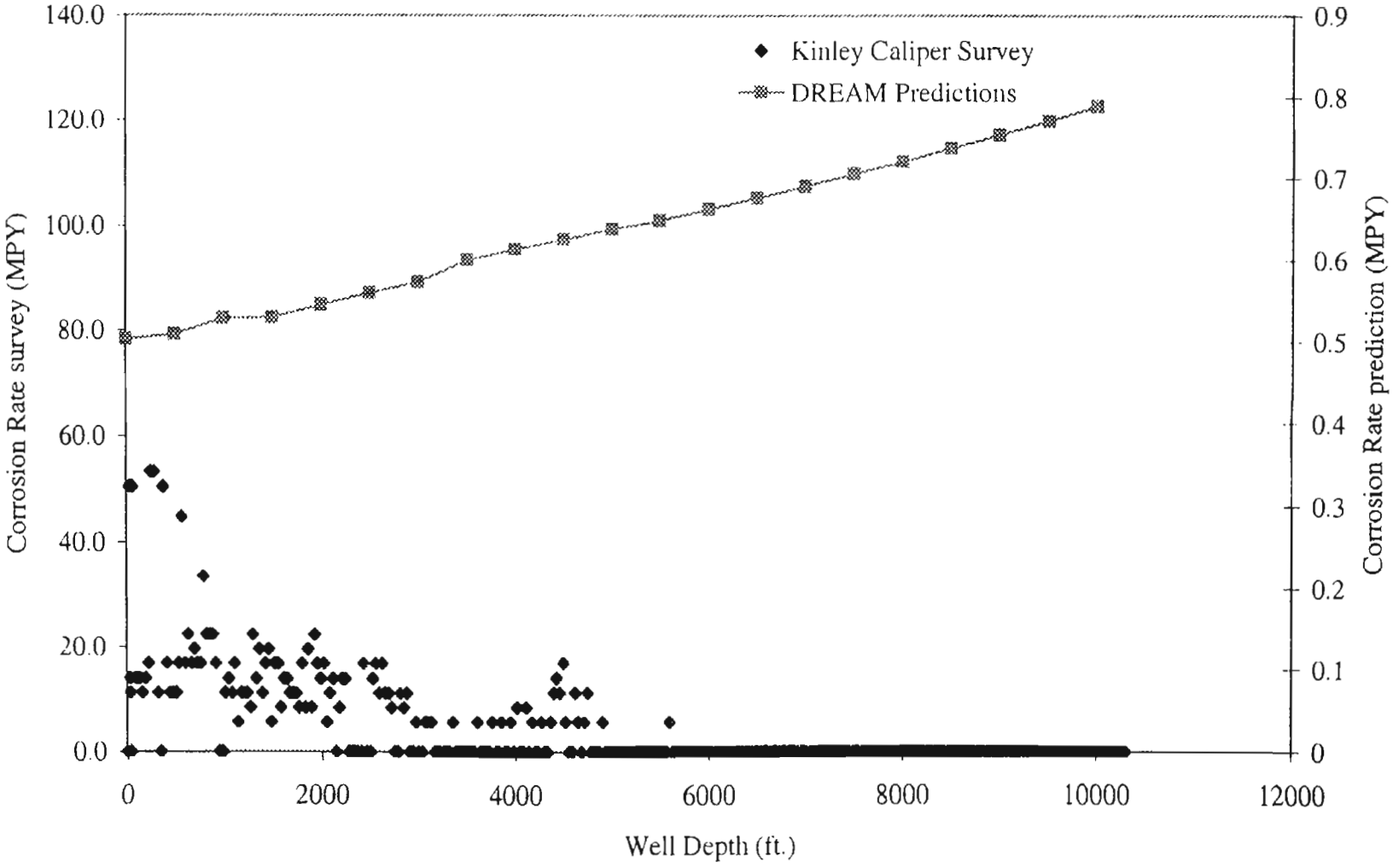

Figure 11. Corrosion Rate Profile along Well Depth: CASE IX

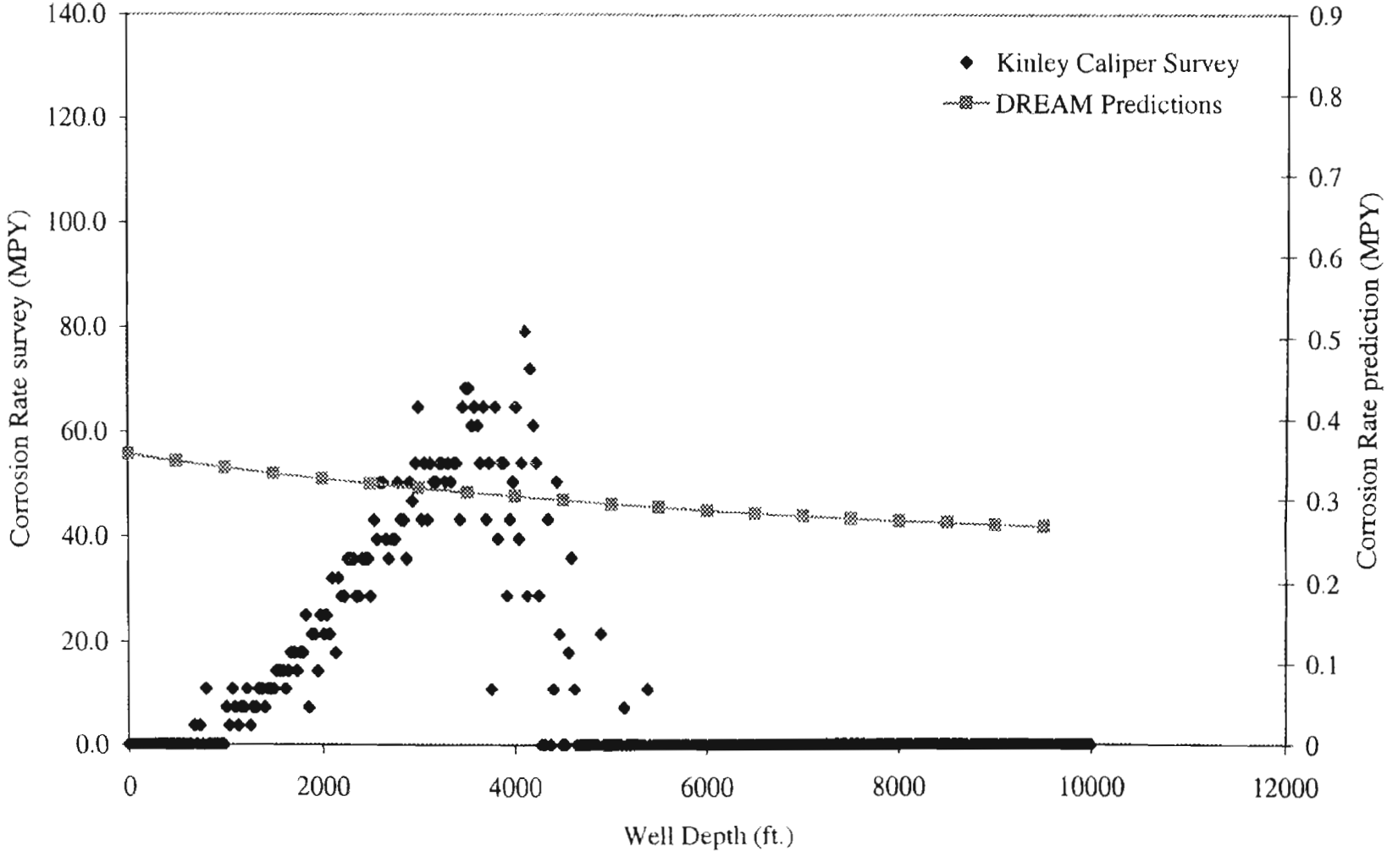

Figure 12. Corrosion Rate Profile along Well Depth: CASE X

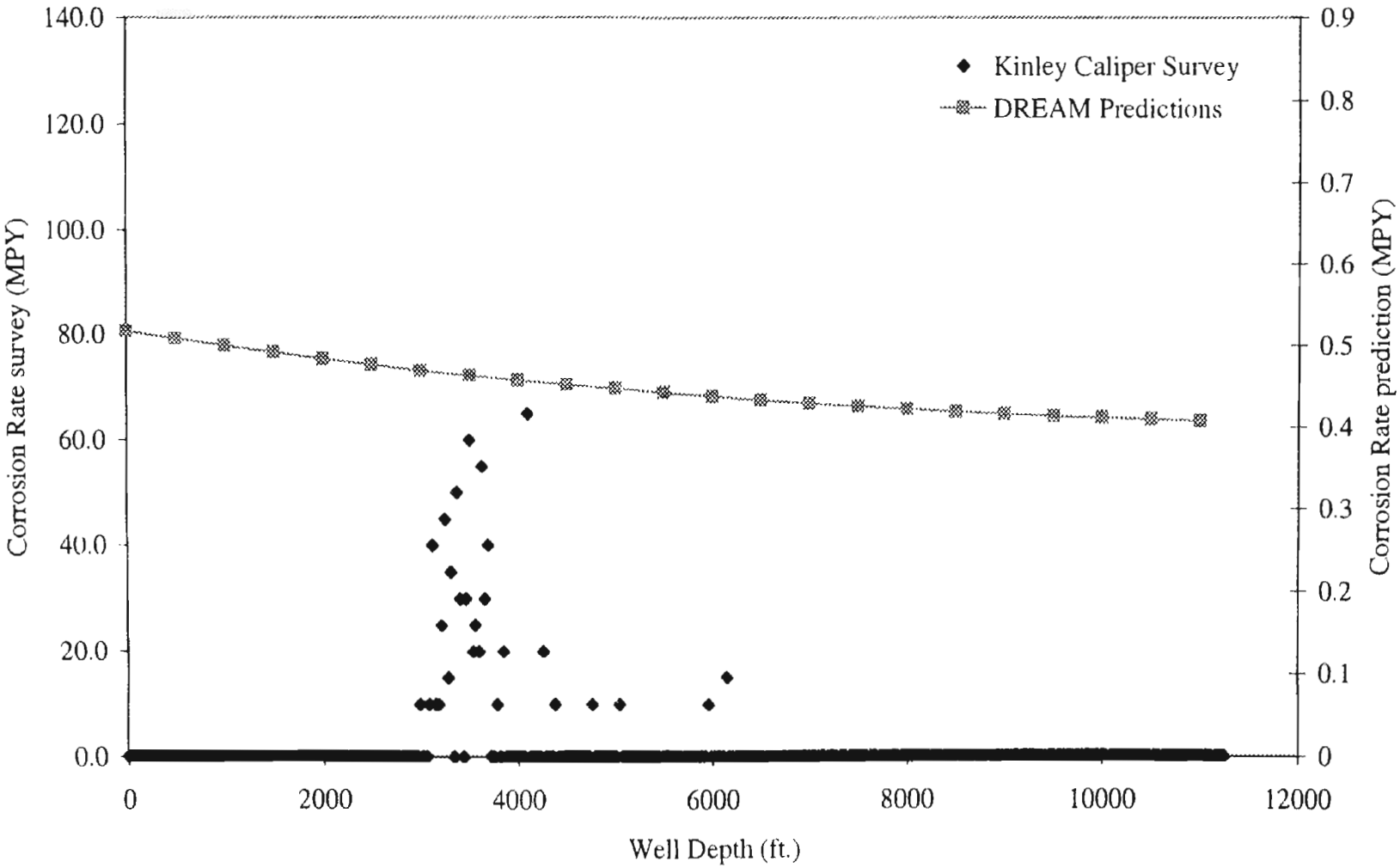

Figure 13. Corrosion Rate Profile along Well Depth: CASE XI

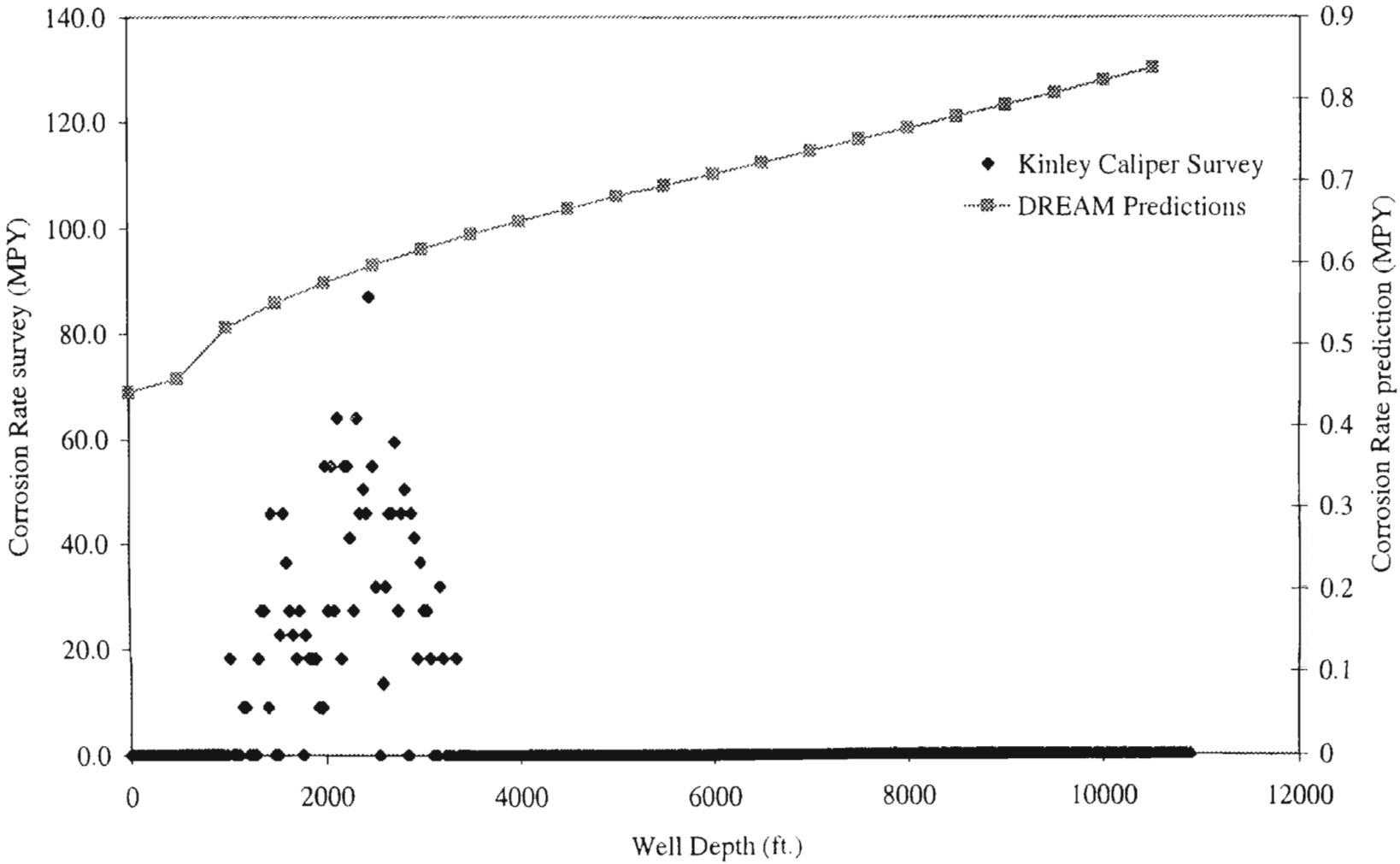

Figure 14. Corrosion Rate Profile along Well Depth: CASE XII

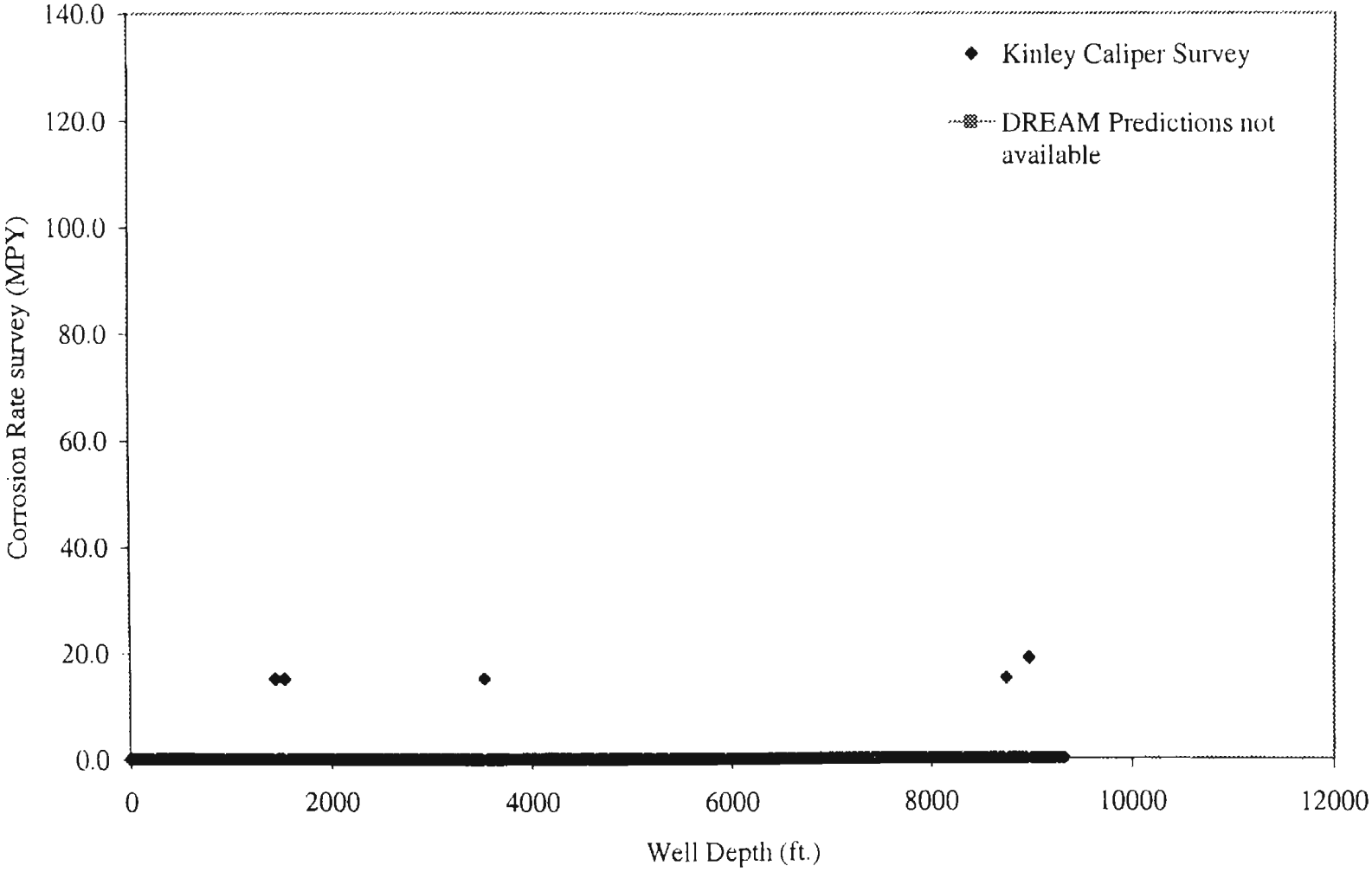

Figure 15. Corrosion Rate Profile along Well Depth: CASE XIII

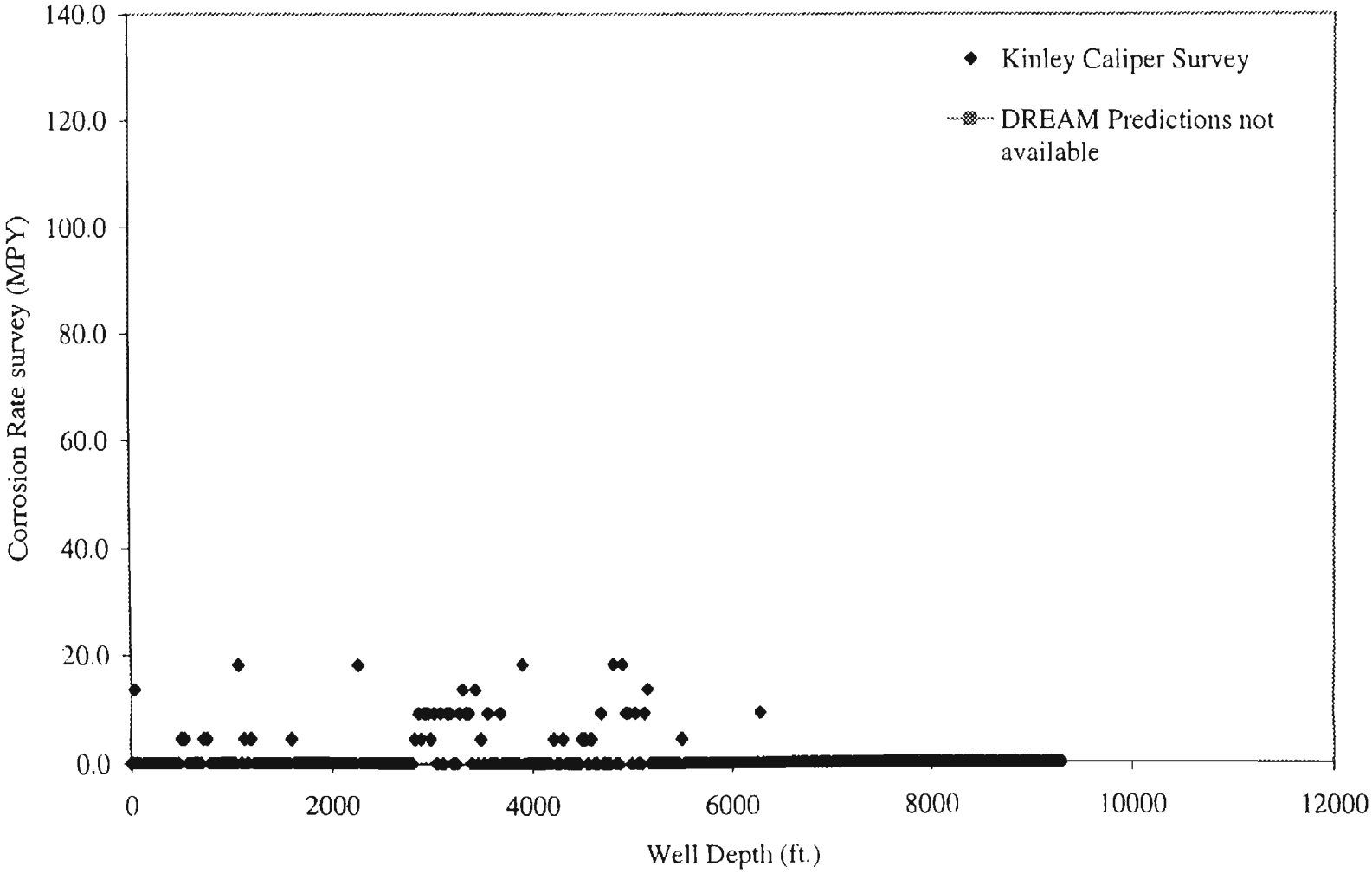

Figure 16. Corrosion Rate Profile along Well Depth: CASE XIV

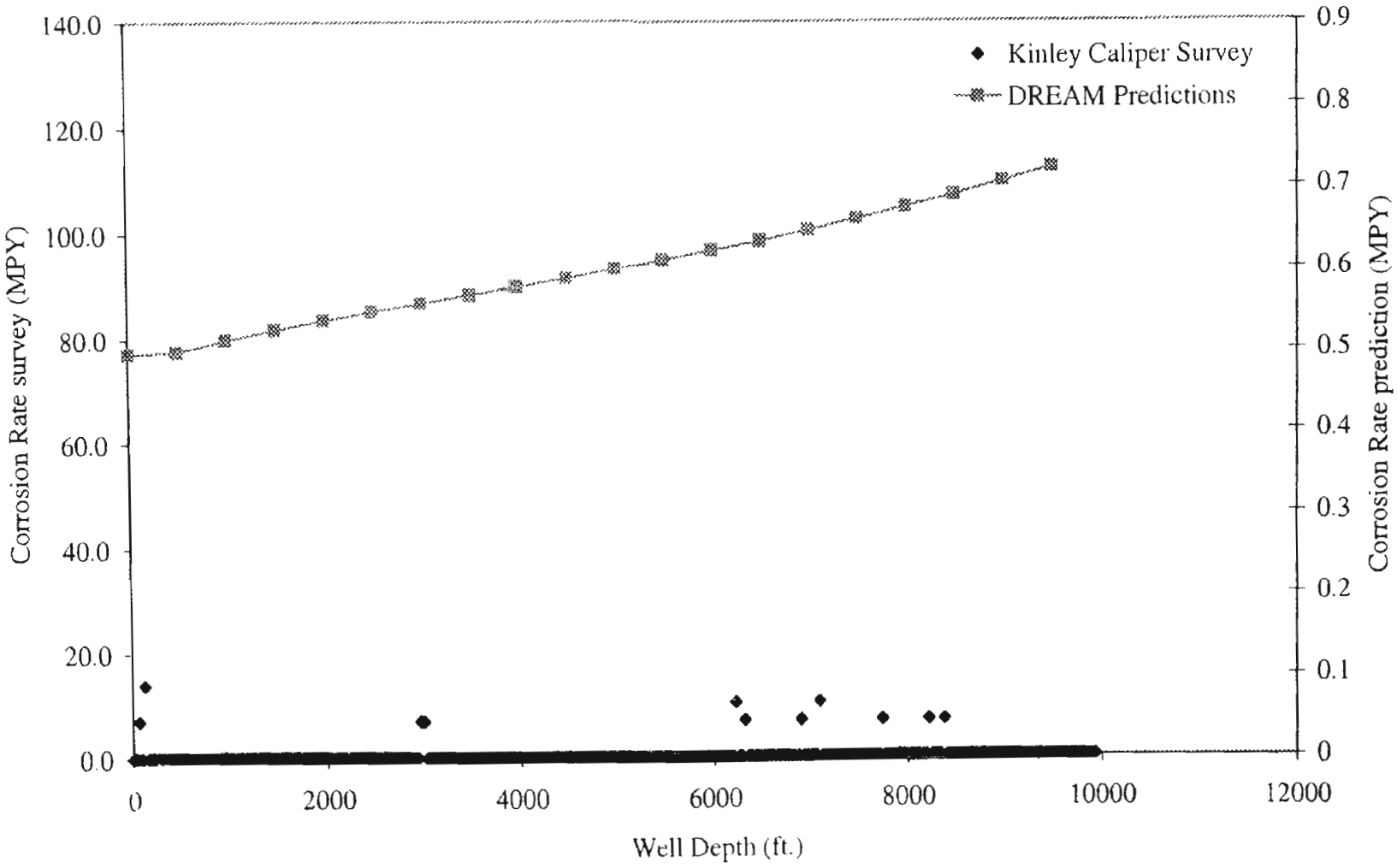

Figure 17. Corrosion Rate Profile along Well Depth: CASE XV

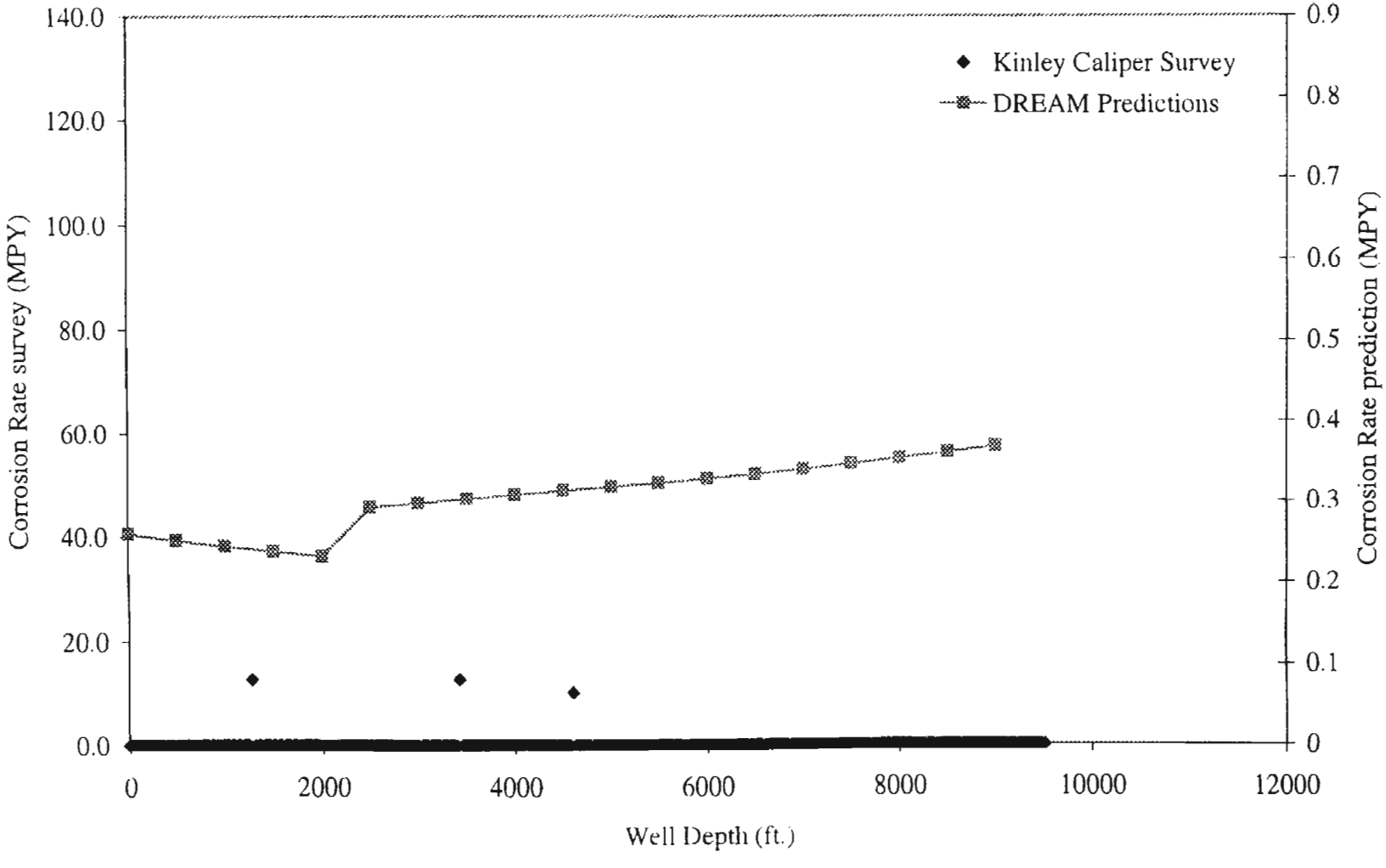

Figure 18. Corrosion Rate Profile along Well Depth: CASE XVI

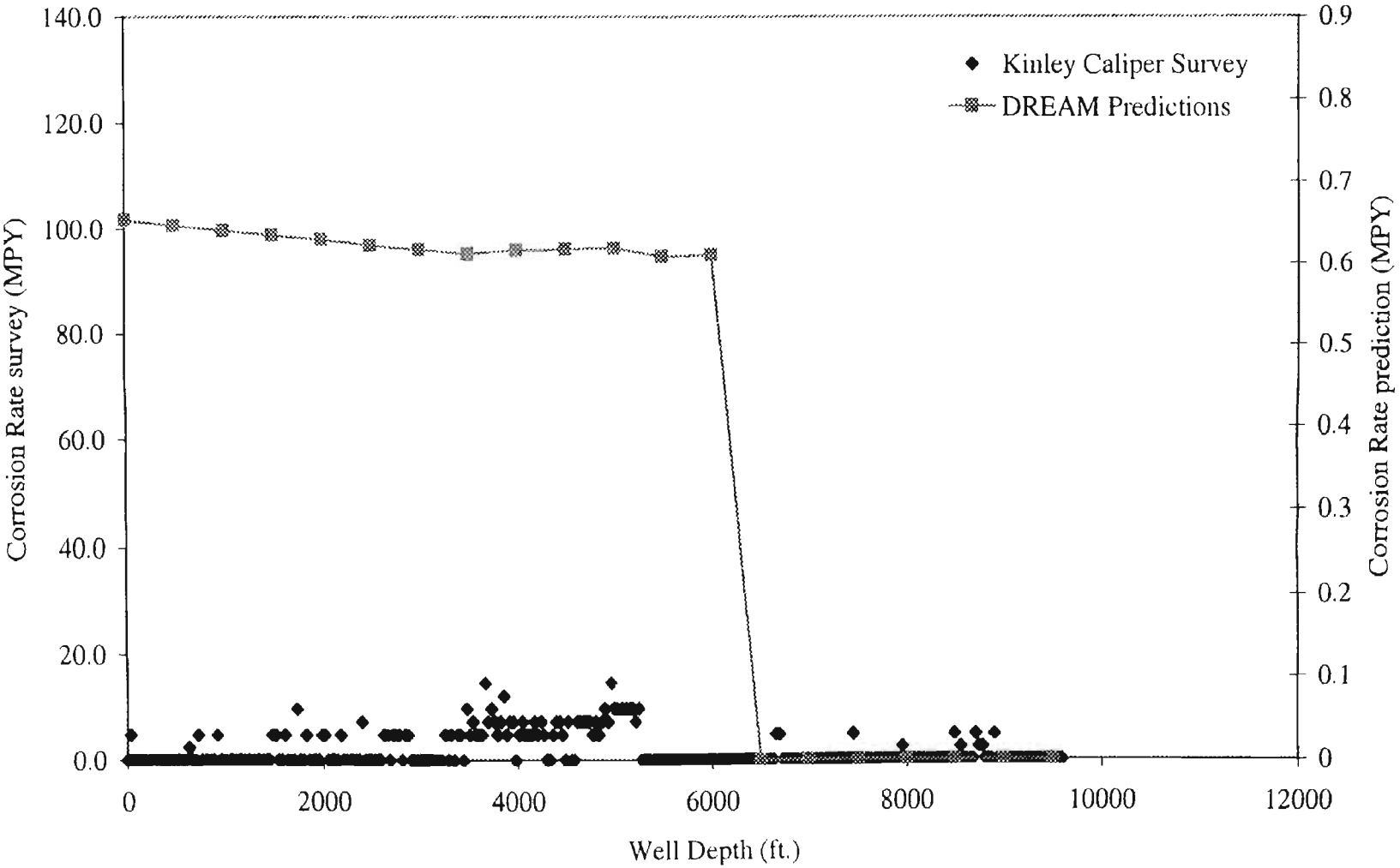

Figure 19. Corrosion Rate Profile along Well Depth: CASE XVII

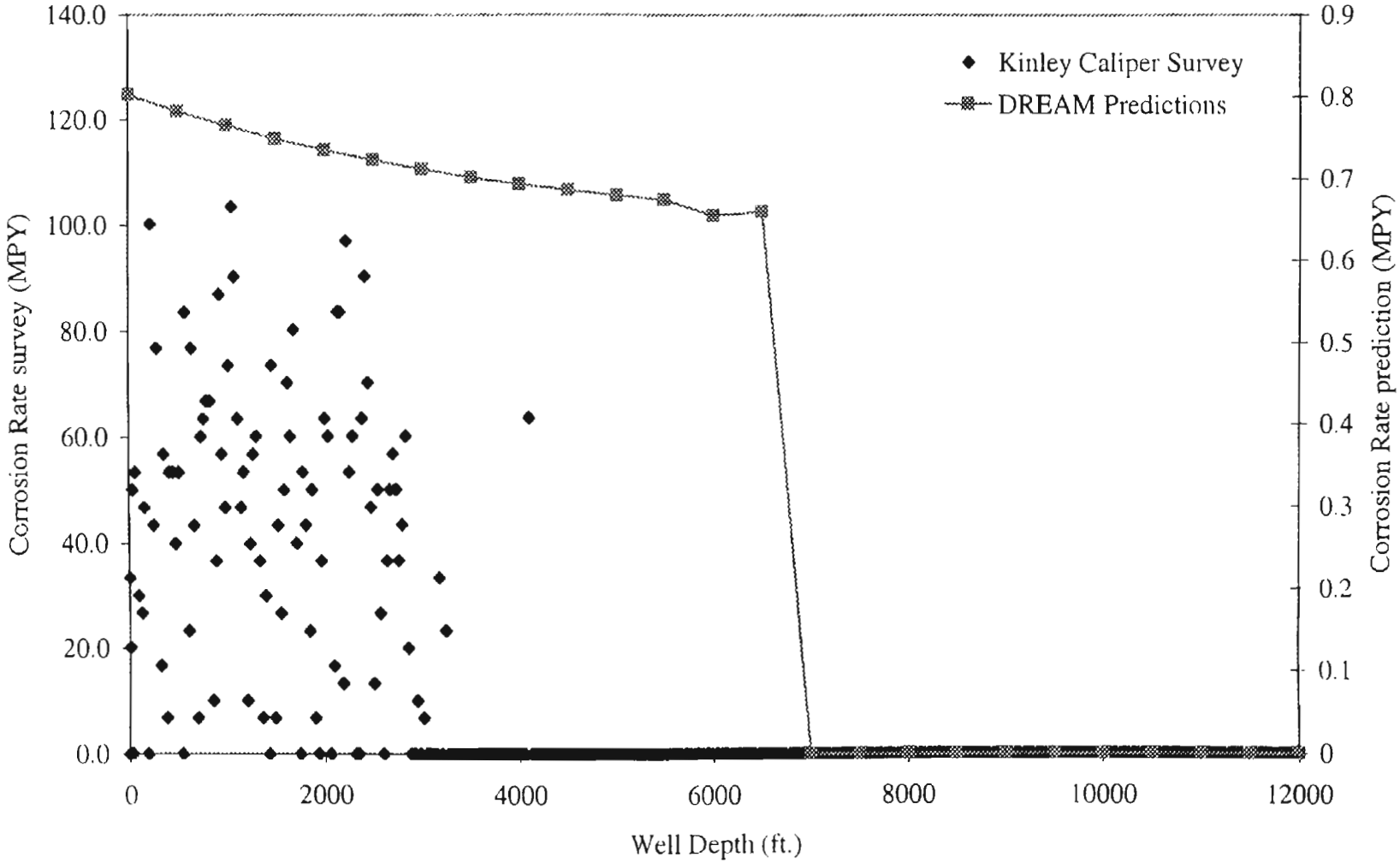

Figure 20. Corrosion Rate Profile along Well Depth: CASE XVIII

some sections in the well where corrosion rate decreases as the well head is approached. In all the cases (except Cases XIII and XIV) the shape of corrosion rate profiles is a mirror image of the pH profiles. As the pH decreases the corrosion rate increases and vice-versa. The increase in predicted corrosion rate as we approach the wellhead is due to the increase in proton concentration in the laminar sublayer. As we approach the wellhead the amount of CO_2 dissolving in the liquid phase increases. This in turn leads to an increase in the amount of protons generated and results in a lower pH and higher corrosion rates as we approach the top. However in Cases I, XVII, and XVIII, there seems to be some exception to the above hypothesis. The exact cause for the exceptions in certain regions in Cases I, XVII, and XVIII is uncertain. That is there are some regions in these cases where the corrosion rate does not increase as we move up. This can be attributed to the pH curve, the shape of which is exactly reflected in the corrosion rate profile. In some cases a maximum is observed in the calculated pH while in others it is not (refer Appendix B). This may be the reason for these exceptions.

In Cases II, III, VII, VIII, IX, XII, XV, XVI the trends predicted were irregular. No consistent pattern was observed in these cases. Further investigation explained that these inconsistent and different trends were caused due to the fact that the pressure drop calculations failed to converge. The convergence problem is further explained later in this chapter.

In Case XIII and Case XIV the FORTRAN program halted execution due to convergence problems in the calculation of the dew point temperatures in the well sections.

In Cases IV, VI, XVII, and XVIII, discontinuities were observed in the corrosion rate profiles. This was further studied and was observed to be related to the transitions between annular and slug flow regimes. The laminar layer thickness decreases as we approach the top of the well. In Case IV below 7500 ft the corrosion rate is zero because of the single-phase region. The laminar layer thickness drops suddenly as we move from 5000 ft to 4500 ft and this can be attributed to the flow regime change from annular to slug flow. This drastic decrease in diffusion layer thickness as we move from annular to slug flow results in the discontinuities in the corrosion rate profile in the cases mentioned above.

4.2.2 Influence of Environmental Parameters

The strength of the DREAM corrosion prediction model is that it is based on the fundamentals and provides an understanding of the effects of various parameters on the corrosion process. Studies have been conducted to observe the effect of different parameters on corrosion rate.

CO_2 Concentration:

The concentration of CO_2 was increased to study its influence on the predicted corrosion rates. Case XVIII was used and the mole percent of CO_2 in the gas analysis was increased from 3.274% to 3.374% and then to 3.474%. In order to compensate for this increase the mole percent of C_7+ components was adjusted accordingly. The results from this study are shown in Figure 21. Figure 21 shows that the corrosion rate predicted increases as the CO_2 concentration is increased. This is an expected phenomenon, as an increase in CO_2 would make the well more corrosive. The study was repeated on Case V,

where the mole percent of CO_2 was increased from 0.26% to 0.46% to 0.66%. The results obtained agreed with the above observation.

Pressure:

The effect of the well pressure on the corrosion rate prediction was studied. Case I and V were used for this study and the well pressures were increased. The changes made to conduct this study are summarized in Table XX.

TABLE XX

INPUTS USED IN STUDYING PRESSURE EFFECT

CASE		Wellhead Pressure (psia)	Bottomhole Pressure(psia)	
			Initial Guess	DREAM Prediction
I	a	1170	6765	1493
	b	1200	7765	1516
	c	1300	8785	1555
V	a	1345	7800	1607
	b	1545	8800	1815
	c	1745	9800	2145

In this study when the input pressures are changed there is the possibility of encountering a problem with the convergence of bottomhole pressure. Such convergence problems were not encountered in the above cases.

The results (Figure 22) indicate that the corrosion rates increase as the well pressures were increased. This was further investigated and it was found that increasing

the pressure leads to an increase in the amount of CO_2 dissolved in the condensed layer. This makes the well more corrosive thereby resulting in higher corrosion rates.

Temperature:

In Case V and XVIII the well temperatures were increased to study its influence on the model predictions. When the temperatures are changed the pressure profiles also change slightly as the pressure drop depends on the well temperatures. The data used for studying the effect of temperature on corrosion rates are summarized in the Table XXI.

TABLE XXI

INPUTS USED IN STUDYING TEMPERATURE EFFECT

CASE		Temperature (°F)	
		Wellhead	Bottomhole
V	a	166	275
	b	190	300
	c	220	330
XVIII	a	95	320
	b	130	350
	c	160	380

It was found that the model predicts lower corrosion rates as the well temperatures were increased (Figure 23). Case V is a well with low corrosion and as we increase the temperature from conditions (a) to (c) it was observed that the corrosion predictions decrease to zero throughout the well. This was found to be due to the fact

that as the temperature was increased the flow regimes changed from two phase to single phase, hence resulting in zero corrosion. In Case XVIII, the flow regimes remained the same for conditions (a), (b) and (c). The corrosion rates were found to decrease with increase in temperatures. This was further investigated and it was observed that increasing the temperature decreases the solubility of CO_2 (Figure 24). The decrease in dissolved CO_2 would then lead to lower corrosion rates.

Laminar layer thickness:

The thickness of the diffusion layer was changed to see its effect on the corrosion rates. The diffusion layer thickness was multiplied by a factor of 2(b), 4(c), and 20(d) and the DREAM predictions were compared with the original results of Case XVIII(a). Figure 25 shows that as the diffusion layer thickness increases the corrosion rate decreases. However, above 6000 ft the decrease is very negligible compared to that in the 6000 – 7000 ft region. This is because above 6000 feet, slug flow regime is encountered. Annular flow regime is predicted for the 6000 – 7000 ft. region and below 7000 ft single phase flow is predicted. In the slug flow regime, the thickness of the diffusion layer is smaller (several orders of magnitude) compared to the thickness in the annular flow regime region. So even increasing the diffusion layer thickness by a factor of 20 does not significantly change the thickness in the slug flow regime as compared to annular flow. This explains the insignificant decrease in the corrosion rate in the slug flow region compared to the annular flow region.

4.2.3 Concentration Profiles

The concentration profiles generated are used to calculate the flux of ferrous ions,

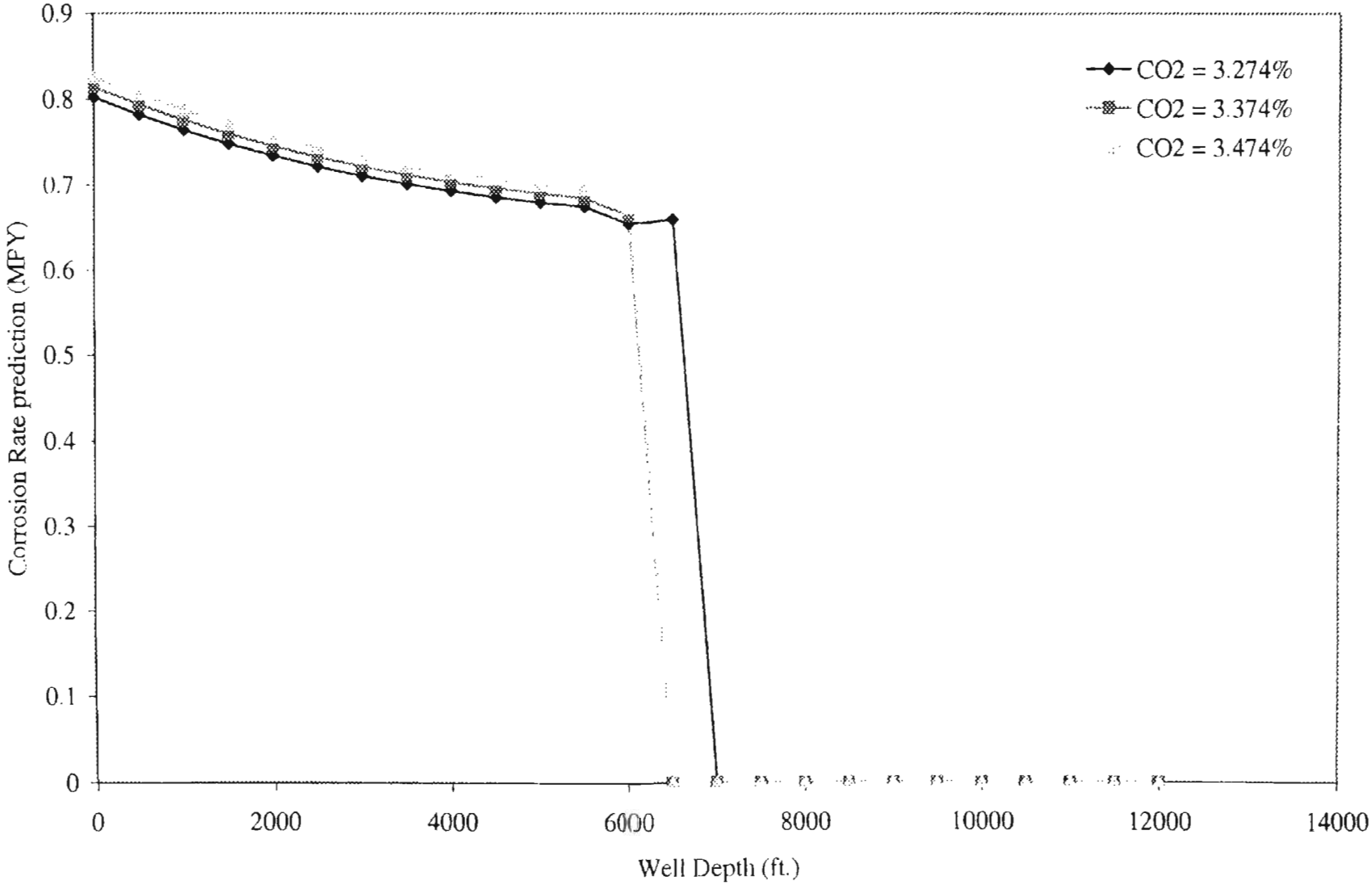

Figure 21. Effect of increasing CO_2 Concentration: Case XVIII

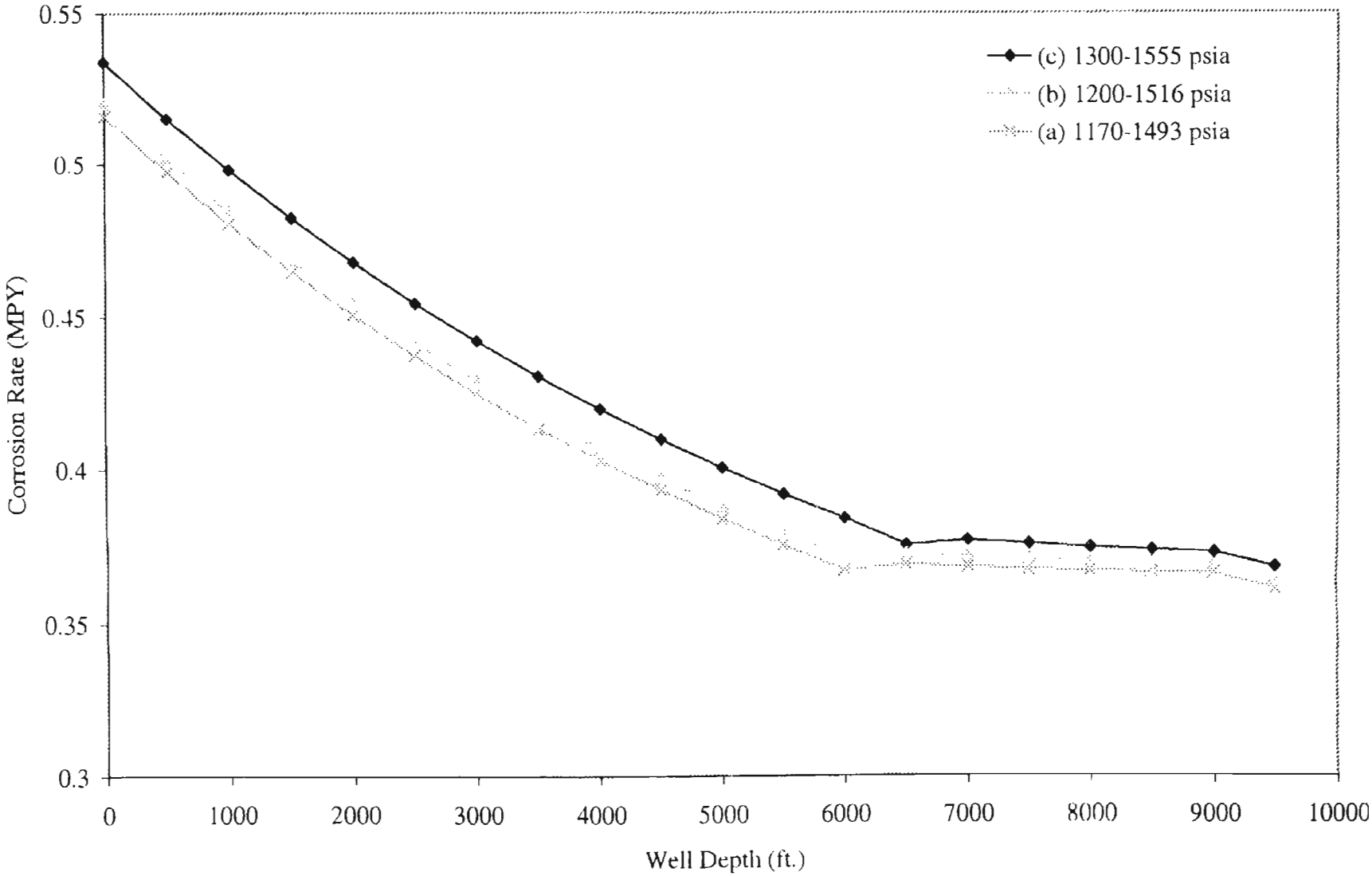

Figure 22. Effect of increasing Pressure: Case I

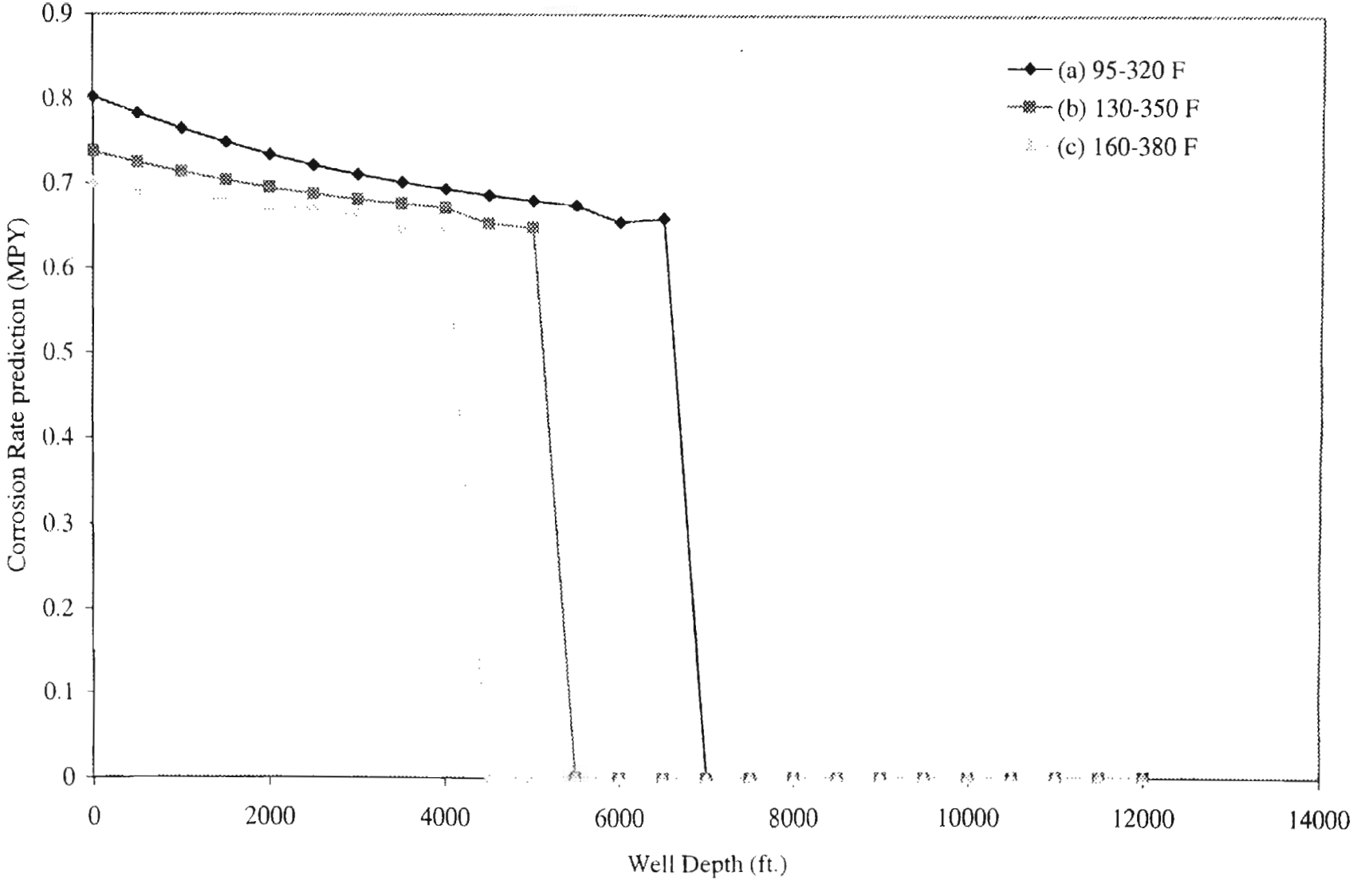

Figure 23. Effect of increasing Temperature: Case XVIII

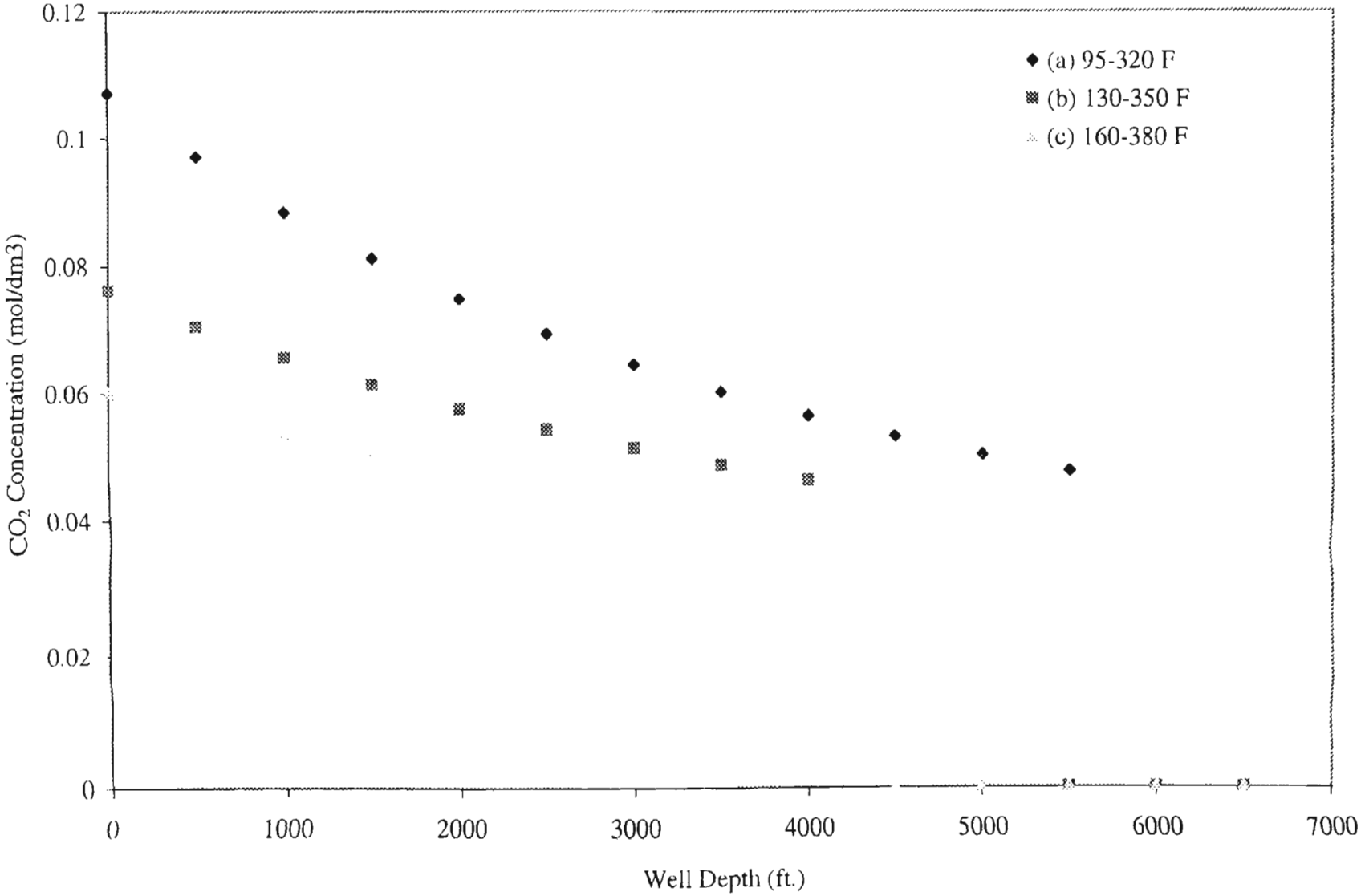

Figure 24. Effect of increasing Temperature on CO_2 Concentration: Case XVIII

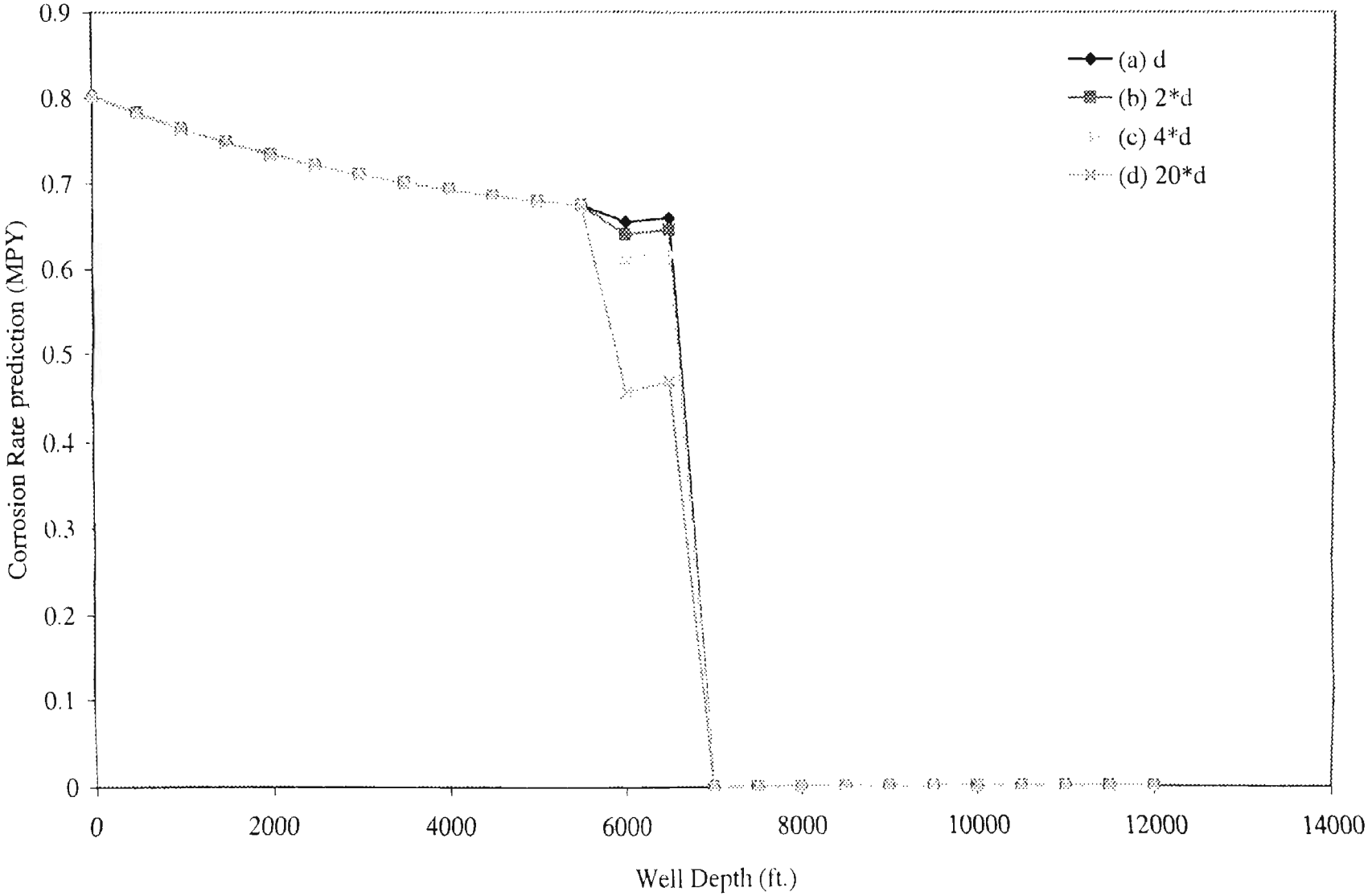

Figure 25. Effect of increasing laminar layer thickness: Case XVIII

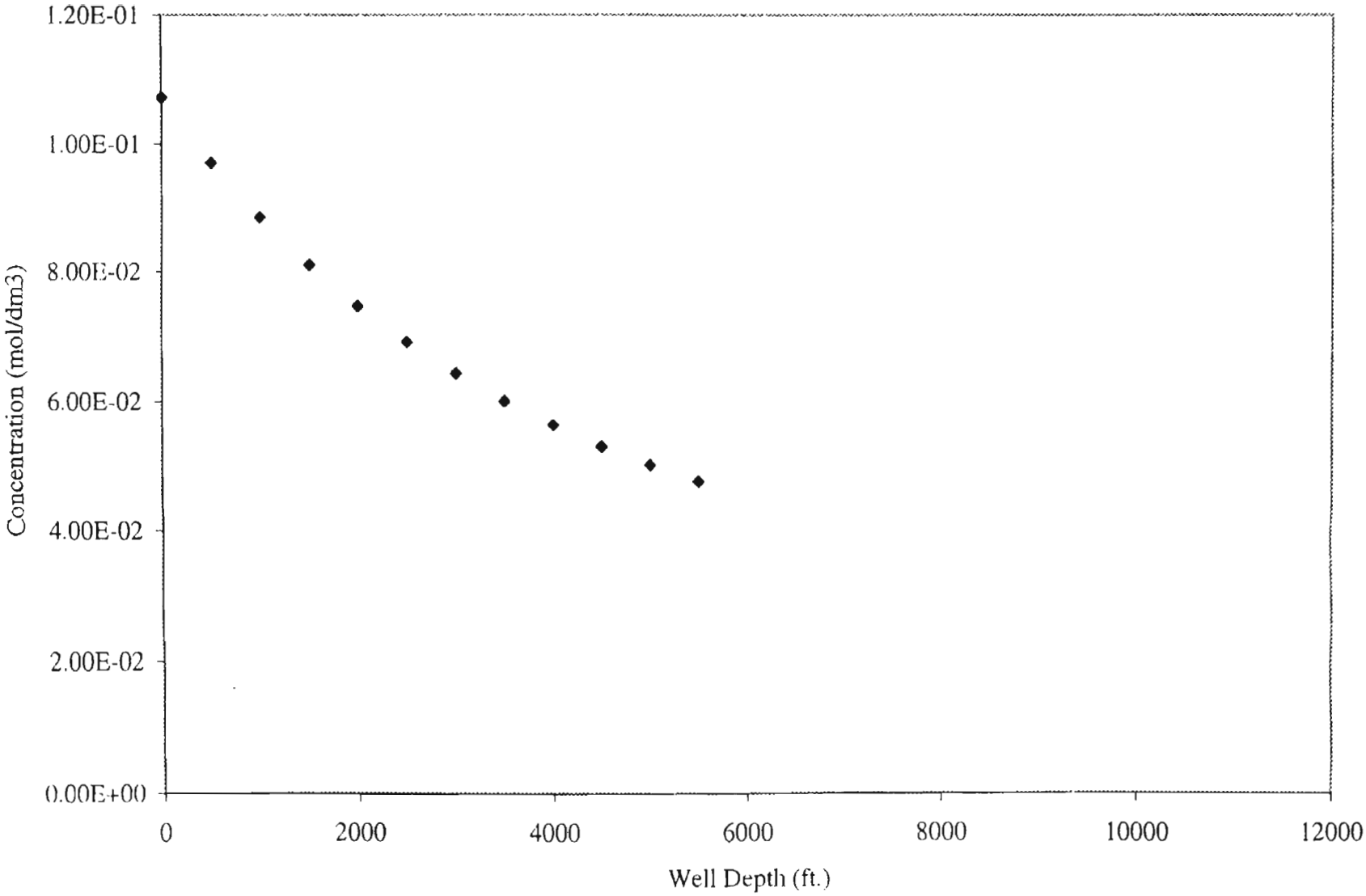

Figure 26. CO_2 Concentration Profile: Case XVIII

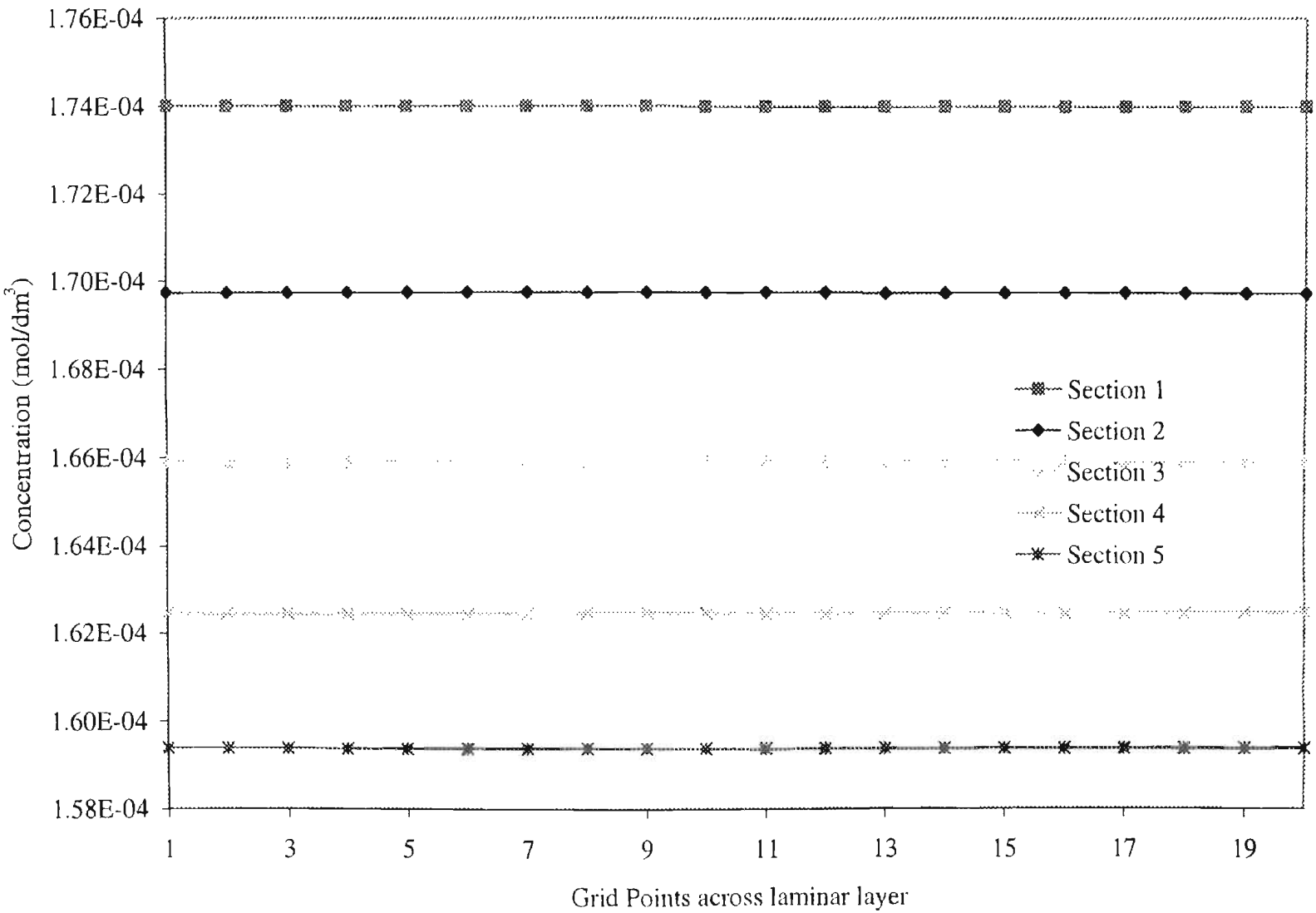

Figure 27. H^+ Concentration Profiles across laminar layer: Case XVIII

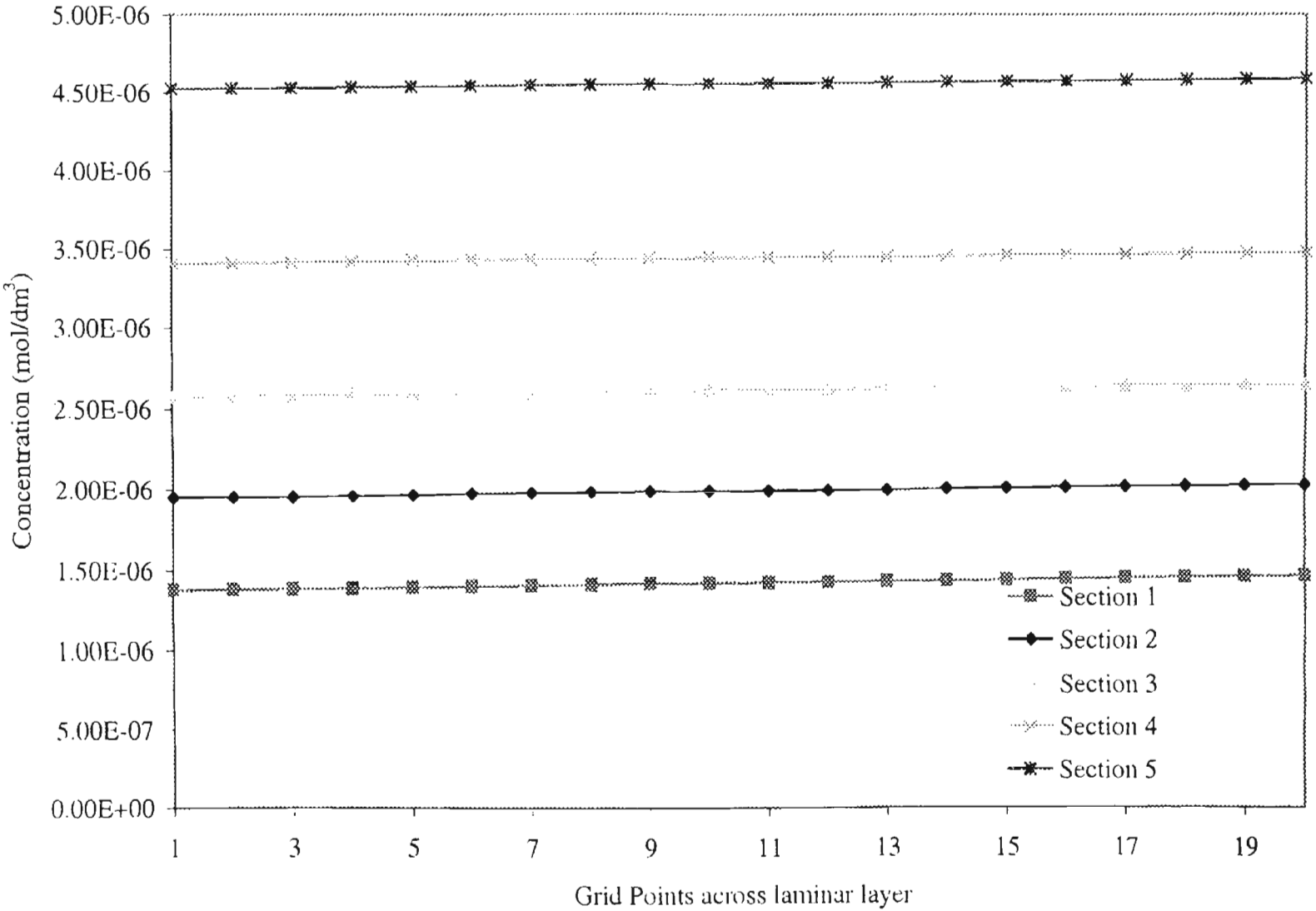

Figure 28. Fe^{2+} Concentration Profiles across laminar layer: Case XVIII

which in turn is related to the corrosion rate via Equation (3.56). The concentration profile in Figure 26 indicates that as the top of the well is approached the amount of dissolved CO_2 increases. This in turn results in an increase in the proton concentration as we go up the well (Figure 27). The increase in proton concentration results in an increase in the predicted corrosion rates (Figure 20). This phenomenon is observed in all the cases where the pressure drop calculations converge.

4.3 Other Discussions

Certain key issues that were identified during evaluation of the DREAM corrosion prediction tool are discussed in this section. These include the discontinuities observed in the corrosion rate profiles and the convergence limitations in the pressure drop calculations. A discussion on the corrosion kinetics model, which has been used in this work, is also included.

4.3.1 Discontinuities in Corrosion Rate Profiles

Discontinuities are observed in the predicted corrosion rate profiles in a few cases that have been modeled using DREAM. The thickness of the laminar liquid layer increases significantly as the flow regime changes from slug to annular flow. The mass transfer coefficient in the turbulent layer in the case of slug flow is also significantly larger than that in the turbulent layer in the annular case. These result in the corrosion rate changing dramatically when such a regime change is encountered in the flow. The discontinuity in certain predicted corrosion rate profiles has been attributed to these flow regime transitions.

4.3.2 Bottomhole Pressure Convergence

Convergence failures were encountered in the pressure drop calculations in some of the cases that were modeled. The user inputs an initial guess for the bottomhole well pressure. DREAM uses this initial guess along with the wellhead pressure to generate an initial pressure profile across the depth of the well. This profile is then used as an initial estimate to perform the pressure drop calculations. The pressure drop calculations result in a new pressure profile which is then used to repeat the calculations until convergence is attained in the bottomhole pressure. However, it was observed that in Cases II, III, VII, VIII, IX, XII, XV, and XVI, convergence problems were encountered in the pressure profile calculations. The pressure profiles generated in these cases were found to be dependent on the initial guess value of the bottomhole pressure input by the user. This should be studied further and corrected as the pressure profile has a strong influence on the corrosion rate.

4.3.3 Corrosion Kinetics Model Limitation

In DREAM the corrosion reaction that occurs at the wall is modeled by

$$Fe + 2H^{+} \leftrightarrow Fe^{2+} + H_{2(g)} \tag{4.2}$$

However, the rate expression used in the current work, given by Equation (3.35), is based on the following reaction mechanism (de Waard et al., 1975)

$$H_2CO_3 + e^{-} \rightarrow H + HCO_3^{-} \tag{4.3}$$

$$H^{+} + HCO_3^{-} \leftrightarrow H_2CO_3 \tag{4.4}$$

Thus, it is clear that there is a discrepancy between the rate expression used in the present work and the corrosion reaction modeled in DREAM. Further, the constants A and B in Equation (3.35) have been obtained at a temperature of 25 ^{o}C (de Waard et al., 1975). This temperature dependence of parameters A and B has been overlooked in the current work.

CHAPTER V

CONCLUSIONS AND RECOMMENDATIONS

5.1 Conclusions

The following conclusions can be made from this study:

1. The model predictions follow expected trends. In general, uniform corrosion in the absence of film formation increases as the well head is approached. The magnitudes of predicted corrosion rates, however, were observed to be much smaller when compared to available caliper data.
2. The model provides a mechanistic perspective of the corrosion process in downhole systems. The different types of studies that are possible with this work enable us to have both a macroscopic and microscopic understanding of the flow-induced corrosion process and the influence of various factors on the corrosion rates.
3. The model could be used as a prediction tool to provide initial estimates of the corrosiveness of a well.

5.2 Recommendations

The following areas should be further studied:

1. The rate expression used has a significant influence on the corrosion rate predictions. The rate expression used in this work is based on a reaction mechanism that is different from the one identified in the DREAM model. The current kinetics model also does not account for the temperature dependence of the corrosion reaction. These may be the reason for the small magnitudes of the corrosion rate predictions. A temperature-dependent rate expression consistent with the overall modeling approach used in DREAM should be identified (Bockris and Reddy, 1970; Kaesche, 1986; Dugan, 1998) and incorporated.
2. The pressure drop calculations do not always result in a converged solution. The well pressures have a significant influence on the predicted corrosion rates. Also, the dew point temperature calculations resulted in convergence problems in Cases XIII and XIV. These issues should be further investigated and improved.
3. Uniform corrosion without corrosion product film formation by itself is a rare situation in reality. Uniform corrosion with the formation of a corrosion product film and localized corrosion are other commonly occurring forms of corrosion in downhole systems. Liu and High (1993) coded the subroutines for the prediction of these additional forms of corrosion. The accuracy of the uniform corrosion rate with film formation has to be studied to see if it can be improved. Further, the subroutines for localized corrosion have to be

activated and investigated further. These would immensely improve the practical applicability of DREAM.

4. At this stage it would be very wise to rewrite the entire code using C. Though it will take considerable amount of time and effort, it will greatly help in making the code more efficient and clear. The issues of interfacing the FORTRAN code with the C++ graphical interface of DREAM would be avoided. Further this would help in future software development work.

REFERENCES

Ansari, A. M., Sylvester, N. D., Sarica, C. et al., "A Comprehensive Mechanistic Model for Upward Two-Phase Flow in Wellbores," SPE Production and Facilities, p. 143, 1994.

Achour, M., and Erbar, R., "Prediction of CO_2 Pitting Corrosion for Downhole Applications," Corrosion Consortium Report, Oklahoma State University, Stillwater, 1992.

Achour, M., Kolts, J., and Johannes, A. H., "Mechanistic Modeling of Pit Propagation in CO_2 Environment under High Turbulence Effects," Corrosion/93, paper 93087, New Orleans, 1993.

Barnea, D., "A Unified model for Predicting Flow-Pattern Transition for the Whole Range of Pipe Inclinations," International Journal of Multiphase Flow, 13, p. 1, 1987.

Bockris J. O'M. and Reddy A. K. N., "Modern Electrochemistry," Second Edition, Plenum Press, New York, Vol. 1-2, 1970.

Camacho, C. A., "Comparison of Correlations for Predicting Pressure Losses in High Gas-Liquid Ratio Vertical Wells," M. S. Thesis, University of Tulsa, Tulsa, 1970.

Chen, H., Wagner, J., Friedemann, J. D., "Phase Equilibria in Aqueous Acid Gas Systems," Proceedings of the 73rd Annual GPA Convention, New Orleans, Louisiana, 1994.

Choi, H. J., Cepulis, R. L., and Lee, J. B., "Carbon Dioxide Corrosion of L-80 Grade Tubular in Flowing Oil-Brine Two-Phase Environments," Corrosion, 45, 943-950 (1989).

Chisholm, D., "Two-phase flow in pipelines and heat exchangers," Pitman Press Ltd., Great Britain, 1983.

de Waard, C., and Lotz, U., "Predictive Model for CO_2 of Carbon Steel," Corrosion/93, paper 69, New Orleans, 1993.

de Waard, C., Lotz, U., and Milliams, D. E., "Predictive Model for CO_2 Corrosion Engineering in Wet Natural Gas Pipelines," Corrosion, 47, p. 976-985, 1991.

de Waard, C., and Milliams, D. E., "Carbonic Acid Corrosion of Steel," Corrosion, 31, No. 5, p. 177-181, 1975.

de Waard, C., and Milliams, D. E., "Prediction of Carbonic Acid Corrosion in Natural Gas Pipelines," Ind. Finishings and Surface Coatings, 28, p. 24-27, 1976.

Dugan, S., "A Mathematical Model for calculating Mass Transfer in the Diffusion Layer," M. S. Thesis, Oklahoma State University, Stillwater, 1998.

Golan, L. P., "An Air-Water Study of Vertical Upward and Downward Two-Phase Flow," PhD Dissertation, Lehigh University, Bethlehem, 1970.

Henstock, W. H., and Hanratty, T. J., "The Interfacial Drag and Height of the Wall Layer in Annular Flows," AIChE Journal, 22, p. 990, 1976.

Ikeda, A., Ueda, M., and Mukai, S., "Influence of Environment Factors on Corrosion in CO_2 Source Well, in Advances in CO_2 Corrosion Vol.2, (Burke, P. A., Symposium Chairman, and Asaphani, A. I., and Wright, B. S., Symposium Co-Chairmen respectively)," NACE, Houston, Texas, 1-22 (1984).

Jepson, W. P., Kanwar, S., "A Model to Predict Sweet Corrosion of Multiphase Flow in Horizontal Pipelines," Corrosion/97, paper 5, New Orleans, 1997.

Jones, D. A., "Principles and Prevention of Corrosion," Macmillan Publishing Company, New York, 1992.

Kaesche, H., "Metallic Corrosion," Second Edition, NACE, TX, p. 79 – 176,1986.

Kvarkeval, J., "A Kinetic Model for Calculating Concentration Profiles and Fluxes of CO_2-Related Species Across the Nernst Diffusion Layer," CORROSION/97, paper no. 5, Houston, Texas, NACE.

Levich, V. G., "Physicochemical Hydrodynamics," Prentice Hall Inc., New Jersey, p. 145 – 155, 1962.

Liu, G., "A Mathematical Model for Prediction of Downhole Gas Well Uniform Corrosion in CO_2 and H_2S Containing Brines," Ph. D. Dissertation, Oklahoma State University, 1991.

Liu, G., and High, M. S., "Documentation Report for the Downhole Corrosion Model and Computer Program," Downhole Corrosion Consortium, 1993.

Newton, Jr., L. E., and Hausler, R. H., "CO_2 Corrosion in Oil and Gas Production," NACE Publication, Texas, p. 3, 1984.

NACE, "Corrosion Basics An Introduction," NACE Publication, Texas, 1992.

Newman, J. S., "Electrochemical Systems," Second Edition, Prentice Hall Inc., New Jersey, p. 539–556, 1991.

Oddo, J. E., and Tomson, M. B., "Method predicts well bore scale, corrosion," Oil & Gas Journal, p. 107-114, 1998.

Palacios, C. A., and Shadley, J. R., "Characteristics of Corrosion Scales on Steels in a CO_2 Saturated NaCl Brine," Corrosion, 47, p. 122-127, 1991.

Patankar, V. S., "Computation of Conduction and Duct Flow Heat Transfer," First Edition, Innovative Research Inc., Minnesota, p. 321–348, 1991.

Perkins, R., Fang, C., Garber, J. D..and Singh, R., "Predicting Tubing Life in Annular Flow Gas Condensate Wells Containing Carbon Dioxide," Corrosion, 52 (10), p. 801, 1996.

Instrument Soc. of America, "Proceedings of the Workshop on Nondestructive Evaluation and Diagnostic Needs for Industrial Impact," October, 1996.

Raman, V., "Downhole Pressure Drop Modeling," M. S. Thesis, Oklahoma State University, Stillwater, 1996.

Reinicke, K. M., and Remer, R. J., "Comparison of Measured and Predicted Pressure Drops in Tubing for High-Water-Cut Gas Wells," Society of Petroleum Engineering 59th Annual Meeting, SPE paper no. 30, Houston, TX, 1987.

Robertson, C. A., "DOWN*HOLE Phase I: A Computer Model for Predicting the Water Phase Corrosion Zone in Gas and Condensate Wells," M. S. Thesis, Oklahoma State University, Stillwater, 1988.

Sundaram, M., "Phase and Electrolyte Equilibrium Modeling in Downhole Environments," M. S. Thesis, Oklahoma State University, Stillwater, 1996.

Sundaram, M., Raman, V. et al., "Deterministic Modeling of Corrosion in Downhole Environments," CORROSION/96, paper no. 30, Houston, TX, NACE.

Sylvester, N. D., "A Mechanistic model for Two-Phase Vertical Slug Flow in Pipes," ASME Journal of Energy Resources Technology, 109, p. 206, 1987.

Taitel, Y., Barnea, D., and Dukler, A. E., "Modeling Flow Pattern Transitions for Steady Upward Gas-Liquid flow in Vertical Tubes," AIChE Journal, 26(3), p. 345, 1980.

Treseder, R. S., and Tuttle, R. N., "Corrosion Control in Oil and Gas Production," NACE Publication, CORUPDATE Inc., Houston, TX, 1998.

Yao, S. C, and Sylvester, N. D., "A Mechanistic model for Two-Phase Annular Mist Flow in Vertical Pipes," AIChE Journal, 33(6), p. 1008, 1987.

Zhang, R., Gopal, M., and Jepson, W. P., "Development of a Mechanistic Model for Predicting Corrosion rates in Multiphase Oil/Water/Gas Flows," Corrosion/97, paper 5, New Orleans, 1997.

APPENDIX A

Species Modeled

TABLE A.1

COMPONENT ID OF SPECIES

Component ID.	Species
1	Sodium
2	Calcium
3	Magnesium
4	Barium
5	Strontium
6	Potassium
7	Ferrous
8	Chloride
9	Sulfate
10	Carbonate
11	Bicarbonate
12	Hydrogen
13	Hydroxide
14	Bisulfide
15	Sulfide
16	Carbon dioxide
17	Hydrogen Sulfide

APPENDIX B

pH Calculation

The pH calculations used in DREAM have been modified using the Oddo and Tomson method. The Oddo and Tomson method is widely known in the oil and gas industry and it enables calculation of pH using the following relations (Oddo et al., 1998)

$$pH = \log_{10}\left[\frac{HCO_3^-}{Py_g f_g}\right] + 8.569 + fn_1(T) + fn_2(P) + fn_3(I) + fn_4(T,I) \tag{B.1}$$

$$\begin{aligned} fn_1(T) &= 5.520*10^{-3}T - 2.830*10^{-6}T^2 \\ fn_2(P) &= -1.330*10^{-5}P \\ fn_3(I) &= -0.425I^{0.5} + 0.346I - 1.716*10^{-2}I^{1.5} \\ fn_4(T,I) &= -1.298*10^{-3}TI^{0.5} \end{aligned} \tag{B.2}$$

$$f_g = \exp\left[\begin{array}{l} \left(-7.66*10^{-3} + 8.0*10^{-4}T^{0.5} - 2.11*10^{-5}T\right)P^{0.5} + \\ \left(-5.77*10^{-4} + 3.72*10^{-5}T^{0.5} - 5.7*10^{-7}T\right)P + \\ \left(4.4*10^{-6} - 2.96*10^{-7}T^{0.5} + 5.1*10^{-9}T\right)P^{1.5} \end{array}\right] \tag{B.3}$$

where T is the temperature (°F), P is pressure (psi), I is ionic strength (molar), y_g is the mole fraction of carbon dioxide in the gas phase and f_g is the fugacity of CO_2 gas at the well section temperature and pressure.

In certain wells that have been modeled the pH decreased as the well head was approached. However, exceptions to the above trend were observed as mentioned in Section 4.2.1. This has been attributed to the interplay of the contributions of the

individual terms in Equation (B.2) to the pH. The term $fn_1(T)$ decreases as the well head is approached (for the range of temperature commonly encountered in gas wells). However, $fn_2(P)$ increases as the well head is approached. The variations of $fn_3(I)$ and $fn_4(T,I)$ are less obvious as they depend on the magnitude of the ionic strength and how it varies along the well depth. Depending on the term, in Equation (B.2), which becomes more significant, the pH profile may increase or decrease as the wellhead is approached.

VITA

Candidate for the degree of

Master of Science

Thesis: MECHANISTIC MODELING OF MASS TRANSFER IN THE LAMINAR SUBLAYER IN DOWNHOLE SYSTEMS

Major field: Chemical Engineering

Biographical:

Personal Data: Born in Chennai, India, On July 17, 1975, the son of Vijayalakshmi, N and Natarajan, M.

Education: Graduated from Padma Seshadri Junior College, Chennai, India in May 1992; received Bachelor of Engineering (Hons) degree in Chemical Engineering with Master of Science (Hons) degree in Chemistry from Birla Institute of Technology and Science, Rajasthan, India, July 1997. Completed the requirements for the Master of Science degree with a major in Chemical Engineering at Oklahoma State University in May, 2000.

Experience: Intern at SPIC Heavy Chemicals Division; co-op at Neyveli Lignite Corporation; employed by the School of Chemical Engineering, OSU as a Teaching Assistant, August to December1997 and then as a Graduate Research Assistant, January 1998 to present.

Memberships: Omega Chi Epsilon, AIChE, NACE.